

NATIONAL ACADEMY OF SCIENCES
NATIONAL RESEARCH COUNCIL

of the
United States of America

UNITED STATES NATIONAL COMMITTEE
International Union of Radio Science



1972 Spring Meeting
13-15 April

Sponsored by USNC-URSI
in cooperation with
Institute of Electrical and Electronics Engineers
Groups on AP, CT, GE, IT, IM, and MTT

The Statler Hilton Hotel
Washington, D.C.

Price \$3.00

USNC-URSI MEETING SCHEDULE

WEDNESDAY, April 12, 1972THURSDAY, April 13, 1972FRIDAY, April 14, 1972SATURDAY, April 15, 1972

0800 Registration (Upper Lobby)	0800 Registration (Upper Lobby)	0800 Registration (Upper Lobby)
0900 Combined Session of all Commissions (Congressional)	0900 1-1 (Galleries I) 2-2 (Senate) 2-3 (Massachusetts) 3-3 (Federal) 3-4 (New York) 4-2 (South American) 5-2 (Galleries II) 6-2 (Pan American) 1020 6-3a(Pan American)	0830 2-5 (Senate) 3-7 (Congressional) 3-8 Joint with 4-4 (South American) 5-4 (Galleries I&II) 6-5 (Pan American) 6-6 (New York)
1345 6-1 (Pan American)	1400 1-2 (Galleries I) 2-4 (Senate) 3-5 (Federal) 3-6 (New York) 4-3 (South American) 5-3 (Galleries II) 6-3b(Pan American) 6-4 (Massachusetts)	1330 2-6 (Senate) 2-7 (Federal) 3-9 (Congressional) 3-10 Joint with 4-5 (South American) 5-5 (New York) 6-7 (Pan American)
1400 2-1 (Senate) 3-1 (Congressional) 3-2 (Federal) 4-1 (Massachusetts) 5-1 (California)		
1600 Registration (Upper Lobby)	1700 C.2 Business (Galleries) C.4 Business (Mass.) C.6 Business (Pan Amer.) 1830 Reception (South American) 1930 USNC (Massachusetts)	1600 C.1 Business (Galleries I) 1700 C.3 Business (Federal) C.5 Business (Galleries II) 1930 USNC (Massachusetts)

Note: Registration and all meeting rooms are located on the Mezzanine floor of the Statler Hilton Hotel, 16th & K Sts. N.W., Washington, D.C.

United States National Committee
INTERNATIONAL UNION OF RADIO SCIENCE

PROGRAM AND ABSTRACTS

1972 Spring Meeting
13-15 April

Sponsored by USNC-URSI in cooperation with IEEE Groups on

Antennas and Propagation
Circuit Theory
Geoscience Electronics
Information Theory
Instrumentation and Measurement
Microwave Theory and Techniques

Washington, D. C.

NOTE

Programs and Abstracts of the USNC-URSI Meetings
are available from:

USNC-URSI
National Academy of Sciences
2101 Constitution Avenue, N.W.
Washington, D. C. 20418

at \$2.00 for meetings prior to 1970 and \$3.00 for subsequent meetings. The full papers are not published in any collected format, and requests for them should be addressed to the authors who may have them published on their own initiative. Please note that these meetings are national and are not organized by international URSI, nor are these programs available from the international Secretariat.

MEMBERSHIP

United States National Committee
INTERNATIONAL UNION OF RADIO SCIENCE

Chairman	A.T. Waterman, Jr., Stanford University
Vice Chairman	F.S. Johnson, University of Texas, Dallas
Secretary	J.V. Evans, Lincoln Laboratory MIT
Editor	S.A. Bowhill, University of Illinois

Immediate Past Chairman E.C. Jordan, University of Illinois

Commission Chairmen

Commission 1: Radio Measurement Methods and Standards

Helmut M. Altschuler
Institute for Basic Standards, 272.10
National Bureau of Standards
Boulder, Colo. 80302

Commission 2: Radio and Nonionized Media

Charles I. Beard
Radar Division (Code 5369)
Naval Research Laboratory
Washington, D.C. 20390

Commission 3: On the Ionosphere

Erwin R. Schmerling
Code SG
National Aeronautics & Space Administration
Washington, D.C. 20546

Commission 4: On the Magnetosphere

Jules A. Fejer
Department of Applied Physics & Information
Science
University of California
P.O. Box 109
La Jolla, California 92037

Commission 5: Radio and Radar Astronomy

Marshall H. Cohen
Owens Valley Radio Observatory
California Institute of Technology
Pasadena, Calif. 91109

Commission 6: Radio Waves and Transmission Information

Leopold B. Felsen
Polytechnic Institute of Brooklyn
Graduate Center ~ Route 110
Farmingdale, N.Y. 11735

Commission 7: Radio Electronics

Robert J. Collins
Department of Electrical Engineering
University of Minnesota
Minneapolis, Minn. 55455

Members at Large	W.I. Axford H.V. Cottony J.W. Findlay R.C. Hansen D.C. Hogg I. Katz	H.C. Ko M.G. Morgan G.C. Reid J.M. Richardson T.B.A. Senior J.R. Wait
------------------	--	--

Officers of URSI resident in the United States

Immediate Past President
Vice President
Chairman, Commission 2
Chairman, Commission 7
Vice Chairman, Commission 3
Vice Chairman, Commission 4
Vice Chairman, Commission 6

S. Silver
H.G. Booker
W.E. Gordon
M. Chodorow
S.A. Bowhill
F.L. Scarf
K.M. Siegel

IEEE

Ernst Weber

United States Government

Department of Commerce
Department of Defense
Air Force
Army
Navy
FCC
NASA
NSF
OTP

A.H. Shapley
E. Paroulek
C.J. Sletten
F.H. Dickson
A.H. Schooley
H. Fine
E.R. Schmerling
R. Fleischer
W. Dean, Jr.

Foreign Secretary, NAS

H.S. Brown

Chairman, NRC Division of Physical Sciences

R. Smoluchowski

Honorary Members

H.H. Beverage
A.H. Waynick

The USNC Executive Committee consists of the Chairman, Vice Chairman, Secretary, Immediate Past Chairman, and Officers of URSI Resident in the United States.

**DESCRIPTION OF
INTERNATIONAL UNION OF RADIO SCIENCE**

The International Union of Radio Science is one of 14 world scientific unions organized under the International Council of Scientific Unions (ICSU). It is commonly designated as URSI (from its French name, Union Radio Scientifique Internationale). Its aims are (1) to promote the scientific study of radio communications; (2) to aid and organize radio research requiring cooperation on an international scale and to encourage the discussion and publication of the results; and, (3) to facilitate agreement upon common methods of measurement and the standardization of measuring instruments. The International Union itself is an organizational framework to aid in promoting these objectives. The actual technical work is largely done by the National Committees in the various countries.

The officers of the International Union are:

President:	W. Dieminger (West Germany)
Immediate Past President:	S. Silver (USA)
Vice Presidents:	W. J. G. Beynon (UK) H. G. Booker (USA) J. Groszkowski (Poland) M. J. Voge (France)
Secretary General:	C. M. Minnis (Belgium)
Honorary Presidents:	B. Decaux (France) R. L. Smith-Rose (UK) J. A. Ratcliffe (UK) C. Manneback (Belgium)

The Secretary's office and the headquarters of the organization are located at 7, Place Emile Danco, 1180 Brussels, Belgium. The Union is supported by contributions (dues) from 37 member countries. Additional funds for symposia and other scientific activities of the Union are provided by ICSU from contributions received for this purpose from UNESCO.

The International Union has seven permanent bodies called Commissions for centralizing studies in the principal technical fields. In addition, Commission 8 was recently established on a provisional basis. The names of the Commissions and the chairmen are as follows:

1. Radio Standards and Measurements
M. E. Zhabotinskii (USSR)
2. Radio and Non-ionized Media
W. E. Gordon (USA)
3. On the Ionosphere
K. Rawer (Germany)
4. On the Magnetosphere
J. W. Dungey (UK)
5. Radio Astronomy
C. A. Muller (Netherlands)
6. Radio Waves and Circuits
H. M. Barlow (UK)
7. Radio Electronics
M. Chodorow (USA)
8. On Radio Noise of Terrestrial Origin
R. Rivault (France)

Every three years the International Union holds a meeting called the General Assembly. The next of these, the XVIIth, will be held in Warsaw, Poland, in August 1972. The Secretariat prepares and distributes the Proceedings of these General Assemblies. The International Union arranges international symposia on specific subjects pertaining to the work of one Commission or to several Commissions. The International Union also cooperates with other Unions in international symposia on subjects of joint interest.

Radio is unique among the fields of scientific work in having a specific adaptability to large-scale international research programs, for many of the phenomena that must be studied are world-wide in extent and yet are in a measure subject to control by experimenters. Exploration of space and the extension of scientific observations to the space environment is dependent on radio for its communication link and at the same time expands the scope of radio research. One of its branches, radio astronomy, involves cosmos-wide phenomena. URSI has in all this a distinct field of usefulness in furnishing a meeting ground for the numerous workers in the manifold aspects of radio research; its meetings and committee activities furnish valuable means of promoting research through exchange of ideas.

COMBINED SESSION

A.T. Waterman, Jr., Chairman

0900 Thursday, April 13

Congressional Room

C-1 RADIO ASTRONOMY EXPLORER (RAE) I OBSERVATIONS OF TERRESTRIAL RADIO NOISE: J.A. Caruso, J.R. Herman, Analytical Systems Corporation, Burlington, Mass.; and R.G. Stone, Goddard Space Flight Center, National Aeronautics and Space Administration, Greenbelt, Md.

Radio Astronomy Explorer (RAE) I data are analyzed to establish characteristics of high-frequency terrestrial radio noise at an altitude of about 6000 km. Time and frequency variations in amplitude of the observed noise well above cosmic noise background are explained on the basis of temporal and spatial variations in ionospheric critical frequency coupled with those in noise source (thunderstorm activity) distributions. It is shown that terrestrial noise regularly breaks through the ionosphere and reaches RAE with magnitudes 15 or more dB higher than cosmic noise background. Maximum terrestrial noise is observed when RAE is over the dark side of the Earth in the neighborhood of equatorial continental land masses where thunderstorms occur most frequently. The observed noise level is 30-40 dB lower with RAE over oceans.

C-2 LASER FREQUENCY MEASUREMENTS IN THE NEAR INFRARED: PROGRESS IN THE MEASUREMENT OF THE SPEED OF LIGHT: K.M. Evenson, National Bureau of Standards, Boulder, Colo.

The synthesis of infrared frequencies to 88 THz has recently been accomplished (Evenson *et al.*, *Appl. Phys. Lett.*, Feb. 1, 1972). The frequency of a cw helium-neon laser tuned to the methane absorption line at $3.39\mu\text{m}$ was measured at the National Bureau of Standards and found to be 88.376245 (55) THz. A second round of experiments to increase the accuracy of this measurement is now well under way. The laser frequency can be combined with the value of the wavelength to obtain a new value of c . The wavelength is being determined by Barger and Hall at JILA and NBS, where the experimental part of the measurement has been completed and systematic errors are now being analyzed. It is also being determined by Giacomo at the BIPM. The accuracy of the frequency measurement should be good to a few parts in 10^9 , and the wavelength measurement should be good to the limits of the present length standard (about 1 part in 10^8). Thus, the value of c obtained from these measurements will be a definitive value. Progress in this series of measurements will be described.

C-3 DIGITIZATION AIDS IONOSPHERIC RESEARCH: J.W. Wright, Environmental Research Laboratories, National Oceanic and Atmospheric Administration, Boulder, Colo.

A successful measurement system should solve more problems than it creates, but historically, HF systems for ionospheric studies have seldom attained their full potential. Multifrequency pulse sounding can provide a wealth of information on the spatial and temporal structure of the ionosphere, with virtually unlimited resolution and dynamic range, but almost none of the many variables comprising this information are directly observable; instead, they are interdependently related to such parameters as frequency, amplitude, phase, group-path, polarization,

COMBINED SESSION

and direction of arrival--and their spatial and temporal dependences. The impossibility of managing all this raw "information" while pursuing a measurement objective by analog methods has caused much of it to be deliberately rejected or ignored. An obvious example is the importance of distinguishing vertical from lateral structure in the ionosphere. Through the introduction of adaptive digital methods in the acquisition, recognition, intercomparison, analysis, and presentation of ionospheric sounding measurements, these problems are near a common solution for diverse applications in ionospheric research and environmental monitoring. We review here, with examples and recent new results, applications of an advanced digital ionosonde system to problems in ionospheric structure, dynamics, and artificial seeding.

C-4 HIGH ANGULAR RESOLUTION STUDIES OF RADIO SOURCES EMPLOYING VERY-LONG-BASELINE INTERFEROMETRY AT METER WAVELENGTHS: W.C. Erickson, Astronomy Program, University of Maryland, College Park, Md.

Very-long-baseline interferometer techniques have been employed recently at meter and decameter wavelengths for a variety of radio astronomical studies. These studies fall into two categories, studies of intrinsic source structure and of propagation effects in the intervening media through which the radiation passes. In the first category, the compact components of radio sources have been observed with angular resolutions from 0.1 to 5 sec of arc at a number of wavelengths from 1 to 11 m. Compact sources do not, in general, display the $f^{2.5}$ spectra predicted on the basis of synchrotron self-absorption and simple models. A number of pulsars have been observed, and a novel technique has been developed for "de-chirping" the pulses to remove the dispersion caused by the interstellar medium. Using this technique, the pulsar NPO532 has been shown to agree in angular position with the compact source in the Crab Nebula to an accuracy of 0.1 sec of arc. Scattering and scintillation effects due to the interstellar, interplanetary, and ionospheric media have been observed. In many cases, the effects caused by the different media are separable due to their differing time scales or dependence upon solar elongation angle. The amplitude-variation spectra, phase-deviation spectra, and coherent bandwidth of the observed scintillations are under investigation.

RECEPTION

1830 Thursday, April 13

South American Room

BANQUET

1930 Thursday, April 13

Federal Room

Dr. John W. Findlay
National Radio Astronomy
Observatory
Edgemont Road
Charlottesville, Va.

"HERE AND THERE: SCIENCE IN EUROPE AND AMERICA"

COMMISSION 1

RADIO MEASUREMENT METHODS AND STANDARDS

H.M. Altschuler, Chairman

<u>Sessions</u>	<u>Page</u>
1. MEASUREMENTS ON AND RELATED TO ANTENNAS OPERATING BETWEEN 10 AND 100 GHZ 0900 Friday, April 14 Galleries I Chairman: R.W. Kreutel COMSAT Laboratories P.O. Box 115 Clarksburg, Md. 20734	10
2. RF TECHNIQUES FOR MEASUREMENT OF POLLUTION OF AIR AND WATER 1400 Friday, April 14 Galleries I Chairman: J.A. Hodgeson Environmental Protection Agency Durham, N.C. 27711	13
BUSINESS MEETING 1600 Friday, April 14 Galleries I	

COMMISSION 1, Session 1

0900 Friday, April 14

Galleries I

MEASUREMENTS ON AND RELATED TO ANTENNAS OPERATING
BETWEEN 10 and 100 GHZ

R.W. Kreutel, Chairman

1-1 DETERMINATION OF POINTING CHARACTERISTICS OF MILLIMETER-WAVE
ANTENNAS: L.E. Telford, Air Force Cambridge Research Laboratories, Bedford, Mass.

Millimeter-wave antennas having beamwidths of the order of one minute of arc require pointing accuracies of less than ten seconds of arc. Therefore pointing errors caused by mechanical misalignments and distortions, wind, solar heating, ice and snow loading, and atmospheric refraction must be determined. Most high-resolution antennas which do not have some form of auto-tracking use pointing correction terms which are determined by measuring apparent radio-source positions and comparing them with the accurately known theoretical source positions. However, radio sources in the 10-100 GHz band are not generally suitable for boresighting since they are weak emitters and require extremely sensitive receivers in order to be detected. The relatively large radio emission from the sun however is easily detectable with much less sophisticated receiver systems. Since most millimeter-wave dishes have beamwidths smaller than the solar radio diameter, the sun appears as an extended source, the center of which must be determined. If the antenna is computer-controlled, procedures for using the sun as a position calibration source are relatively straightforward, and it should be possible to obtain RMS pointing accuracies approaching ten seconds of arc. However, the effects of active regions and their positions on the solar disk must be taken into account. A series of solar measurements were conducted with the AFCRL 29-ft antenna at a wavelength of 8.6 mm, and it is shown that correction terms can be generated to correct for mechanical misalignments and distortions. Pointing corrections obtained from optical star sighting data, electronic level data, and solar measurements are compared.

1-2 PHOTOGRAMMETRIC MEASUREMENT OF ANTENNA REFLECTORS: J.F. Kenefick, Photogrammetric Services Division, DBA Systems, Inc., P.O. Drawer 550, Melbourne, Florida

Analytical photogrammetric stereotriangulation is a least-squares triangulation process in which two-dimensional measurements of an unlimited number of discrete points on two or more photographic records are processed simultaneously to generate a unique set of three-dimensional coordinates for each point measured. Applications of analytical photogrammetry to the measurement of antenna reflectors were first introduced by DBA in 1963. Since that time over 50 surface measurements have been performed over a wide range of test conditions. Recent advances have enhanced the capabilities of the photogrammetric process through hardware designed to operate within solar vacuum chambers and through increases in accuracy upwards to 1 part in 100,000 of the aperture of the antenna. Accuracies on the order of 1 part in 200,000 are within the state of the art. After a brief conceptual outline of the mathematical basis for analytical photogrammetric stereotriangulation, specific examples of actual measurements performed are detailed.

COMMISSION 1

1-3 BORESIGHT MEASUREMENTS UTILIZING A COMPACT RANGE: T.G. Hickman, Scientific-Atlanta, Inc., Atlanta, Ga; and R.C. Johnson, Engineering Experiment Station, Georgia Institution of Technology, Atlanta, Ga.

A compact range was constructed and evaluated. The design of this range was based on information gained from the evaluation of existing ranges at Georgia Tech. The design was directed toward providing a range which would give precision measurement capability for antennas measuring up to 4 ft in diameter and operating primarily in the 8-18 GHz frequency bands. Evaluation of this range is discussed and actual measurement data presented. The capability of this range for making precision antenna measurements is the object of the paper. Particular emphasis will be placed on making boresight measurements with the compact range. Since there is no visible point which may be considered the apparent source of radiation, boresight measurements cannot be made in the conventional manner. Boresight techniques are discussed and measurement accuracies presented.

1-4 GENERALIZED THREE-ANTENNA GAIN AND POLARIZATION MEASUREMENTS AT REDUCED RANGE DISTANCES: A.C. Newell, National Bureau of Standards, Boulder, Colo.

An accurate method has been developed at the National Bureau of Standards for determining both polarization and power gain of three unknown microwave antennas at reduced distances. This new technique requires no prior quantitative knowledge of the polarization of any of the antennas. Neither does it require that the antennas be identical or even similar in characteristics. This has made possible more accurate gain standards (errors of about 0.10 dB) and, for the first time, absolute polarization standards. The method requires that for each combination pair, the amplitude and relative phase of the received signal be measured for two orientations of the receiving antenna. The two orientations differ by a 90° rotation about the axis of measurement. These two orientations for each of the three pairs of antennas yield six equations involving six unknowns. These unknowns are the components of the transmission spectrum in the on-axis direction for each antenna. When these are solved for, the gain and polarization are easily determined. One means of obtaining the necessary data is by using an extrapolation technique which allows accurate measurements to be made at distances less than $2a^2/\lambda$. Near-zone and multipath errors are carefully evaluated and corrected for in this technique which involves measuring the received signal as a function of antenna separation distance. The measured data is then fitted with a series in powers of 1/distance, and the resulting series used to extrapolate to infinite distance to obtain the far-field characteristics.

1-5 THE MEASUREMENT OF CROSS-POLARIZED INTERFERENCE IN DUAL-POLARIZED ANTENNA SYSTEMS: R. W. Gruner, COMSAT Laboratories, Box 115 Clarksburg, Md.

For future satellite communications applications, considerable attention has been focused on the use of orthogonally polarized beams to increase channel capacity of a satellite link. In order for such a system to be tractable, sufficient isolation between the two beams must be obtained.

COMMISSION 1

The accurate measurement of this isolation is fundamental to the design of such a satellite system. By virtue of their curvature, reflector antennas generate cross-polarized signals. In addition, the primary feed also radiates a cross-polarized field. Depolarization also occurs due to scattering off of the feed and feed support structure. The highly frequency-sensitive nature of the cross polarization, in particular the scattered energy, necessitates the use of swept-frequency measurement techniques. A measurement system is outlined which directly measures the cross-polarized isolation on a swept-frequency basis. This measurement method is applicable to a dual-polarized system in which the polarization may be either nominally linear or nominally circular. The measurement equipment was implemented in a large anechoic chamber. Estimates of the error bounds due to anechoic chamber limitation and test equipment are given. Measurement results for a typical dual-polarized antenna are presented and discussed.

1-6 CALIBRATION PROCEDURES AND RESULTS FOR THE UNIVERSITY OF TEXAS 16-FT ANTENNA: J.H. Davis and J.R. Cogdell, Electrical Engineering Research Laboratory, University of Texas, Austin, Texas

In 1965, the 16-ft antenna was refurbished and moved from Austin to Mt. Locke, Texas. A complete calibration program has been conducted, including gain and patterns, pointing, and atmospheric losses. As initially installed at Mt. Locke, the antenna had a severe astigmatism problem. Diagnostic procedures were developed to detect and correct this problem, which is common in high-resolution antennas. A novel technique for determining the peak gain of the antenna was developed based on inferring the gain at a low frequency with high precision from a measurement made at a high frequency with a scaled feed system. A way of isolating the effects of random (Ruzian) and systematic (astigmatic and high-order) phase errors is presented. The calibration state of the antenna in the range 35-140 GHz will be discussed to illustrate the theory and viewpoint of the program.

COMMISSION 1, Session 2

1400 Friday, April 14

Galleries I

RF TECHNIQUES FOR MEASUREMENT OF POLLUTION OF AIR AND WATER

J.A. Hodgeson, Chairman

2-1 A MODERN MICROWAVE SPECTROMETER AND ITS POSSIBLE APPLICATION TO AIR POLLUTION CONTROL: J.R. Hearn, Hewlett-Packard Company, Palo Alto, Calif.

The principles of microwave spectroscopy are described, and some of the features of the technique are illustrated. Some important specifications and the design of a practical instrument are discussed. The potential of the technique as a dry, physical method for analyzing mixtures of small polar molecules typical of air pollutants is evaluated.

2-2 MICROWAVE MEASUREMENTS WITH ACTIVE SYSTEMS--POSSIBLE POLLUTION APPLICATIONS: R.C. Ajmera, East Carolina University, Greenville, N.C.; and D.B. Batchelor and H. Lashinsky, University of Maryland, College Park, Md.

Conventional systems used to determine dielectric constants or refractive index at microwave frequencies depend on the measurement of a shift in time phase, space phase, or frequency, caused by the introduction of a sample into a "passive" configuration, i.e., one in which the required microwave power is supplied by an external source. Passive systems have certain shortcomings: (1) ambiguities of factor of 2π , nonlinearity, and limited sensitivity (time-phase systems); (2) the need for expensive precision mechanical elements (space-phase systems); (3) subjective and time-consuming observations (frequency-shift systems). We describe here a new approach to the measurement of microwave refractive index in which the microwave elements and the sample are introduced into a positive-feedback loop that contains a broadband amplifier, typically a travelling-wave tube. This "active" configuration comprises a microwave oscillator whose frequency and output level depend on the complex dielectric constant of the sample. Active systems have certain interesting features with regard to response time, sensitivity, accuracy, and dynamic range. They also have self-telemetering capabilities and weaker requirements on circuit Q because of the availability of positive gain. These features are discussed together with certain measurements with possible pollution applications.

2-3 PASSIVE MICROWAVE DETERMINATION OF OIL SLICK THICKNESS: J.P. Hollinger and R.A. Mennella, E.O. Hulbert Center for Space Research, Naval Research Laboratory, Washington, D.C.

A promising method for the remote determination of the thickness of oil slicks using a multifrequency passive microwave technique is presented. A knowledge of the thickness over the areal extent of the slick allows the volume of the oil spill or discharge to be determined, and gives necessary information for appropriate legal or cleanup actions. The use of passive microwaves offers the advantages over optical and infrared techniques of allowing much thicker slicks to be measured and providing day-or-night and more nearly weather-independent operations.

COMMISSION 1

In effect the oil acts as a matching layer between free space and the water, increasing the emissivity of the surface. The use of several frequencies permits ambiguities resulting from interference effects to be removed and a unique thickness determined. Laboratory measurements at 19.3 and 69.8 GHz are presented which verify the predicted behavior. An aircraft-borne measurement program of controlled oil spills off Chesapeake light tower is currently under way to investigate this technique on an operational basis. Preliminary results from this program will be described.

2-4 MICROWAVE ROTATIONAL SPECTROSCOPY -- A TECHNIQUE FOR SPECIFIC POLLUTANT MONITORING: L.W. Hrubesh, Lawrence Livermore Laboratory, Livermore, Calif.

The properties of microwave rotational spectroscopy that make it a promising technique for gaseous pollutant monitoring are presented. Recent advances in instrumentation and technique that have suggested feasibility of in situ monitoring are discussed. A laboratory model of a potentially portable cavity spectrometer has been interfaced to the atmosphere by way of a multistaged membrane separator. Results of testing this system under controlled experimental conditions as a specific monitor for NO_2 and SO_2 are given. Determinations of optimum sensitivity, specificity, and stability expected for this system are discussed along with considerations for its calibration.

COMMISSION 2
RADIO AND NONIONIZED MEDIA
C.I. Beard, Chairman

<u>Sessions</u>	<u>Page</u>
1. REMOTE SENSING OF ATMOSPHERES I 1400 Thursday, April 13 Senate Room Chairman: Isadore Katz Applied Physics Laboratory Johns Hopkins University Silver Spring, Md. 20910	17
BUSINESS MEETING	
1700 Thursday, April 13 Galleries I and II	
2. EARTH-SATELLITE PROPAGATION ABOVE 10 GHZ 0900 Friday, April 14 Senate Room Chairman: A.W. Straiton Engineering Sciences Bldg 541 University of Texas Austin, Texas 78712	21
3. SURFACE AND SUB-SURFACE PROPAGATION 0900 Friday, April 14 Massachusetts Room Chairman: J.T. deBettencourt Raytheon Corporation 40 Second Avenue Waltham, Mass. 02154	25
4. REMOTE SENSING OF SURFACES I 1400 Friday, April 14 Senate Room Chairman: J.W. Rouse, Jr. Remote Sensing Center Texas A&M University College Station, Texas 77843	28
5. REMOTE SENSING OF ATMOSPHERES II 0830 Saturday, April 15 Senate Room Chairman: D.A. deWolf David Sarnoff Research Center Radio Corporation of America Princeton, N.J. 08540	32
6. REMOTE SENSING OF SURFACES II 1330 Saturday, April 15 Senate Room Chairman: S.H. Durrani COMSAT Laboratories P. O. Box 115 Clarksburg, Md. 20734	36

COMMISSION 2

<u>Sessions</u>	<u>Page</u>
7. REMOTE SENSING OF ATMOSPHERES III 1330 Saturday, April 15 Federal Room Chairman: A.H. LaGrone Electrical Engineering Research Laboratory University of Texas Austin, Texas 78712	39

COMMISSION 2, Session 1

1400 Thursday, April 13

Senate Room

REMOTE SENSING OF ATMOSPHERES I

Isador Katz, Chairman

1-1 ACOUSTIC ECHO-SOUNDING OF THE ATMOSPHERIC BOUNDARY LAYER: C.G. Little, NOAA Research Laboratories, Boulder, Colo.

The theory of the scatter of acoustic waves by inhomogeneities in the atmospheric velocity, temperature, and humidity fields is outlined and contrasted with the corresponding scatter of radio and optical waves. Examples of acoustic echo-sounding records obtained under stable and unstable atmospheric conditions are presented, together with the corresponding temperature profiles. Monostatic acoustic sounders typically show records of one of three types - intermittent, irregular quasi-vertical echoing regions associated with thermal plumes; intermittent quasi-periodic inclined echoing regions (apparently associated with gravity waves) during radiation inversions; and elevated, quasi-horizontal echoing regions, which often show undulations characteristic of gravity waves and occasionally the "braided" echoes characteristic of breaking waves. Comparisons of C_T measured remotely by the acoustic echo sounder and in situ by fast response, differential temperature sensors show agreement to within $\pm 50\%$ for the convectively unstable atmosphere, and comparable accuracy for marginally stable, well-mixed regions just above temperature inversions. In strong inversion layers, the sounder consistently indicates higher C_T values, possibly because of partially coherent scattering of the 20-cm wavelength acoustic radiation from such regions of nonisotropic turbulence. In layers characterized by large temperature gradients, the remotely measured C_T has been found to be as much as 400% higher than in situ results. The Doppler technique gives values of velocity which are in good agreement with those recorded by an anemometer at the same height.

1-2 RADAR STUDIES OF WAVE PATTERNS AND CLEAR AIR TURBULENCE: K.R. Hardy, Air Force Cambridge Research Laboratories, Bedford, Mass.

Two occurrences of aircraft clear air turbulence have been investigated using sensitive radars at Wallops Island, Virginia, and direct sensors. One of the occurrences was characterized by a deep layer of strong wind shear (rapid increase of the wind with height) and by widespread aircraft turbulence which persisted for more than 4 hours. The radar observations of the clear atmosphere revealed three different wave like structures, one of which was perpendicular to the other two. Each pattern had a distinctive wavelength which varied from about 20 km for the longest pattern to 1.5 km for the shortest. The second occurrence of turbulence was associated with Kelvin-Helmholtz waves or billows. It was observed by an instrumented aircraft and radar. The detailed structure of the waves and the mesoscale synoptic features associated with the life cycle of the waves will be described.

1-3 LIDAR: R.T.H. Collis, Stanford Research Institute, Menlo Park, Calif.

The application of radar principles at optical or near-optical wavelengths made practicable by the advent of lasers is still in an evolutionary phase. Most progress has been made with lidars using crystal

COMMISSION 2

lasers only as a convenient source of high intensity, short pulses. Such lidars, relying on Rayleigh and Mie scattering have been used widely to observe the distribution of particulate material in visually "clear" atmospheres or the structural features of ice and water clouds. More sophisticated techniques exploiting the wave nature of the energy are being increasingly studied. These include the use of the Doppler principle to measure air motion; Raman shifts of the backscattered energy to distinguish gaseous species, such as pollutants, in the lower atmosphere; and resonant scattering to observe atomic elements in the thermosphere. The various possibilities will be reviewed briefly with emphasis on recent results.

1-4 THE ROLE OF RESONANCE SPECTRA IN REMOTE SENSING OF THE ENVIRONMENT:

V.E. Derr, Wave Propagation Laboratory, Environmental Research Laboratories, National Oceanic and Atmospheric Administration, Boulder, Colo.

Inspite of the generally small cross sections of molecules for Raman scattering, it has been successfully used in laser ranging devices to measure atmospheric profiles of water vapor and temperature (Derr, Little, 1970; Strauch, Derr, Cupp, 1971; Strauch, Cupp, Derr, 1972). The extension of the method in range and sensitivity for detection of atmospheric pollutants and the detection and measurement of oceanic and terrestrial solutes, minerals, and biological materials depend on improvements in lasers and receivers and on choosing resonant exciting frequencies. Theory and experiment indicate that many materials of environmental interest, perhaps a preponderance, exhibit resonant effects which enhance cross sections. Data will be presented on experimentally determined resonant cross sections of gases, liquids, solutes, solids, and biological materials determined by the use of a tunable dye laser.

1-5 SIMULTANEOUS MEASUREMENTS OF RADAR REFLECTIVITY AND REFRACTIVE INDEX SPECTRA IN CLEAR AIR CONVECTION: T.G. Konrad and F.L. Robison, Applied Physics Laboratory, Johns Hopkins University, Silver Spring, Md.

A quantitative comparison between the radar reflectivity and the spectral characteristics of the fluctuations in the radio refractive index measured simultaneously in clear air convection has been made. The results are in good agreement with the theory and show that the radar returns in clear air are a result of backscattering from fine scale refractivity fluctuations due to turbulent mixing. The data also give strong evidence as to the applicability of the $-5/3$ spectral decay in refractivity fluctuations generally assumed in scattering theory. This value of the spectral slope is the only value for which the measured reflectivity and extrapolated refractivity spectra agree. The results of this experiment confirm the conclusions drawn in earlier attempts to relate theory with experiment and extend the range over which the measurements are compared with theory by an order of magnitude. Fluctuations in the index of refraction and the consequent radar reflectivity are greatest at the top of the convective field while little or no radar return is received from refractivity variations in the lower reaches of the field.

COMMISSION 2

1-6 APPLICATIONS OF POLARIZATION TECHNIQUES TO REMOTE SENSING BY MICROWAVE WEATHER RADAR: G.C. McCormick and A. Hendry, Radio and Electrical Engineering Division, National Research Council, Ottawa, Ontario, Canada

Polarization techniques have been used in various parts of the electromagnetic spectrum for remote sensing. At the National Research Council of Canada, a medium power experimental radar is used for the study of the polarization properties of precipitation particles, at a wavelength of 1.8 cm. The radar includes an antenna with polarization diversity having uniformity of the polarization pattern throughout the beam, and a dual-channel receiving system. The dual channel receiving system permits the simultaneous measurement of four quantities, viz.,

$\langle r_1 \cdot r_1^* \rangle$, $\langle r_2 \cdot r_2^* \rangle$, $\langle \text{Re}(r_1 \cdot r_2^*) \rangle$, and $\langle \text{Im}(r_1 \cdot r_2^*) \rangle$ where r_1 and r_2 are the two RF receiver input signals. The first two quantities are determined by the size, shape, and physical properties of the scattering body or bodies. The last two are correlation signals, from which the orientation angle of a single scattering body may be determined; or if there is an assembly of scattering particles they yield a measure of the degree of randomness of their orientations and their mean orientation angle. The orientation and other information is of interest in the fields of radar, meteorology, and communications. Vertical profiles are presented showing the way in which the degree of orientation varies through thunderstorms. Extensive data on the mean orientation angle for rainstorms are included. The melting layer is readily identified by its polarization characteristics. Results typical of the various forms of precipitation occurring in the Ottawa area are discussed.

1-7 DOPPLER MEASUREMENTS ON A LONG RANGE 16-GHZ BISTATIC SCATTER LINK: U.H.W. Lammers, Air Force Cambridge Research Laboratories, Bedford, Mass.; and R.L. Olsen, Communications Research Centre, Ottawa, Canada

The AFCRL-CRC 500-km scatter system is operated in various position scan modes, where the common volume of the two narrowbeam antennas (free-space beamwidth 0.15°) is moved through space by synchronized motion in azimuth and elevation of either antenna beam. The linear resolution of the scatter volume is approximately 700 m in height and width in the midpath region, thus yielding good spatial definition of the scatter signals received and of the average Doppler shifts imposed on them. This is particularly the case relative to the total range through which the scatter volume is scanned in height, along the great circle path and transverse to it. In a series of tests Doppler measurements have been taken at several heights in the vicinity of the midpath point, which indicate that the system is quite capable of monitoring the average crosspath wind continuously and with radiosonde accuracy or better. Likewise, under uniform crosspath wind and standard propagation conditions the Doppler results are evidence for correct antenna pointing. The wind field has been mapped over extended portions of the midpath plane. A number of cases indicate that turbulence may have contributed to the measured shifts. This is also true for the great circle plane where only vertical wind components are expected to yield Doppler offsets. At the same time anomalies in the

COMMISSION 2

Doppler characteristics may not only be indicative of the anomalies in the wind field, but may stem from nonstandard wave propagation mechanisms. Hence these results will contribute in the evaluation of the potential of long range radar techniques in determining tropospheric parameters.

COMMISSION 2, Session 2

1700 Thursday, April 13

Senate Room

EARTH-SATELLITE PROPAGATION ABOVE 10 GHZ

A.W. Straiton, Chairman

2-1 THE ATS-5 MILLIMETER WAVE EXPERIMENT: J.L. King, Goddard Space Flight Center, National Aeronautics and Space Administration, Greenbelt, Md.

The fifth Applications Technology Satellite (ATS-5) was launched August 12, 1969 marking the start of the first NASA Goddard Space Flight Center millimeter wave experiment. The experiment was designed to determine both short- and long-term propagation characteristics for operational millimeter wavelength earth-space links as a function of defined meteorological conditions. Data were collected at sites scattered throughout North America (U.S. and Canada) utilizing 15.3-GHz spacecraft transmitters with an earth-coverage antenna pattern. The experiment also included a 31.65-GHz spacecraft receiver to make on-board attenuation measurements of the signal from a 1-kw transmitter located at Rosman, N.C. This paper will emphasize the hardware implementation and operational constraints that have confronted this experiment. The satellite was planned to be 3-axis gravity-gradient-stabilized. However, control problems during the transfer orbit injection caused the satellite to become spin-stabilized, rotating at approximately 75 rpm. This condition caused the experiment antenna pattern to sweep across the earth yielding a pulsed signal resulting in reduced measurement dynamic range. The spinning also resulted in loss of the short-term data (<2 Hz) and meaningful phase measurements. The spin-stabilized ATS-5 was placed in a geosynchronous orbit located at 104°W longitude. However, this orbit had a 2° inclination with the equator which resulted in a 2.5 dB diurnal signal variation. This variation depends on the site's latitude, and in order to maintain the desired 1-dB measurement accuracy, this variation had to be removed from the attenuation data during processing. The orbit and spin conditions were aggravated by spacecraft hardware problems. The primary 15.3-GHz transmitter suffered a 6-dB, and then an additional 3 dB, loss of power early in the program which limited the dynamic measurement range. The second 15.3-GHz backup transmitter had thermal problems which limited its operating time to about 2.5 hours per day. Near the end of the experiment in the summer of 1971, the primary transmitter failed completely which also resulted in the loss of the local oscillator for the 31-GHz receiver. Even with these problems the various sites had adequate measurement ranges to acquire a significant data base on the long-term propagation characteristics at 15.3 and 31.65 GHz. The satellite data were supplemented by radiometric and rain-gauge data to fill in voids when the satellite was not available.

2-2 STATISTICS ON ATTENUATION AT 15 GHZ and 31.2 GHZ: A.W. Straiton, University of Texas, Austin, Texas

This paper presents a survey of available information on the percent of time the attenuation of radio waves at 15 and 31.2 GHz exceeded various levels over earth-satellite paths. The data were obtained by measurements of the signals transmitted from or to the ATS-5 satellite,

COMMISSION 2

by observation of the radiation received at the earth from the sun, and by converting sky temperature data to associated attenuation levels. ATS-5 provided the first opportunity to obtain direct measurements of the levels of coherent signals transmitted through the entire atmosphere at these frequencies. Statistical data at 15 GHz were obtained at 5 locations with similar phase-lock receivers and at 4 other locations with other types of receivers. The signal level at the satellite at 31.2 GHz was monitored by Goddard Space Flight Center. Data relating to earth-satellite transmission at these frequencies have also been obtained by measuring the level of the radiation received at the earth from the sun. Indirect attenuation information has been obtained by sky temperature observations associated with and independent of the satellite tests. These data provide reliable values of the attenuation for loss levels up to approximately 12 dB. The statistical data at the various locations are related to the associated total rainfall during the observation period. Comparison of the attenuation levels is made, and various models for extrapolating the observations from one location to another are considered.

2-3 RELATIONSHIP BETWEEN THE ATMOSPHERIC ATTENUATION OF SATELLITE PATH SIGNALS AND GROUND RAIN RATE: E.A. Robertson, COMSAT Laboratories, Clarksburg, Md.; and D.E. Sukhia, Martin Marietta, Orlando, Florida

Measurements of atmospheric attenuation at 15.3 GHz using the ATS-5 satellite transmissions and/or radiometric techniques have been in progress since the launch of ATS-5 in August 1969. In conjunction with these measurements several experimenters have also made simultaneous measurements of ground rain rate using a variety of rain-gauge types. The objective has been to determine the nature of the relationships between elevated path attenuation and ground rain rate if any, and to determine if elevated path attenuation can be predicted from ground rain-rate measurements. The paper reviews the attenuation-rain-gauge measurements obtained by several participants in the ATS-5 program. Conclusions obtained from comparing the several measurements are presented.

2-4 THE RELATIONSHIP BETWEEN SATELLITE SIGNAL ATTENUATIONS AND SKY TEMPERATURE MEASUREMENTS IN THE RAIN ENVIRONMENT: D.A. Gray, Bell Telephone Laboratories, Crawford Hill Laboratory, Holmdel, N.J.

The ATS-5 satellite and sun-trackers have afforded an evaluation of the ability to obtain earth-to-space path attenuation statistics through radiometric measurements of the sky temperature. Experiments using the satellite show that directly measured attenuations of the ATS-5 signals (15.3 and 31.65 GHz) and attenuations derived from concurrent sky temperature measurements compare favorably. In computing attenuations from sky temperature measurements on the basis that rain is a pure absorber, best agreement with directly measured attenuations is achieved when the value taken for the kinetic temperature of the rain is colder than one would expect, in some cases below freezing. This experimental result agrees with theoretical computations of the effects of scatter by rain. At 15.3 GHz, for example, an assumed kinetic temperature of 273 K gives good agreement for many storms.

COMMISSION 2

The comparison experiments have shown that radiometers are a viable, alternate means for obtaining attenuation statistics on earth-space paths when the effect of scatter is taken into account.

2-5 SIMULTANEOUS DIRECT, RADIOMETRIC, AND RADAR MEASUREMENTS OF PRECIPITATION ATTENUATION AT 15.3 GHZ: J.I. Strickland, Communications Research Centre, Ottawa, Canada

During 1970, the signal strength received at 15.3 GHz from the ATS-5 satellite was measured using a 9-m antenna. The receiving antenna, with a beamwidth of 0.15° , was also connected as a total-power radiometer providing simultaneous measurements of the sky noise temperature at 15.3 GHz. Attenuations, calculated from the measured sky noise temperature, show very good agreement with the directly measured attenuations. Also during the occurrence of rain, the 3-m antenna of an S-band radar located nearby was directed at the satellite. The output of the logarithmic radar receiver was sampled at accurately determined intervals to provide digital A-scans with a range resolution of 100 m. Three-dimensional plots of successive digital A-scans show the temporal variation in evolution of the spatial distribution of precipitation along the propagation path. For many attenuation events, there was evidence of a bright band. The mean reflectivity at each range is calculated, and path attenuations at 15.3 GHz derived. Generally good agreement between measured and calculated attenuation is obtained for most meteorological conditions. The effects on the calculated attenuation of radar returns from the bright band and snow aloft will be discussed.

2-6 THE USE OF SPACE DIVERSITY IN THE RECEPTION OF MILLIMETER WAVELENGTH SATELLITE SIGNALS: D.B. Hodge, Department of Electrical Engineering, Ohio State University, Columbus, Ohio

The various meteorological parameters that influence millimeter wavelength satellite-to-ground space diversity links will be summarized. Space diversity propagation statistics obtained using the 15.3-GHz down-link on ATS-5 will be presented. These results include comparison of data obtained using site separations of 4 and 8 km. Propagation data were recorded at Columbus, Ohio, during 1970 using a site separation of 4 km and during 1971 using a site separation of 8 km. The radiometric temperature as well as attenuation of the satellite signal was recorded in both cases for correlation purposes. Both statistics of individual storm events and cumulative statistics have been analyzed yielding single site and joint fade distributions, correlation between attenuation experienced at the two receiving terminals, and correlation between path radiometric temperatures observed at the two receiving terminals. These data indicate that the use of space diversity is indeed effective in improving the reliability of millimeter wavelength satellite-to-ground communication links.

2-7 THE ESTIMATION OF ATTENUATION STATISTICS FOR EARTH-SPACE MILLIMETER WAVELENGTH PROPAGATION: L.R. Zintsmaister, Department of Electrical Engineering, Ohio State University, Columbus, Ohio

The attenuation probability distributions for a millimeter wavelength earth-space propagation path will be estimated for a single site and

COMMISSION 2

for a diversity configuration. The precipitation attenuation phenomenon will be modelled by a cylindrical storm cell having a homogeneous rain rate. The attenuation probability distributions will be calculated from this storm cell model in terms of the rain-rate probability density function, the cell diameter as a function of rain rate, and a fixed cell height. A rain-rate probability density function which can be related to National Weather Service rain-rate measurements will be used in the calculations. Data from ATS-5 measurements for single sites in Clarksburg, Maryland; Rosman, North Carolina and Columbus, Ohio will be compared to results calculated using typical storm parameters. In addition, diversity calculations will be compared with ATS-5 diversity measurements in Columbus, Ohio.

2-8 SUMMARY AND EVALUATION OF RESULTS FROM THE ATS MILLIMETER WAVE EXPERIMENT: L.J. Ippolito, Goddard Space Flight Center, National Aeronautics and Space Administration, Greenbelt, Md.

A summary of propagation measurements from eleven locations in the continental U.S. and Canada operating with the ATS-5 millimeter wave experiment's 15.3-GHz earth-space link is presented, along with results of 31.65 GHz uplink measurements performed from Rosman, N.C., over a period of two years. Included are attenuation statistics comparisons at the various locations, and the correlation of attenuation measurements with rainfall rate, sky temperature, and radar observations. Attenuation ratio measurements of simultaneous 15.3- and 31.65-GHz transmissions are utilized to provide bounded cumulative distributions at the higher frequency. An overall assessment of the ATS-5 results and their impact on earth-space communications system performance are presented. In conclusion, future millimeter wave flight experiments planned for the ATS-F satellite are described; these will hopefully extend and improve upon the measurements obtained to date.

COMMISSION 2, Session 3

0900 Friday, April 14

Massachusetts Room

SURFACE AND SUB-SURFACE PROPAGATION

J.T. deBettencourt, Chairman

3-1 910-MHZ URBAN MOBILE RADIO PROPAGATION: MULTIPATH TIME DELAY MEASUREMENTS IN NEW YORK CITY: D.C. Cox, Bell Telephone Laboratories, Crawford Hill Laboratory, Holmdel, N.J.

Amplitude and time delays associated with multipath propagation have been measured between a base station antenna on top of a 400-ft building in New York City and a vehicle moving along streets up to 2 mi away. The vehicle usually was shadowed from the transmitting antenna by intervening buildings. The measuring system, which was described at the 1971 USNC/URSI spring meeting, measures the 910-MHz complex bandpass impulse response (amplitude and phase of the multipath propagation) with a resolution of 0.1 μ sec in time delay. Individual power delay profiles illustrate that frequently more than 10 paths with significant amplitudes (less than 6 dB below the strongest path) exist. A multitude of weaker paths also is evident. Often the multipath structure is significant at excess delays as large as 10 μ sec. The strongest paths are frequently a microsecond or more delayed from the shortest path observed. Local statistics for vehicle travel distances of about 100 ft, such as average power delay profiles and distributions of signal amplitude at fixed delays, are presented. RF Doppler spectra associated with some particular delays (cross-sections of delay-Doppler scattering functions) are illustrated.

3-2 DISTRIBUTION OF THE MULTIPATH RANGE ERROR IN A FREQUENCY MODULATED PHASE RANGING SYSTEM OPERATING IN AN URBAN AREA: S.G. Gustafsson, Raytheon Company, Sudbury, Mass.

A "phase ranging system" employs narrow-band, frequency modulation of a carrier in the VHF/UHF bands. Generally, the received signal in the system will be composed of several components. This is particularly accentuated in an urban area where a large number of paths generally are of significance. The group delay, as measured after an ideal frequency demodulator, can be expressed as the quotient between two double sums. This expression provides a deterministic relationship between the measured group delay and the amplitude a_n , RF-phase ϕ_n , and group delay τ_n of the individual components. It is shown that the numerator of this expression is gaussianly distributed and the denominator Rayleigh-distributed when all a_n 's and ϕ_n 's are independent. By a proper choice of time origin, these two functions will also become statistically independent. It then follows that the measured group delay is governed by Student's t-distribution with two degrees of freedom. The parameters of this distribution are given by the spatial distribution of the group delay of the individual components. An interesting analogy with angular glint in radar is observed. It is also shown that the theoretical distribution correlates well with measurements performed in a dense urban area.

COMMISSION 2

3-3 NUSC WISCONSIN TEST FACILITY ELF TRANSMITTING ANTENNA PATTERN AND STEERING TESTS: P.R. Bannister, Naval Underwater Systems Center, New London Laboratory, New London, Conn.

During August-September 1971, NUSC/NL performed pattern and steering measurements on both the NS and EW Wisconsin Test Facility (WTF) antennas. The pattern measurements were made at 13 different locations in eastern Minnesota and southern Wisconsin (covering approximately 120° of arc), while the steering tests were taken in Mars Hill, Maine, and Swansboro, North Carolina. In order to be certain that the receiving sites were acceptable, at least six components of the received magnetic field were measured at each site and then plotted on a normalized cosine curve. The 45- and 75-Hz pattern measurements were made at a range of approximately 300 km, while the steering measurements were performed at 1.7 Mm. The principal results obtained from the pattern and steering measurements were (1) the WTF EW antenna pattern is skewed clockwise; (2) the WTF NS antenna pattern is skewed counterclockwise; and (3) the effective conductivity under the WTF EW antenna is greater than the effective conductivity under the WTF NS antenna.

3-4 NUSC ELF PROPAGATION MEASUREMENTS DURING THE PERIOD OF MARCH/ APRIL 1971: P.R. Bannister, Naval Underwater Systems Center, New London Laboratory, New London, Conn.

During the period of March-April 1971, NUSC/NL conducted a far-field ELF attenuation constant measurement test. Two sites located along the same great circle path were utilized. One site (3.9 Mm) was located in St. Johns, Virgin Islands, while the other site (1.7 Mm) was situated near Swansboro, North Carolina. Horizontal magnetic field strength measurements were performed at a band of frequencies centered at 45 and 75 Hz in order to determine the attenuation rate during both daytime and nighttime propagation conditions. The EW antenna of the Navy ELF Wisconsin Test Facility was employed as the source of the transmissions. The principal results obtained from these measurements were (1) the daytime attenuation rate is higher than the nighttime attenuation rate at both 45 and 75 Hz; and (2) the ionospheric excitation factors are quite different for daytime and nighttime propagation conditions. A comparison of these results with other data taken previously and concurrently shows excellent agreement.

3-5 DETERMINATION OF THE HF IN SITU GROUND CONDUCTIVITY AND RELATIVE DIELECTRIC CONSTANT VIA THE TWO-LOOP METHOD USING A SWEPT FREQUENCY EXCITATION: R.J. Lytle, Lawrence Livermore Laboratories, University of California, Livermore, Calif.

Coaxial, coplanar, and perpendicular orientations of transmitter and receiver loops located at the same height over ground are considered. Both conduction and displacement currents have been included in the mathematical model. The governing integrals were evaluated numerically, and no mathematical approximations have been made, not even the usual quasi-static one. A ratio measurement scheme is proposed as it helps to eliminate many of the difficulties inherent in an experimental procedure based upon absolute measurements. Two cases

COMMISSION 2

are considered, the coaxial/perpendicular and the coplanar/perpendicular. In the first case the plane of the transmitter loop is oriented vertically. The induced voltage is measured as a function of frequency for two orientations of the receiver loop plane (vertical and horizontal). Thus the ratio of the voltage magnitudes (in dB) and their phase difference (in degrees) are obtained. In the second case, the transmitter loop plane is oriented horizontally and the comparisons between the horizontal and vertical receiver loop orientations are repeated. Numerical results for the coaxial/perpendicular and coplanar/perpendicular situations with transmitter and receiver loops 0.68 above ground and separated by 5 and 10 m are presented. A frequency range of 0.1-25 MHz and relative dielectric constants of 5, 10, and 25 were used in the calculational model. Conductivities of 10^{-4} - 10^{-1} mho/m were considered. The experimental procedure and a swept frequency experimental system operable over the range 0.1-25 MHz are described. Sample experimental results are discussed.

3-6 ELECTROMAGNETIC SCATTERING BY A SMALL SPHERICAL TARGET NEAR THE GROUND: D.A. Hill, Institute for Telecommunication Sciences, Office of Telecommunications; and J.R. Wait, Environmental Research Laboratories, National Oceanic and Atmospheric Administration, Boulder, Colo.

We first obtain an apparently novel exact solution for the static problem of an ungrounded sphere in a vertical electric field. The derivation is facilitated by the use of bispherical coordinates and known solutions of closely related problems. For comparison, we obtain an approximate result that considers only dipole mode interactions with the interface. The two solutions are nearly identical when the sphere center is at least 1.5 radii above the interface, and all interface coupling can be neglected when the sphere center is more than 3 radii above the interface. By extrapolating to the quasi-static regime, we obtain the vertical electric and horizontal magnetic dipole moments induced by a low-frequency ground wave. From these dipole moments, the reradiated, far-zone, backscattered field is computed. This result reduces to twice the free-space result when the sphere height is more than a few radii.

COMMISSION 2, Session 4

1400 Friday, April 14

Senate Room

REMOTE SENSING OF SURFACES I

J.W. Rouse, Jr., Chairman

4-1 CONCEPTS AND VERIFICATION OF A DIRECTIONAL REFLECTANCE MODEL FOR VEGETATIVE CANOPIES: G.H. Suits, Willow Run Laboratories, University of Michigan, Ann Arbor, Mich.; Gene Safir and A. Ellingboe, Michigan State University, East Lansing, Mich.

The concepts used in a directional reflectance model of a vegetative canopy are presented. The causes of the non-Lambertian reflectances are dependent upon the nature of the vertical structure of the canopy and the sun angle. The model is tested by predicting and measuring the directional spectral reflectance of two cornfields.

4-2 THE MICROWAVE RESPONSE OF VEGETATION: W.H. Peake, Department of Electrical Engineering, Ohio State University, Columbus, Ohio

To interpret the radar imagery of vegetated surfaces, one must know that properties of the vegetation influence the radar return. Here, two single scattering models are considered for predicting the absolute levels of scattering and the microwave emissivity of vegetation. The first, an older model, is based on a random distribution of cylinders appropriate for such linear crops as oats, wheat, and sudan grass. A more recent model is based on high- and low-frequency approximations to scattering from a thin disc (Lommel-Seeliger model) and is appropriate for volume distribution crops such as cotton and soybeans. The model results are compared with data from a variety of sources and show good agreement for angular and frequency dependence and absolute scattering cross-section. Although the absolute levels might be considered forced because of the number of parameters in the model, it is shown that certain parameter combinations are directly related to agriculturally significant properties of the vegetation (e.g., the total moisture per unit volume). Thus the models offer a rational approach to explaining certain anomalies in the radar imagery and to extracting useful information from it.

4-3 MICROWAVE SPECTRAL MEASUREMENTS OF AGRICULTURAL TARGETS: F.T. Ulaby, R.K. Moore, R. Moe, and J. Holtzman, Center for Research, Inc., University of Kansas, Lawrence, Kansas

Octave-bandwidth (4-8 GHz) radar spectrometer measurements were obtained in an attempt to associate signature definitions with agricultural crops. The spectral response data were concentrated on agricultural targets covering 87 fields with 4 crop types -- corn, sorghum, soybeans, and alfalfa -- and plowed ground. The experiment consisted of measuring the spectral responses of the agricultural crops across the 4-8 GHz frequency band at look angles of 0°, 10°, 20°, 30°, 50°, and 70° for both horizontal and vertical polarizations. The system used was an FM-CW radar positioned atop a 42-ft truck-mounted boom. Target signature techniques were applied to the data by color-combining the spectral return. For each crop type, polarization, and look angle, the 4-8 GHz data were divided into three sub-bands. The averaged return over each of the sub-bands was used to set the intensity level of the corresponding

COMMISSION 2

light beam of a three-beam color combiner (4-5.2 GHz = red, 5.2-6.8 = green, and 6.8-8 = blue). The color signatures of the four crop types were then grouped by look angle and polarization. The results very clearly indicate the usefulness of octave-bandwidth measurements of radar return in delineating and classifying agricultural targets.

4-4 MICROWAVE BRIGHTNESS TEMPERATURE OF A WINDBLOWN SEA: F.G. Hall, Manned Spacecraft Center, National Aeronautics and Space Administration, Houston, Texas

A computer simulation of a windblown sea has been developed at NASA/MSC. Some results of this model and a comparison to results from Stogryn's model at 19.35 GHz are presented. This computer simulation calculates the expected microwave brightness temperature T_B at an arbitrary microwave frequency, as a function of wind speed for a windblown sea. This simulation models the combined effects of clear water and white water (sea spray, foam, or white caps) on T_B . The computer program allows atmospheric effects to be calculated either from radiosonde data or from sky temperatures obtained by in situ measurement. The results of this model are compared at 19.35 GHz to Stogryn's results using Stogryn's model atmosphere. For the most part, when no foam coverage exists, the results from the two models are identical. However, in contrast with Stogryn's model, which predicts no increase in T_B at nadir, the computer model indicates, for nadir look angles, an increase of 0.20° K/m/sec in T_B with increasing wind speed. As a consequence of this nadir increase in T_B and the increase in T_B above 8 m/sec due to foam coverage, the 52° crossover of the vertically polarized T_B does not occur. Significant deviations from Stogryn's model can be seen above 8 m/sec where foam coverage of the sea surface becomes an important contributor to the brightness temperature. These effects at different frequencies and nadir angles are presented.

4-5 THE EFFECT OF SEA STATE ON A RADAR ALTIMETER PULSE: D.E. Barrick, Battelle Columbus Laboratories, Columbus, Ohio

A closed-form expression is derived for the average power as a function of time received by a satellite or aircraft microwave altimeter looking vertically at the sea. The specular point theory for sea scatter is employed, and gaussian shapes for the altimeter pulse and antenna beam are assumed for convenience. The resulting simple model shows the dependence of the time return on the various parameters of the altimeter and sea, i.e., H = altimeter altitude, τ = half-power (compressed) altimeter pulselength, ψ_B = half-power (one-way) antenna beamwidth, with σ_h and s being the rms sea surface height and total slope, respectively. The (compressed)altimeter power pulse and antenna pattern, $g(\psi)$, are both normalized to unity at the center. The expression for the radar cross section times the antenna pattern factors is then

$$g^2 \sigma(t) = (\pi^{3/2} H x_w / s^2) \exp\left[\left(t_p/t_s\right)^2 - 2t/t_s\right] [1 - \Phi(t_p/t_s - t/t_p)] ,$$

where $x_w = ct/(4\sqrt{2\pi})$, $t_p = 2\sqrt{x_w^2 + \sigma_h^2}/c$, $t_s = H\psi_e^2/c$, $1/\psi_e^2 = (8\ln 2)/\psi_B^2 + 1/s^2$, c being the velocity of light and Φ being the error function. The time $t = 0$ occurs when the pulse center strikes the mean spherical sea. The quantity t_p is interpreted as the equivalent pulse width

COMMISSION 2

after stretching by the sea waves, and t_s is the two-way time of flight to the bottom of the effective specular scattering region illuminated by the altimeter antenna. This expression simplifies for beam-limited illumination, where $t_s \ll t_p$. For fully developed wind-driven seas, the following relations can be used to relate σ_h and s to u , the wind speed (m/s): $\sigma_h = .016 u^2$ meters and $s = .074\sqrt{u}$. Using the above equation, the altimeter can be designed either to measure sea state (and hence wind speed), or to determine the mean surface position after removing sea-state effects.

4-6 REMOTE SEA SENSING: R.K. Thomas, General Electric Company, Valley Forge, Pa.; and H.N. Kritikos, University of Pennsylvania, Philadelphia, Pa.

The apparent temperature of the slightly rough surface has been investigated at radio frequencies by using the formalism first introduced by Rice and later refined by Barrick. While in general the albedo is mainly determined by the specular contribution, there is one exception. For this case, the sea is viewed at the Brewster angle at vertical polarization; here the scattered energy contribution is of the same order of magnitude as the specular one. It was found that the scattered contribution shows a resonant effect with varying correlation lengths of the sea surface. This opens the interesting possibility of detecting the sea wave number distribution by passive means. The spatial coherence of the scattered field due to an incident plane wave has also been examined. Since the spatial coherence function is related to the statistical parameters of the sea surface, this method also offers the possibility of determining the sea wave number distribution.

4-7 ON MICROWAVE REMOTE SENSING OF ARCTIC ICE: J.W. Rouse, Jr., Texas A&M University, College Station, Texas

Radar backscatter measurements at 2.25-cm wavelength, vertical polarization, were obtained by the NASA Manned Spacecraft Center over arctic ice in 1967 and 1970. Both data sets show the distinctly different scattering behavior of sea ice of different ages. These distinctions have also been observed by NASA Goddard Space Flight Center using multiple frequency microwave radiometers. The radar data were compared to an analytical model based on the Kirchhoff method following Fung and Leader. A fit of the model to the experimental measurements provided predicted values of relative dielectric constants of both young ice and open water which agreed with waveguide measurements reported by Hoestra. However, the same procedure led to predicted dielectric constants of older ice which were considerably larger than expected, by as much as one order of magnitude. A very similar situation was found when independently evaluating microwave emission from older ice, i.e., the magnitude of the signal from multi-year ice differs from that from young ice by an amount greater than can be accounted for by a standard model using expected values of dielectric constant. The results suggest that either the accepted physical model of multi-year ice is inaccurate or the scattering mechanism yields reflection and emission components, perhaps due to volume scatter, that are not adequately handled in the models.

COMMISSION 2

4-8 BISTATIC SENSING OF PLANETARY SURFACES WITH A UHF LANDER-TO-ORBITER LINK: P.F. Sforza, Raytheon Co., Sudbury, Mass.

The feasibility of using the measurements of relative received power at the orbiter of a UHF lander-to-orbiter communications link to determine the complex dielectric properties of slightly rough planetary surfaces has been analyzed. A new graphical iterative method to compute the dielectric constant and conductivity of the surface has been developed. It is shown that the ratio of power received by an antenna with the same polarization sense as the transmitter to the power received by the antenna with opposite polarization sense can be used to determine the dielectric constant of the surface. For elliptically polarized antennas with ellipticities of 1.5 and a surface of $\epsilon/\epsilon_0 = 3$ and $\sigma = 10^{-5}$ mhos/m it is found that an experimental error of ± 0.3 dB in the relative power ratio results in a value of ϵ/ϵ_0 between 2.1 and 4.8. As the ellipticities of the antennas approach unity the measured value of ϵ/ϵ_0 can be more accurately determined with a value between 2.9 and 3.15 with ellipticities of 1. For ellipticities greater than 1 the uncertainty in ϵ/ϵ_0 can be reduced by measuring the relative power ratio on the antenna with polarization sense opposite to that of the transmitter for different positions of the orbiter. It is also shown that surface conductivities can be measured with sufficient accuracy when they are larger than 10^{-3} mhos/m.

COMMISSION 2, Session 5

0830 Saturday, April 15

Senate Room

REMOTE SENSING OF ATMOSPHERES II

D.A. deWolf, Chairman

5-1 MEASUREMENT OF ATMOSPHERIC WINDS BY OBSERVATION OF STELLAR SCINTILLATIONS: G.R. Ochs and S.F. Clifford, Environmental Research Laboratories, National Oceanic and Atmospheric Administration, Boulder, Colo.

The light from a star is distorted by refractive-index irregularities when it passes through the atmosphere. When these irregularities are carried along by winds, the distorted starlight forms a moving pattern of light and dark areas on the ground. This pattern contains information about the speed and direction of the wind, as well as the distribution of refractive-index fluctuations along the light path. We derive upper atmospheric winds by observing the fluctuating light from Polaris in two sets of receiving apertures. These four apertures are mounted on a rotating mount, with the axis of rotation pointed toward Polaris. The slope of the normalized covariance at zero delay of one set of apertures controls the rotation of the mount, which turns until this slope, an indication of pattern motion, is zero. At this point the aperture separation is at right angles to the motion of the light pattern, and the wind direction may be derived from the mount position. The other set of apertures, at right angles to the first, is now aligned with the motion of the light pattern. The delay to the peak of the time-lagged covariance of light fluctuations in these apertures is inversely proportional to pattern speed, and atmospheric wind velocity may be derived from this measurement. These calculations are actually performed in an on-line analog computer. We have measured, on clear nights, wind velocity and direction in the altitude region above 6000m over a period of two months. The measurement compares favorably with Weather Service radiosonde data.

5-2 PATH DIVERSITY FOR MILLIMETER-WAVELENGTH EARTH-TO-SATELLITE LINKS: K.N. Wulfsberg, Air Force Cambridge Research Laboratories, Bedford, Mass.

The rapidly increasing demand for wide-band communications with global coverage has led to recent frequency allocations in the millimeter wave spectrum for earth-satellite links. From measurements conducted over the past decade it is evident that the major obstacle in utilizing these frequencies is the high attenuation that may result under conditions of rain, and that earth terminals in non-arid regions would experience unacceptably high outage times due to rain attenuation. Since heavy rain is generally quite localized it has been proposed that the required reliability could be achieved by path diversity, which involves two or more earth receiving terminals sufficiently spaced so that the simultaneous outage time of all terminals is acceptably low. At present the only generally available source for diversity experiments is the sun. This paper describes a year-long diversity experiment in the Boston area involving two sun trackers spaced 7 mi and operating at 35 GHz. The results show an 18-fold improvement in outage time at the 27-dB attenuation level, the maximum measureable by the system, and that for an outage time of one hour per year the power

COMMISSION 2

transmitted by the satellite would have to be increased 18 dB above that needed to overcome free-space loss, as compared to an increase of over 33 dB for a single-site system.

5-3 DIVERSITY ANTENNA SPACING FOR LINE-OF-SIGHT MICROWAVE LINK: C.K. H. Tsao and J.F. Roche, Raytheon Company, Norwood, Mass.

The successful application of space diversity to achieve high propagation reliability over line-of-sight microwave links requires proper separation between diversity antennas. Criteria for antenna spacing exists whereby the signal received at the antennas are sufficiently decorrelated. These criteria lead to contradictory results in the antenna spacing. The different propagation mechanisms which cause signal fading are examined and related to the established formula for spacing. An empirical approach is considered which makes due allowance for different fading phenomena.

5-4 A SECOND-ORDER EQUATION FOR INTENSITY FLUCTUATIONS: J.W. Strohbehn and Ting-I. Wang, Dartmouth College, Hanover, N.H.

In studying the propagation of optical waves in the clear atmosphere it has been shown that the perturbation solution is incorrect for predicting the variance of the logarithm of the amplitude fluctuations even over relatively short paths near the earth's surface. Numerous approaches have been tried, many of which lead to very complex partial differential equations for the fourth-order coherence function. In this paper it is shown that if it is assumed that the amplitude fluctuations are log-normal a much simpler equation may be derived.

5-5 THE EFFECT OF SCATTER ON RADIOMETRIC OBSERVATIONS OF RAINFALL: D.A. Gray, Bell Telephone Laboratories, Crawford Hill Laboratory, Holmdel, N.J.

Radiometers offer indirect means for obtaining statistics of rain-induced attenuation on earth-to-space transmission paths. If the rain medium were a pure absorber (does not scatter energy), and its kinetic temperature known, then the sky temperature measured by a radiometer can conveniently be used to compute the attenuation of the earth-space path. Unfortunately, rain scatters energy in addition to absorbing it, and the effect of scatter should be taken into account in the interpretation of radiometric data. In this paper we discuss scatter by rain, providing theoretical calculations of its effect on the measurement of several idealized rainstorms. From these idealized cases we draw guidelines to the interpretation of experimental data. Basically, one can continue to consider rain a pure absorber, but one must assume a temperature for the rain which is less than the kinetic temperature. We call this assumed temperature the apparent absorber temperature. As an example, at 16 GHz the apparent absorber temperature turns out to be approximately 15 K lower than the kinetic temperature to account for the effect of scattering.

COMMISSION 2

5-6 POLARIZATION EFFECTS IN MILLIMETER WAVE PROPAGATION THROUGH RAIN: A REVIEW OF PRESENT THEORY AND A DISCUSSION OF CURRENT EXPERIMENTS: P.H. Wiley, C.W. Bostian, W. L. Stutzman, and R.E. Marshall, Virginia Polytechnic Institute and State University, Blacksburg, Va.

Rainfall attenuation and scattering are important factors in millimeter wave communications system design. A thorough understanding of how these effects depend on wave polarization would benefit future millimeter wave communication systems in the following ways: (1) the polarization giving the minimum average attenuation could be used; (2) increased reliability through polarization diversity might be possible, and (3) more efficient frequency sharing would result if cross-polarization scattering could be predicted. Existing theories are reviewed. Their prediction of cross-polarization effects is based primarily on differential attenuation; possible depolarization by single or multiple scattering should be investigated theoretically and experimentally. Previous measurements of differential attenuation and depolarization are summarized. An 18-GHz experiment is described which the authors are conducting to measure (1) simultaneous attenuation on vertically and horizontally polarized signals and (2) cross-polarization scattering as a function of rainfall rate.

5-7 EMPIRICAL RAINFALL ATTENUATION AT MILLIMETER WAVELENGTHS: J.T. deBettencourt, Raytheon Company, Equipment Division, Waltham, Mass.

The variation of excess rainfall attenuation α vs. path average rainfall rate R may be expressed as $\alpha = K R^P$, dB/km (with R in mm/h). Analyzing 21 "world-wide" sources of experimental (α, R) data at frequencies from 8 to 100 GHz, empirical polynomial expressions were derived for the frequency dependencies of the coefficients K and P , independent of R . Additional data when available will be analyzed and resulting changes presented later.

5-8 THE MEASUREMENT OF THE SCATTERING MATRIX OF VARIOUS BODIES: L.E. Allan and G.C. McCormick, National Research Council of Canada, Ottawa, Ontario, Canada

There is no lack of literature regarding the backscattering matrix and its measurement. But specific results even for elementary bodies are notably lacking. If the body is such that the matrix can be diagonalized so that $S_{xy} = 0$, then in terms of right-hand and left-hand circular polarization components the significant quantities are ν and δ where $\nu e^{i\delta} = \frac{S_{xx} - S_{yy}}{S_{xx} + S_{yy}}$. Average values of ν and δ for some targets,

e.g., raindrops, should be directly observable with radars having polarization capability. For small lossless bodies to which Rayleigh theory or Stevenson theory is applicable $\delta = 0$. It has been our purpose to obtain measurements of ν and δ for bodies in an approaching the resonance region, specifically oblate spheroids, prolate spheroids, and circular cylinders. The target body is illuminated by S-Band CW radiation from a dual-mode horn fed by a turnstile junction. RHC polarization is radiated and reception of RHC and LHC polarizations is available in the two receiver channels. The receivers are simul-

COMMISSION 2

taneously nulled when looking into empty space. Small spheres used as reference targets generate an RHC-to-LHC receiver-amplitude ratio of 0.023 (-32.7 dB) instead of the ideal value of zero. A correction is made for this noncircularity of the incident radiation. Measured values of ν and δ will be presented for 3 metal prolate spheroids, 3 dielectric oblate spheroids, and several metal and dielectric cylinders.

COMMISSION 2, Session 6

1330 Saturday, April 15

Senate Room

REMOTE SENSING OF SURFACES II

S.H. Durrani, Chairman

6-1 BOEING/FAA AIRCRAFT-TO-ATS-5 OVEROCEAN MULTIPATH MEASUREMENTS AT L-BAND: A.D. Thompson, Boeing Company, Seattle, Wash.

Results from the Boeing/FAA ATS-5-to-aircraft overocean L-band multipath propagation tests are presented. Experimental configurations were designed to measure the amplitude characteristics, circular polarization-sense reversal properties, and Doppler spectrum associated with the L-band multipath channel. Separate direct and multipath antenna systems and a composite (direct plus multipath) antenna system, all with known gain distributions, were employed thereby enabling the relative energy level in the scattered signal and the fading characteristics of the composite signal to be determined. All measurements of the scattered signals' amplitude and sense reversal characteristics were performed with the multipath antenna operating in its vertical, horizontal, right-hand circular, and left-hand circular polarization modes. Estimates of the mean Doppler spectrum were obtained through use of a spectral averaging technique which operates on a burst-by-burst basis. Approximately 30 hours of flight test data, covering a range of elevation angles from 10° to 30° and typical North Atlantic winter sea-surface conditions, have been reduced for presentation. Near-simultaneous sea-surface measurements were also conducted for each flight test and are used to correlate the measured multipath characteristics with those predicted by theory.

6-2 POLARIZATION CHARACTERISTICS OF INCOHERENT GROUND MULTIPATH: D.W. Swayze, Philco-Ford Corporation, WDL Division, Palo Alto, Calif.

Some experimental data are available on ground multipath in the case of satellite-aircraft links, but none are presently available in the case of satellite-satellite links. Thus, what happens when a signal is transmitted from one satellite, scattered from an extended region of the earth's surface, and received on another satellite has to be predicted theoretically for the design of satellite-satellite links. This paper describes the predicted characteristics of diffuse multipath arising in satellite-satellite links for various polarization states. Among the techniques that can be used to minimize the multipath interference are: the use of only the parallel polarized component for which the reflection coefficient is generally smaller than for the perpendicular polarized component, the use of circularly polarized antennas in which discrimination against multipath is afforded by the change in sense of polarization upon reflection, and the use of polarization diversity in which the polarization component with the optimum signal/multipath ratio is selected. Results of a computer simulation study are presented which show the polarization dependence of the average scattered power, the delay power spectrum, and the Doppler power spectrum in a form that permits comparison of these techniques.

COMMISSION 2

6-3 NEAR-NORMAL-INCIDENCE SCATTERING FROM A DIRECTIONAL, PHILLIPS-TYPE OCEAN SURFACE AND GROUND TRUTH LIMITATIONS: G.S. Brown, G.S. Hayne, and L.S. Miller, Research Triangle Institute, Research Triangle Park, N.C.

The utility of radar altimetry as a remote sensor of ocean surface characteristics is based primarily on the results obtained from theoretical models of rough surface scattering. In order to verify these results and, subsequently, the theory, it will be necessary to compare actual radar-altimeter-derived data with the theoretical model. This comparison is not quite so straightforward, however, since the theoretical model requires certain experimentally derived data on the ocean surface (i.e., ground truth data). It is the purpose of this paper to consider the implications of erroneous or incomplete ground truth data when used in the theoretical model for near-normal-incidence backscattering. Theoretical models of microwave scattering from the ocean's surface presume a rather detailed knowledge of the wave height spectrum. Instrumentation and time limitations usually force one to consider this spectrum as independent of direction, i.e., isotropic, and thus the two-dimensional character of the spectrum is disregarded. Furthermore, available instrumentation becomes increasingly inaccurate at the high wavenumber end of the spectrum; so, for all intents and purposes, the one-dimensional wave height spectrum is truly known only over a limited wavenumber range. In view of these measurement constraints, this paper will consider the effects of spectral inaccuracy and anisotropy on the theoretical scattering backscattering cross-section of the ocean's surface for near-normal incidence. A slight modified form of the Pierson-Moskowitz spectrum will be assumed to be an accurate representation of the isotropic wave height spectrum. Formulas will be derived for the backscattering cross section of the ocean's surface when the spectrum is truncated at either the low or high wavenumber region to simulate spectral resolution inaccuracies. It will be shown that spectrum measurements need not go beyond 1 cm^{-1} in wavenumber but should be as accurate as possible in the extremely low wavenumber range ($\sim 0.0001 \text{ cm}^{-1}$). It will also be demonstrated that the infinite range wave height spectrum results in a surface height correlation function which is neither linear nor quadratic at the origin. Finally, based on either the Cote or Longuet-Higgins directional spectrum models, it will be demonstrated that the isotropic assumption should be accurate enough for backscattering computations.

6-4 WAVE SCATTERING FROM STATISTICALLY KNOWN ROUGH SURFACES: R. Axline and A.K. Fung, Center for Research, Inc. University of Kansas, Lawrence, Kansas

The backscattering cross sections of two statistically known one-dimensional rough surfaces have been computed by moments method at four different wavelengths and incident angles ranging from 0° to 40° . This was done by first evaluating an integral equation to yield the surface currents on forty samples of the rough surfaces. The backscattered fields from individual samples were then found, squared, and averaged to obtain the scattering cross section. The correlation coefficient of surface heights of surface number 1 is the same as that of surface number 2. The correlation length is 6 mm. The standard deviation of surface number 1 is 0.85 mm and that of surface number 2 is about 3

COMMISSION 2

times larger. The backscattered fields were also computed using surface currents estimated by the tangent plane method (tpm). Comparisons were made between both the scattered fields and the scattering cross sections computed by the two different methods. It has been found that for the smoother surface (surface number 1) the tpm is satisfactory for wavelengths varying from 5 to 35 mm for incident angles smaller than about 25°. For larger incident angles, the tpm gets worse as the wavelength increases from 5 to 20 mm. However, it gets better when the wavelength is further increased. This seems to indicate that beyond 20-mm wavelength, the problem has been reduced to a perturbation problem. It is known that to the first order of approximation the results of the tpm are very close to that of the small perturbation method over the range of incident angles considered. For surface number 2 the results of the tpm shows increasing deviation from those of the moments method as either the wavelength or the incident angle increases. This indicates a breakdown of the tpm due to large curvature.

6-5 WAVE PROPAGATION IN THE PRESENCE OF A SINUSOIDAL INTERFACE: D.J. Fang, Radio Physics Laboratory, Stanford Research Institute, Menlo Park, Calif.

Wave propagation in the presence of a sinusoidal interface is analyzed based upon the Rayleigh assumption. The media separated by the interface are assumed to be either dielectric or conductive. Both vertical and horizontal polarizations for the incident waves are taken into consideration. Fourier-Bessel series is used to expand the wave factors at the interface. Boundary conditions are then matched by the perturbation technique. The final solution contains two algebraic recurrence formulas. It suggests a new computer solution, more accurate and much simpler than those "brute-force" numerical methods currently used. It provides better insight into the behavior of reflected waves as well as transmitted waves due to scattering from the interface. Important aspects of the present approach will be discussed, including convergence, energy conservation, and validity of the Rayleigh assumption.

COMMISSION 2, Session 7

1330 Saturday, April 15

Federal Room

REMOTE SENSING OF ATMOSPHERES III

A.H. LaGrone, Chairman

7-1 REMOTE SENSING AND KALMAN FILTERING: V.J. Falcone, Jr., Air Force Cambridge Research Laboratories, Bedford, Mass.

The problem of estimation of temperature profiles from passive microwave measurements has been shown by the use of Bayes theorem and the assumption of gaussian distributions to result in a recursive relation. Expanding on this work it is shown that the a priori data used in Bayes theorem is interpreted mathematically as measured data so that no distinction is made between the preconceived (a priori) idea of a temperature at a specific height and the radiometric measurement. The recursive relation may be identified as a Kalman formulation of the problem for the case of gaussian distributions. In this case it is shown that the stabilization matrix (a Penrose pseudoinverse) is identical to the Kalman gain matrix with the consequence that it is optimal in a least-squares sense.

7-2 PROPAGATION OF RADIO WAVES THROUGH THE LOWER ATMOSPHERE OF VENUS: K.R. Richter, Goddard Space Flight Center, National Aeronautics and Space Administration, Greenbelt, Md.

Venus atmosphere modes are based on results of the experiments conducted by the USSR entry probes, Venera, and by the U.S Mariner 5 spacecraft. Based on these results this paper deals with the determination of radio frequencies providing maximum signal-to-noise ratios (SNR) for different modes of operation at a constant antenna area. Considering the constraints in aerospace systems on the antenna dimensions it follows that the SNR may be increased by using higher operational frequencies. However, the attenuation in the atmosphere increases with the square of the frequency. The variability of these two parameters determine the maximum SNR. In this paper it is shown that the optimum frequency differs for communication (a) from a probe located on the surface of the planet to an orbiting spacecraft, (b) from a probe to an earth-based station, and (c) for a radar system operating from an orbiting spacecraft. Furthermore, the frequency to be selected depends also on the communication angle or on the slant angle of the radar antenna. The theoretical results show that microwave frequencies in the range between 2 to 5 GHz encompass the optimum for the three cases stated above and should be used for experiments performed by future probe and orbiter missions.

7-3 CHARACTERISTICS OF RADAR ECHOES FROM BIRDS IN FLIGHT: J.L. Green, Aeronomy Laboratory, National Oceanic and Atmospheric Administration, Boulder, Colo.; and W.L. Flock, Department of Electrical Engineering, University of Colorado, Boulder, Colo.

Birds are a phenomenon of the troposphere and are responsible for a large percentage of the radar echoes which in previous years were referred to as radar angels. Thus radar can be used as a tool for studying bird migration and play a role in minimizing the hazard of collisions between birds and aircraft. Also radar echoes from birds

COMMISSION 2

show characteristic amplitude and frequency modulation associated with the wing beat of the birds. Two types of X-band radar were used to study the characteristics of birds in flight. A surveillance radar was used for monitoring the local movements of birds around a fresh water lake near Boulder, Colorado. The PPI display was photographed, and these records were useful in documenting the times and directions of departure and arrival of bird populations. A low-power CW radar was used for studying the motions of flight of individual birds. Whereas previous radar signatures of birds have emphasized amplitude variation, the Doppler output of this radar was recorded. These records, which are presented as velocity-versus-time plots, show not only the mean velocity of the bird in flight, but the distinct motion of both wings. These studies give evidence that at least the type of bird, if not the species, can be recognized from these "Doppler signatures."

7-4 RADIO ASPECTS OF A TORNADO: J.B. Smyth, Smyth Research Associates San Diego, Calif.

It is well accepted that thunderstorms generate lightning which emits radio waves. There remains considerable controversy over the electrical properties of the tornado. While observing radio transmissions from the ATS-3 satellite on 137 MHz at Ocilla, Georgia, an unusual interference was recorded between 1400 and 1800 EST on 29 April 1971. Around 1600 at least one tornado touched the earth 80 mi southwest of the receiving station. A radio model of the tornado is proposed that is consistent with a number of observations on different tornadoes.

7-5 PROBING ATMOSPHERIC WATER VAPOR PROFILES VIA MULTIPLE SCATTERING OF ELECTROMAGNETIC WAVES: C.C.H. Tang, Bellcomm, Washington, D.C.

A theoretical analysis on the multiple scattering of electromagnetic waves propagating in a finite inhomogenous medium is presented and applied to synthesizing the water vapor density profile in a clear atmosphere (fine weather conditions). When an electromagnetic plane wave of centimeters or longer wavelength propagates vertically through a clear atmosphere and produces a reflection, the reflection is always associated with some identifiable and abnormally steep gradients of dielectric constant due to inhomogeneities in the water vapor density in the atmosphere. Anomalies in dielectric constant gradients of the atmosphere, however, are not always accompanied by reflections. These observed features cannot be explained satisfactorily by present available theories that do not take into consideration the effects of small internal reflections or multiple scattering of electromagnetic waves. However, these observed features can be readily explained by the results of this analysis with multiple scattering considerations. It is shown that (1) for a prescribed profile of water vapor density the resultant reflection due to multiple scattering from the density profile is sensitive to the frequency used in probing, (2) by measuring the resultant reflections at several different frequencies the water vapor density profile can be synthesized. The solutions of the multiple scattering approach are shown to be more accurate than those of the WKB method, which neglects the multiple scattering effects.

COMMISSION 3
ON THE IONOSPHERE
E.R. Schmerling, Chairman

<u>Sessions</u>	<u>Page</u>
1. INCOHERENT SCATTER I 1400 Thursday, April 13 Congressional Room Chairman: J.S. Nisbet Electrical Engineering Department Pennsylvania State University University Park, Pa. 16802	43
2. PROPAGATION PROBLEMS 1400 Thursday, April 14 Federal Room Chairman: T.P. Quinn Field Projects Programs (418) Office of Naval Research Washington, D.C. 20360	46
3. INCOHERENT SCATTER II 0900 Friday, April 14 Federal Room Chairman: J.S. Nisbet Electrical Engineering Department Pennsylvania State University University Park, Pa. 16802	51
4. DISTURBANCES 0900 Friday, April 14 New York Room Chairman: E.A. Mechtly 1003 Mumford Drive Urbana, Ill. 61801	54
5. IONOSPHERIC PROCESSES 1400 Friday, April 14 Federal Room Chairman: T.A. Seliga Electrical Engineering Department Ohio State University Columbus, Ohio 43210	58
6. IRREGULARITIES AND MOTIONS 1400 Friday, April 14 New York Room Chairman: J.M. Kelso ITT Electro-Physics Laboratories, Inc. 9140 Old Annapolis Road Columbia, Md. 21043	61
BUSINESS MEETING 1700 Friday, April 14 Federal Room	

COMMISSION 3

<u>Sessions</u>	<u>Page</u>
7. IONOSPHERIC PERTURBATION I 0830 Saturday, April 15 Congressional Room Chairman: R.S. Cohen National Oceanic and Atmospheric Administration, R44 Boulder, Colo. 80302	66
8. CONJUGATE EFFECTS IN THE IONOSPHERE AND MAGNETOSPHERE I (Joint with Commission 4) 0830 Saturday, April 15 South American Room Chairman: W.H. Campbell National Oceanic and Atmospheric Administration Boulder, Colo. 80302	69
9. IONOSPHERIC PERTURBATION II 1330 Saturday, April 15 Congressional Room Chairman: R.S. Cohen National Oceanic and Atmospheric Administration, R44 Boulder, Colo. 80302	72
10. CONJUGATE EFFECTS IN THE IONOSPHERE AND MAGNETOSPHERE II (Joint with Commission 4) 1330 Saturday, April 15 South American Room Chairman: W.H. Campbell National Oceanic and Atmospheric Administration Boulder, Colo. 80302	75
PANEL DISCUSSION: FUTURE OF CONJUGATE RESEARCH Chairman: E.R. Schmerling National Aeronautics and Space Administration, Code SG Washington, D.C. 20546	

COMMISSION 3, Session 1

1400 Thursday, April 13

Congressional Room

INCOHERENT SCATTER I

J. Nisbet, Chairman

1-1 CHATANIKA, ALASKA, AURORAL-ZONE INCOHERENT-SCATTER FACILITY:
R.L. Leadabrand, M.J. Baron, and J. Petriceks, Stanford Research Institute, Menlo Park, Calif.; and H.F. Bates, Geophysical Institute, College, Alaska.

The Stanford Research Institute L-bank incoherent-scatter radar has been moved to Chatanika, Alaska ($L = 5.7$), an auroral-zone location near Fairbanks, Alaska. The siting of the radar is such that D-, E-, and F-region incoherent-scatter measurements can be made without ground-clutter interference. Coherent auroral clutter echoes that are seen do not interfere with the incoherent-scatter measurements. The capabilities of the system and samples of the type of incoherent-scatter results being obtained are outlined as an introduction to the more specific studies that are presented in detail in companion papers.

1-2 A SUMMARY OF EARLY INCOHERENT-SCATTER OBSERVATIONS AT CHATANIKA, ALASKA: T.M. Watt and J. Petriceks, Stanford Research Institute, Menlo Park, Calif.; and H.F. Bates, Geophysical Institute, College, Alaska.

Initial incoherent-scatter observations of the ionosphere at Chatanika, Alaska, are reported here. Vertical profiles of electron densities, electron temperature, and ion temperature have been obtained for several 24-hour periods using 20-minute integration times. Latitudinal variations of the F region and plasma drifts in the E region have been observed by scanning the radar antenna in elevation and azimuth. The observations indicate that the auroral-region ionosphere is vastly different from the normal midlatitude ionosphere. In particular, very large and very rapid variations of electron density, especially at E-region altitudes, regularly have been observed. During the period of these observations, F-region densities and temperatures often exhibited large variations, with periods from minutes to hours, not related in any obvious way to solar zenith angle. Frequently it was observed that the vertical ionization profile had been completely dominated by a single, thick layer at E-region altitudes. On some occasions, very large horizontal drifts of plasma in the E region were observed. Some solar-zenith-angle dependence of various parameters was observed.

1-3 INCOHERENT-SCATTER MEASUREMENTS OF THE IONOSPHERE DURING DISTURBANCES: IMPLICATIONS TO HF PROPAGATION: H.F. Bates, Geophysical Institute, University of Alaska, College, Alaska; and T.M. Watt, Radio Physics Laboratory, Stanford Research Institute, Menlo Park, Calif.

Incoherent-scatter measurements have been made into the ionosphere near or into the aurora. The auroral ionization forms a dense, thick, auroral E layer. Above 200 km the electron density is almost constant up to 500 km, supporting previous suggestions of an upward drift of ionization during auroral activity. The aurora makes the F layer disappear in the sense that the auroral ionization obscures the normal maximum of the F layer. Soundings made into the F layer during a summer

COMMISSION 3

magnetic storm showed that the disturbed ionosphere was almost constant in electron density from 125 to 300 km for several hours about local noon; temperatures were higher than during quiet periods. The absence of an F-layer maximum during these disturbances would have considerably modified long-range HF propagation through these latitudes, quite apart from absorption.

1-4 ELECTRON DENSITIES WITHIN AURORAE AND OTHER AURORAL E-LAYER CHARACTERISTICS AS DETERMINED FROM INCOHERENT SCATTER OBSERVATIONS:
M.J. Baron and J. Petriceks, Stanford Research Institute, Menlo Park, Calif.; and R. Hunsucker, Geophysical Institute, College, Alaska

The L-band incoherent-scatter radar located at Chatanika, Alaska (latitude 65° N) has been used to measure the characteristics of the auroral E layer. In this paper, the term "auroral E layer" refers to nighttime ionization between 90 and 150 km produced by particle precipitation and generally associated with visual auroral forms. Electron-density profiles have been measured using time resolutions as short as 2 sec and range resolutions of 5 to 10 km. The statistical accuracy of the measurement for the shortest integration times is of the order of 8 percent. The results obtained to date have shown peak electron densities approaching $2 \times 10^6 \text{ el/cm}^3$ within the layer. The altitude of peak density varies from 95 to 120 km, and the layer thickness at the half-density points varies between 10 and 30 km. Density gradients on the bottomside of the layer are typically very sharp, with the density increasing from about 10^4 (minimum detectable) to 10^6 el/cm^3 within the 10-km pulse width. From the short-term temporal behavior of the layer, production rates ($\sim 2 \times 10^5 \text{ el/cm}^3/\text{sec}$) and recombination coefficients ($\sim 1 \times 10^{-7} \text{ cm}^3/\text{sec}$) have been estimated. In addition, estimates of the energy and flux of the precipitating electrons have been made. Simultaneous measurements of the incoherent-scatter spectra have shown some evidence of heating of the plasma coincident with the electron-density enhancements.

1-5 SIMULTANEOUS INCOHERENT-SCATTER, IONOSONDE, AND RIOMETER OBSERVATIONS OF THE FORMATION OF A DISTINCT AURORAL D LAYER: R.D. Hunsucker, Geophysical Institute, University of Alaska, College, Alaska; and M.J. Baron, Radio Physics Laboratory, Stanford Research Institute, Menlo Park, Calif.

During the period 0826 to 1024 UT, 23 November 1971, electron-density distributions obtained with the auroral-zone incoherent-scatter radar showed distinct D and E layers in the aurorally disturbed ionosphere. The existence of a distinct maximum in the D layer indicates that the spectrum of the auroral primaries had two discrete maxima, one a few keV and the other several tens of keV. This suggests the existence of two distinct populations of auroral electrons. Absorption, as measured by a riometer and an ionosonde, correlated with the appearance and disappearance of the D layer. Visual aurora was observed in the beam of the radar during this period.

COMMISSION 3

1-6 INCOHERENT-SCATTER MEASUREMENTS OF LATITUDINAL VARIATION OF F LAYER FROM TROUGH TO AURORA: H.F. Bates, Geophysical Institute, University of Alaska, College, Ala.; and J.D. Petriceks, Radio Physics Laboratory, Menlo Park, Calif.

The auroral-zone incoherent-scatter radar has scanned along the magnetic meridian on a number of quiet to slightly disturbed nights. At F-layer heights the radar scanned roughly 60 to 70° magnetic latitude. E- and F-layer electron densities were found to increase markedly as the latitude of visual aurora was approached. On those nights when no aurora was observed above the northern horizon, little or no increase with latitude was found. This result confirms earlier findings that the aurora increases the ionospheric electron density. At times, the increase began well equatorward of the visual aurora; this result supports the notion of a "drizzle" region of precipitation equatorward of the visual auroral precipitation. This increase forms the poleward boundary of the trough; during quiet times the trough is apparently quite broad.

1-7 AURORAL-ZONE RADAR MEASUREMENT OF IONOSPHERIC MOTION AND DETECTION OF CURRENTS: C.L. Rino, Stanford Research Institute, Menlo Park, Cal.

The technique of measuring ionospheric motion from the shift in the incoherent-scatter ion plasma line has been known for some time. The underlying assumption in the adaptations of the technique applied so far is that there are no detectable current-induced asymmetries in the spectrum. In the auroral zone this assumption is often violated during magnetospheric storms. To cope with current-induced asymmetries we use an estimate of the first moment of the spectrum together with a matched-filter-like estimate that is a slightly modified version of the optimum estimate proposed by Evans *et al.* (1970). The first moment is the sum of the first moment of the unshifted spectrum plus the Doppler shift. The matched-filter estimate, while not unaffected by asymmetries, tends to give an estimate closer to the Doppler shift. Hence, a difference between the two estimates is an indication of a current flowing in the range gate where the spectrum is measured. We assume that no other sources of asymmetry are present. In principle, the difference can be calibrated to give the magnitude of the current. This step is not yet completed, owing to uncertainties in the composition of the ionosphere at low altitudes and a loss of frequency resolution due to the finite pulse length. The detectability of the currents by our method, however, is not affected by poor frequency resolution. Preliminary results from the Chathanika auroral-zone incoherent-scatter radar are presented that show large velocities correlated in detail with simultaneous magnetometer data. Also, an indication of a current flow has been observed in pre-midnight data taken on a very active night. An azimuth scan showed the sense of the current to be predominantly westward.

COMMISSION 3, Session 2

1400 Thursday, April 13

Federal Room

PROPAGATION PROBLEMS

T. Quinn, Chairman

2-1 PROPAGATION MEASUREMENTS IN THE ELF RANGE: D.P. White and D.K. Willim, Lincoln Laboratory MIT, Lexington, Mass.

An experimental measurement program has been undertaken to determine the parameters for propagation in the 40- and 70-Hz range. A transmitter in Wisconsin (WTF) transmitted simple sinusoidal signals for two 8-hour periods per day for 20 days. The radiated power was 0.25 w at 45 Hz and 0.5 w at 75 Hz. Receiver sites were located in Utah, Nova Scotia, and Hawaii. Subject to the constraints detailed in the talk, estimates of the attenuation rates and the mode excitation factors have been determined with high accuracy. The daytime attenuation rates were found to be higher than those estimated previously on the basis of theoretical calculations. The nighttime excitation factor was also found to be a few dB smaller than previously expected. A careful analysis shows that directional differences in the attenuation rates ($|\alpha_{EW} - \alpha_{WE}|$) are less than 0.2 dB/Mm for both the 40- and 70-Hz range. A detailed report of the results can be found in a Lincoln Laboratory Technical Note 1972-1, ELF Propagation Study (Phase II, Spring 1971).

2-2 IONOSPHERIC REFLECTION HEIGHT DETERMINATION AT ELF FREQUENCIES FOR USE IN FIELD-STRENGTH CALCULATIONS BY EMPLOYING A STRATIFIED-IONOSPHERE MODEL IN THE ZONAL-HARMONIC-SERIES FIELD-STRENGTH CALCULATION: R.L. Lewis, Institute for Telecommunication Sciences, Office of Telecommunications, Boulder, Colorado.

A spherically stratified model of the earth-ionosphere waveguide is considered. Each layer of stratification requires a converging-ray reflection coefficient, a diverging-ray reflection coefficient, and an interlayer transmission coefficient for a complete description of each layer's effect on the field-strength calculation. By use of a recursive formula, starting from the topmost layer, any number of layers of stratification can be specified. The field strength calculation for such a stratified model is best accomplished by summing the zonal-harmonic series, since the solution of a modal equation which contains an iterative sequence would be quite time-consuming. For frequencies near 100 Hz, approximately 250 terms are sufficient for convergence of the series solution. Using a two-layer ionosphere model the effects of stratification can be highly exaggerated, particularly if the outermost layer is highly conducting. With an extremely low conductivity for the inner layer, only the highly conducting outer layer affects the field, while with a low conductivity inner layer, the appearance of a trapped wave dominates the field strength in the earth-ionosphere waveguide. Yet with only moderate conductivity for the lowest ionosphere layer the effects of the highly conducting upper layer are completely masked, even when the layer thickness is extremely thin. It is apparent that pre-assignment of a single ionosphere reflection height may lead to erroneous field-strength predictions. Rather a realistic ionospheric profile which accounts for both ion and electron densities should be used to allow the field-strength calculation program to select the proper reflection height. The actual reflection height

COMMISSION 3

can then be deduced by deleting superfluous layers.

2-3 WORLDWIDE PROBABILITIES OF SPREAD-F OCCURRENCE AND ITS EFFECT ON HF PROPAGATION: R.M. Davis, Jr., Office of Telecommunications, Boulder, Col.

The probability of spread-F occurrence is analyzed by use of vertical-incidence data taken at the network of ionosondes in 1958 and 1964. Twenty-four numerical maps are formed from the data; they provide computer predictions of spread-F probability for general time and space conditions. The mapping error, in terms of the standard deviation of residuals, varies between 11 and 17 percent. Widely different patterns of spread-F probability arise at low, middle, and high latitudes. The dependences on season and solar activity are different in the pre-midnight and post-midnight periods, in the range of invariant latitudes $\pm 25^\circ$. Pre-midnight spread-F in this range has a higher probability in the eastern hemisphere than in the western. Seasonal effects also depend on longitude. Frequency usage likely to minimize the harmful propagation effects of spread-F is recommended for the various latitude and time blocks.

2-4 AURORAL ABSORPTION PREDICTIONS FOR HIGH-LATITUDE HF PROPAGATION: Richard Vargas-Vila and J.H. Dillingham, Analytical Systems Corporation, Burlington, Mass.

This paper describes a method for computing the amount of auroral absorption that would be observed by a high-latitude HF radio communications circuit. It is based upon data gathered by three different chains of riometer stations. A similar distribution in space and time of auroral absorption events is observed by the three networks. This allows cumulative probability distributions of the occurrence of auroral absorption to be generated from the data. To calculate attenuation on a given radio propagation path, the corrected geomagnetic coordinates of the D-region penetration and exit points are first determined. Next, a probability distribution showing percent time that the vertical-incidence auroral absorption exceeds a given level is calculated for these D-region points, where absorption is assumed to occur. A secant law is assumed in order to translate vertical-incidence absorption to oblique-incidence absorption, and an inverse-square frequency relationship is assumed to extrapolate to other frequencies. The total path loss is then given by the sum of the attenuations incurred on the up-going and downgoing portions of the path as they traverse the D region. Results are presented as contours of constant absorption for any specified percentage of time up to the median value. All computations and plotting are performed by computer.

2-5 SOME RESULTS OF CALCULATIONS OF RADAR REFLECTION COEFFICIENTS FROM PLASMA GRADIENTS WITH COLLISIONS: W.G. Chesnut, Radio Physics Laboratory, Stanford Research Institute, Menlo Park, Calif.; and M.S. Tierney, University of California, Los Alamos Scientific Laboratory, Los Alamos, N.M.

The magnitude and frequency dependences of radar reflections from gradients in plasma density are used in many applications as diagnostics for determining the properties of the plasma gradient. Well-known

examples are ionospheric sounding, radar reflections from the solar corona, radar reflections from cesium and barium clouds released in the ionosphere, and laboratory plasma probing. The Epstein density profile often may be fitted to these plasma density profiles, so that this profile form has very great practical utility. We have computed radar reflection coefficients from Epstein profiles for two limiting situations of general interest. These limiting conditions are electron-neutral collision dominated and electron-ion collision dominated plasmas. In order to evaluate these coefficients we have found a relatively simple but accurate analytical approximation to the ratio of gamma functions of complex arguments found in the reflection coefficient equations. The simplicity of the formulation greatly enhances one's ability to estimate reflection coefficients without resorting to evaluation of the generally unfamiliar gamma functions themselves. For the case of an electron-ion collision dominated plasma that exponentiate to very high density, we have found an extremely simple analytical approximation for the reflection coefficient that is valid for most radar/plasma systems of practical interest. This form complements the well-known form that pertains to electron-neutral collision dominated plasmas that exponentiate to infinite density. Some interesting pseudo-resonance phenomena have been discovered and will be discussed.

2-6 THE ACOUSTIC-GRAVITY MODES OF A REALISTIC, DISSIPATIVE ATMOSPHERE:
S.H. Francis, Bell Telephone Laboratories, Whippany, N.J.

The acoustic-gravity modes of a realistic, dissipative atmosphere are discussed. The underlying analysis differs from previous treatments by including dissipation (viscosity, thermal conductivity, and ion drag) and by using a realistic sound speed profile throughout the thermosphere. The upper-atmospheric modes exhibit several characteristics which conflict with previous results concerning leaky modes in dissipationless atmospheres. At long periods, there are upper-atmospheric modes with speeds up to 800 m/sec, all composed at F-region heights of internal gravity waves with nearly horizontal phase fronts. Attenuation distances, defined as the horizontal distance in which a mode is attenuated by a factor of $1/e$, are about 1/8 of the way around the earth (5000 km) or less. These characteristics agree with those observed for F-region traveling disturbances (TID's). Ion drag is not found to be particularly important, but changes of the upper-atmospheric temperature structure due to diurnal and solar cycle variations are found to have quite appreciable effects.

2-7 RAY TRACING ANALYSIS OF CHARACTERISTIC HF PROPAGATION EFFECTS:
M.S. Wong, Air Force Cambridge Research Laboratories, Bedford, Mass.

Effects on the usable frequency bands, and distance coverage, due to various ionospheric electron distributions are analyzed by ray tracing. These distributions include linear variations with distance, and trans-equatorial, polar, and sunrise models. Frequency gaps, and abnormally high values of the lowest usable frequency, occur in the computed effects. It is suggested that the LUF is sometimes set by ray-pattern geometry rather than by ionospheric absorption. Sample oblique-incidence ionograms obtained with a step-frequency Granger sounder operating between Puerto Rico and Uruguay in 1964-1965 show features similar to those computed from electron-distribution models. Also discussed is

COMMISSION 3

the construction of frequency-distance coverage diagrams useful for propagation predictions on one-way circuits or skywave ground backscatter.

2-8 REGULAR AND IRREGULAR VARIATIONS OF F-REGION PARAMETERS: A.K. Paul, Environmental Research Laboratories, National Oceanic and Atmospheric Administration, Boulder, Colo.

A new method of anharmonic frequency analysis is applies to several years of hourly values of $f_{\text{c}}F2$ and $M(3000)$. It is found that a set of 12 frequencies with their amplitudes and phases provides an accurate description of the diurnal and seasonal variation of those quantities by comparison with monthly median values. Those regular variations are subtracted from the observed values, and the residual is studied. This still contains strong irregular variations, which can be partly associated with solar and magnetic activity. It is assumed that the remaining variations are due to dynamic processes in the F region. By comparison of the residuals among several stations some insight concerning those processes can be gained.

2-9 RAY THEORY AND VARIATIONAL RESULTS: J.A. Bennett, Institute of Earth and Planetary Physics, University of Alberta, Edmonton, Alberta

The propagation of radio waves in the ionosphere may be studied by constructing an asymptotic solution, the limiting situation representing an ideally slowly varying medium. This may be called a short wavelength solution since the medium changes slowly on the scale generated by the wavelength. In this approximation, the phase and amplitude of the wave are calculated by integration along the familiar radio rays. It is a consequence of the variational principle satisfied by the rays that the formulae for the phase changes, due either to movement of the ray endpoints or perturbations of the medium, are greatly simplified. Results will be presented in the form of Hamiltonian expressions for successive variations of the phase path, and a number of applications including Doppler shifts, group propagation, polarization rotation, and ray reciprocity will be discussed.

2-10 SCATTERING OF HF RADIO WAVES BY ELLIPTICAL ELECTRON-DENSITY DISTRIBUTIONS: V.L. Corbin and M.M. Klein, Air Force Cambridge Research Laboratories, Bedford, Mass.

The differential and total cross sections for ellipsoids and elliptic cylinders having gaussian electron-density distributions have been obtained by a ray-tracing procedure. Calculations for the case of an external magnetic field were restricted to the ellipsoidal distributions. The results show that the scattering is extremely sensitive to the orientation of the body. A peak in cross section occurs at the scattering angle corresponding to the ray normal to the critical surface and increases as the surface becomes flatter. The cross section is sensitive to the ratio of peak density to critical density for moderate values but becomes relatively insensitive when the ratio exceeds 3. The total cross section is a very sensitive function of both orientation and ratio of major to minor axes. The introduction of a magnetic field decreases the ordinary ray cross section; the extraordinary ray exhibits higher values only in the forward-scattering region but is always higher

COMMISSION 3

for the spherical case. Comparison of the gaussian ellipsoid with the corresponding conducting ellipsoid shows that the gaussian has a large cross section in the forward region but considerably lower values in the backscatter region.

0900 Friday, April 14

Federal Room

INCOHERENT SCATTER II

J. Nisbet, Chairman

3-1 EXOSPHERIC TEMPERATURE VARIATIONS AT MILLSTONE HILL: J.E. Salah, Department of Meteorology and Lincoln Laboratory, MIT, Cambridge, Mass.; and J.V. Evans, Lincoln Laboratory, MIT, Lexington, Mass.

Based upon the assumption of ion thermal energy balance, incoherent-scatter measurements using the Millstone Hill UHF radar have been reduced to give neutral temperatures in the altitude region 300-450 Km for 48 days between March 1969 and March 1971. The results support the models of exospheric temperatures based on earlier incoherent-scatter results. The temperature maximum occurs at 16.5 ± 1.5 h and the diurnal variation changes with season to reflect the length of the day. The maximum-to-minimum ratio of the exospheric temperature is about $1.3 \pm .05$ with no apparent seasonal dependence. The long- and short-term variations observed provide strong support for the Waldteufel (1971) model, but indicate a larger seasonal variation. The results also show that the Jacchia (1971) model is in better agreement with incoherent-scatter measurements than earlier models based on satellite drag observations, but does not accurately predict the diurnal temperature variation. A harmonic analysis has been conducted of the exospheric temperatures and the results compared with Lindzen's (1971) theory. The observed amplitude and phase variations of the diurnal and semidiurnal thermal tides show no evidence for a propagating semidiurnal tide from the mesosphere. The *in-situ* semi-diurnal tide is observed to have an amplitude of less than about 30% of the diurnal component and exhibits seasonal phase variations. Analytical expressions that represent the observed exospheric temperature variations in terms of frequency harmonics are presented.

3-2 INCOHERENT-SCATTER OBSERVATIONS OF HORIZONTAL DRIFTS IN THE E AND F REGIONS AT MILLSTONE HILL: J.V. Evans, Lincoln Laboratory, MIT, Lexington, Mass.

A steerable 23-cm wavelength radar system has been employed for incoherent-scatter observations of the ionosphere at oblique incidence. With the beam at an elevation of 15° , it has been possible to measure the horizontal drift of the ionospheric plasma with a height resolution of ~ 30 km. The direction of the drift was determined by making measurements alternately looking north and west. Drift velocities are typically less than 30 m/sec, and the direction of drift normally rotates clockwise during the course of the day. In the F region the drift appears height-independent, suggesting that it is produced by electric fields. The direction of the E-region drift lags behind that of the drift in the F region indicating that the source of the electric field is the dynamo region (and not the magnetosphere). On one day electric fields of magnetospheric origin developed following a magnetic storm sudden commencement. The clockwise progression of the drift was then reversed, and the drift reached a speed of 200 m/sec toward the west at sunset. This motion may be connected with sunward surges of the plasma in the plasmasphere bulge at times of substorms reported by Carpenter (1970).

COMMISSION 3

3-3 INCOHERENT-SCATTER OBSERVATIONS AT ARECIBO USING COMPRESSED PULSES: G.Ioannidis and D.T.Farley, School of Electrical Engineering, Cornell University, Ithaca, N.Y.

Pulse-compression techniques are now being used successfully in incoherent-scatter observations at Arecibo. In most observations a 13-bit Barker code and 6- μ sec band length are used, giving a compression ratio of 13 to 1 (i.e., the signal-to-noise ratio is 13 times greater than for a single 6- μ sec pulse) with very low range "sidelobes" and an altitude resolution of 0.9 km. Even better resolution should be obtainable in the near future. A few of the first measurements with this technique are presented and include observations of (1) the E region and sporadic E layers, (2) the D-region ledge near 80 km, and (3) narrow enhanced echoes associated with HF heating of the ionosphere.

3-4 PROTONOSPHERE-IONOSPHERE COUPLING - NIGHTTIME BACKSCATTER OBSERVATIONS AT ARECIBO: Y.S. Hsu, R.A. Behnke, and B.S.Tanenbaum, Case Western Reserve University, Cleveland, Ohio

Experimental observations using backscatter techniques at Arecibo, Puerto Rico, of composition and particle flux up to 1000 km, are presented. The data show the so-called "transition" height from O^+ to H^+ descends to very low altitudes around midnight local time. We believe this is the first time both O^+ and H^+ fluxes have been measured simultaneously by the radar technique. The lowering of the transition level is accompanied by large downward velocities, suggesting that transport processes play a dominant role in the topside nocturnal ionosphere. The effects of this flux on the maintenance of the nighttime ionosphere will be discussed.

3-5 HIGH-RESOLUTION INCOHERENT-SCATTER MEASUREMENTS OF THE NIGHTTIME E REGION AT ARECIBO: J.F.Rowe, Jr., Arecibo Observatory (NAIC), Arecibo, Puerto Rico

The lower ionosphere over Arecibo is being studied with the use of phase-coded radar pulses and newly installed digital signal processing equipment. The technique in use is well suited to D- and E-region altitudes where the correlation time of the medium is large compared to the 78- μ sec 13-bit Barker coded pulse in use. Using the pulse compression technique, the nighttime E region over Arecibo has been analyzed with 9-km height resolution. High-resolution profiles taken over several nights in the 90-120 km altitude range are presented. The variation of altitude, electron density, and electron content of the relatively stable nighttime E layer are analyzed and discussed within the context of current theoretical models applicable to this region.

3-6 OBSERVATIONS OF REVERSIBLE HEATING BY TIDES IN THE E REGION: R.H. Wand, Electrical Engineering Department, Sydney University, Sydney, Australia (Present address: Lincoln Laboratory, MIT, Lexington, Mass.)

Incoherent-scatter measurements of E-region ion temperature were made at the Arecibo Observatory. The technique involves transmitting five separate short (20- μ sec) pulses in a group. The pulse spacings within

the group are selected so that the separation between any two pulses is unique. This allows the correlation function of the ionospheric electron-density fluctuations to be obtained simultaneously at 10 time delays. Analysis of the correlation functions gave daytime ion temperature (and hence neutral temperature) over the altitude range 108-135 km with a resolution of 4 km. The measured temperatures show the presence of a wave with a 12-h period which is interpreted as reversible adiabatic heating by the solar semidiurnal tide. The fractional amplitude of the temperature wave is quite variable from day to day and on occasion may be as large as 20%. A downward phase progression (corresponding to upward energy propagation) of the wave is evident with a vertical wavelength near 30 km.

3-7 ELECTRON TEMPERATURE CHANGES IN THE EQUATORIAL IONOSPHERE DURING GEOMAGNETIC STORMS: T.B.Jones, Environmental Research Laboratories, National Oceanic and Atmospheric Administration, Boulder, Colo.

Observations of the electron temperature and density in the equatorial ionosphere made at Jicamarca, Peru, have been examined during five geomagnetic storms. In all cases the nighttime electron-temperature increases and temperature increases of up to 500 K are also observed during some of the daytime storms. In no case were temperature decreases observed, in contrast with the results reported for temperate latitudes during comparable disturbances. The largest temperature increases during daytime were always observed in the height range 300-400 km. Electron-density increases and decreases were observed during these storms. Some of the possible mechanisms for the production of the observed storm changes are discussed, and the results are compared with those reported for the temperate-latitude ionosphere during similar disturbances.

COMMISSION 3, Session 4

0900 Friday, April 14

New York Room

DISTURBANCES

E.A. Mechtly, Chairman

4-1 STUDY OF CHARACTERISTICS OF SATELLITE-MEASURED PARTICLE PRECIPITATION WITH SIMULTANEOUSLY MEASURED RADAR AURORA: W.G. Chesnut, J.C. Hodges, and R.L. Leadabrand, Stanford Research Institute, Menlo Park, Calif.

The characteristics of auroral particle precipitation as measured during 14 passes by the Lockheed OV1-18 satellite over Alaska have been compared with radar aurora simultaneously detected at 139 and 398 MHz beneath the satellite orbit using the SRI auroral radar located at Homer, Alaska. All measurements were made near local midnight while the E region was in darkness. The study has revealed the following: (1) Protons with energies above 10 keV regularly precipitate to the south of electrons with energies above 800 eV. (2) Electron precipitation in regions of radar aurora seems sufficiently intense to produce the E-region ionization needed to explain the observed radar scattering. (3) Radar aurora (on 11 of 14 passes) was not associated with regions of intense proton precipitation. (4) No obvious relationship existed between regions of radar aurora and regions of most intense flux of electron precipitation power (number flux times average electron energy), though there may be a tendency for these to be spatially anticorrelated. (5) There seems to be a tendency for the electrons incident into regions of radar aurora to have a slightly lower average energy (order of 80%) than electrons precipitating elsewhere. (6) There is a tendency for the average electron precipitation power to be less in regions of radar aurora than in other precipitation regions. We have not found a deterministic relationship between the character of precipitating electrons and radar aurora--only subtle, statistical tendencies were found.

4-2 A SUMMARY OF IONOSPHERIC EFFECTS DURING PCA EVENTS, 1. PARTICLE CHARACTERISTICS: A.J. Zmuda and T.A. Potemra, Applied Physics Laboratory, Johns Hopkins University, Silver Spring, Md.

Ionospheric disturbances during PCA (polar cap absorption) events have been observed since 1957 through effects on practically all types of ionospherically propagated radio transmissions from LF to VHF. The disturbed polar cap region has been observed as low as Washington, D.C. Observations of solar protons, alpha particles, and electrons obtained by near-earth and interplanetary satellites during 30 major PCA's in the period 1965-1969 were consolidated to provide a summary of near-earth particle characteristics important for the evaluation and possible prediction of ionospheric effects. The particle properties reviewed are as follows: (1) the range of proton fluxes and spectrums observed; (2) a definition of the proton polar cap region and its variation with proton energy and geomagnetic activity; (3) the variation of proton fluxes over the polar caps; (4) the regions of anisotropic and 2π -isotropic flux; (5) arrival time and fluxes of solar alpha particles and electrons.

COMMISSION 3

4-3 A SUMMARY OF IONOSPHERIC EFFECTS DURING PCA EVENTS, 2. IONOSPHERIC CHARACTERISTICS: T.A. Potemra and A.J. Zmuda, Applied Physics Laboratory, Johns Hopkins University, Silver Spring, Md.

The particle characteristics discussed in the previous paper were used in combination with ground-based HF riometer and VLF phase observations and various rocket measurements to analyze and review ionospheric effects during PCA's. These may be listed as follows: (1) the altitude deposition of ionization in the ionosphere and the range of maximum effect for a number of events; (2) the day and night D-region aeronomy; (3) variation of electron density distribution for a range of events; (4) evaluation of radio propagation models for predicting HF and VLF effects during PCA's; (5) the importance of solar alpha particles and electrons to the ionosphere during PCA's; (6) the importance of the radio station locations with respect to the time-varying polar cap, in conjunction with a possible explanation for the midday recovery effect observed on riometer absorption, the delayed disturbances observed on midlatitude VLF transmissions, and the effect of low ground-conductivities on VLF transmissions.

4-4 EFFECTS OF PRECIPITATING ENERGETIC ELECTRONS ON VLF PHASE AT MID-LATITUDES: T.A. Potemra, Applied Physics Laboratory, Johns Hopkins University, Silver Spring, Md.; T.J. Rosenberg, Institute for Fluid Dynamics and Applied Mathematics, University of Maryland, College Park, Md.; and R.A. Helliwell, Radioscience Laboratory, Stanford University, Stanford, Calif.

Perturbations to the phase of long distance VLF transmissions at mid-latitudes ($\sim 50^\circ$ geomagnetic latitude) associated with magnetic activity have been observed for some time. Evidence is presented showing that precipitating electrons with energies > 30 keV are the cause of a particular VLF disturbance and further, that a wave-particle interaction involving cyclotron resonance between energetic trapped electrons and whistler-mode VLF waves is the cause of this electron precipitation. On January 2, 1971, phase disturbances were simultaneously observed on 13 midlatitude VLF paths which correlated with the following observations: (1) magnetic bays measured at several midlatitude stations; (2) 1-4 kHz VLF emissions measured at Siple Station, Antarctica ($\sim 60^\circ$ geomagnetic latitude); (3) Bremsstrahlung x-rays ($E > 30$ keV) measured by balloon-borne detectors over Siple; (4) increases in trapped electron fluxes at 40 keV, 75 keV, 120 keV and > 5 keV measured at synchronous altitude by ATS-5. The flux of electrons with $E > 30$ keV required to account for the phase disturbances is estimated to be $1000/\text{cm}^2\text{sec ster}$ which is near the sensitivity of most other indicators of electron precipitation such as x-rays or riometer absorption.

4-5 POLAR D-REGION RESPONSE TO A SOLAR PROTON FLUX: W.J. Helms and R.L. Livingston, University of Washington, Seattle, Wash.

A vertical-incidence stepped-frequency VLF sounder operated near Byrd Station, Antarctica, is used to monitor the D-region response to a large solar proton event from September 25 through October 1, 1969. Explorer 41 solar proton data indicates a substantial increase in proton flux with energies greater than 10 MeV at approximately 0900 UT on September 25, with a peak flux at 1200 UT followed by a classic

COMMISSION 3

exponential decay with a time constant of about 6 hours. The VLF phase height of the D region above Byrd Station is seen to drop from an initial height of 79 km at 0946 to a minimum of 60 km at 1401 UT. Electron-density profiles obtained using the full wave technique on VLF sounder amplitude data indicate a general lowering and flattening of the electron-density profile, and the development of a sharp ledge at approximately 65 km. The D-region recovery is seen to occupy approximately two days.

4-6 MEDIUM SCALE TRAVELING IONOSPHERIC DISTURBANCES ATTRIBUTED TO MID-LATITUDE CHANGES IN GLOBAL CIRCULATION FOLLOWING A SEVERE MAGNETIC STORM: G.B. Goe, Environmental Research Laboratories, National Oceanic and Atmospheric Administration, Boulder, Colo.

Traveling ionospheric disturbances with periods of 12 to 20 min are examined for 14 days following the severe magnetic storm of November 1, 1968. The disturbances appear to be typical for midlatitude, daytime, winter. The horizontal trace velocities vary from 80 to 150 m/sec and are directed 110° to 175° east of north. Their continued appearance for a two-week period of time is, however, unexpected and is explained by the modification of global circulation following the magnetic storm. This suggests that the changing unstable tropopause wind patterns are the source of the disturbances. It is usual for the ionospheric data to show 3 to 5 day trends, the time required for the troughs or ridges of the planetary waves as observed on the tropopause wind analysis maps to pass over Boulder (40° N, 105°W).

4-7 RADAR-AURORAL POLEWARD EXPANSIONS: E.J. Fremouw, Stanford Research Institute, Menlo Park, Calif.; and C.R. Wilson, Geophysical Institute, University of Alaska, College, Alaska.

An examination of radar records obtained at Homer, Alaska, in October and November 1970 has disclosed a repeating feature of radar-auroral motion that occurs during the expansive phase of polar substorms. This substorm radar signature consists of a rapid poleward excursion of one or more strongly backscattering regions, readily identifiable range-time-intensity records. The signatures were found in such records obtained at 139 and 398 MHz, using radar beamwidths of 9° and 3°, respectively, and pulses giving respective range resolutions of 11 km and 150 km. The radar beam was held fixed in such a position that its center intersected the E layer nearly perpendicularly to the geomagnetic field at L=6, between College and Fort Yukon, Alaska. This operation led to identification of seven poleward-expansion signatures in six weeks of nighttime observation. Radar range-rates of 1 to 2 km/sec, sustained for several minutes, typified the events. They all were accompanied by negative bays in H, typically of several hundred v, on College magnetograms. The onsets of the bays were coincident, within about a minute, with the arrival time of the radar aurora at the range of College. When skies were clear, poleward motions of visible aurora also were observed.

COMMISSION 3

4-8 D-REGION SEASONAL AND LATITUDINAL VARIATIONS DERIVED FROM IONOSPHERIC PERTURBATIONS PRODUCED BY SOLAR X RAYS: R.H. Doherty and R.L. George, Office of Telecommunications, Institute of Telecommunication Sciences, Boulder, Colo.

Low-frequency pulse transmissions are received over reciprocal paths after being once reflected from the ionospheric D region. Daytime signals show considerable phase and amplitude sensitivity to solar x rays which produce sudden ionospheric disturbances. The changes observed are not always the standard phase advance and amplitude increase normally seen on VLF CW signals. Consequently, a study was made over a period of one year on the percentage of the total number of SID's that produced phase advances or amplitude enhancements. The remainder of the SID's produced phase retardations or amplitude decreases or both. Actually the phase and amplitude statistics are treated separately, but it is obvious from the results that there is a strong tendency for phase retardations and amplitude decreases to occur together. Three paths at roughly 25°, 35°, and 60° N latitude have been examined for the one-year period. The results show that for all these northern latitude paths solar x-ray events tend to attenuate the LF signal in the winter and to enhance the signal in the summer. At the lowest latitude, solar x-ray events produce nearly 100% phase advances, whereas at the highest latitude phase retardations occur more than 50% of the total time and nearly 100% during winter months. Seasonal variations are observed on all three of these paths with amplitude decreases and phase retardations more common during winter months. The latitude variations, the seasonal variations, and variations relative to the solar zenith angle all suggest that the amplitude changes occur at a different ionospheric height than that where the phase changes occur.

COMMISSION 3, Session 5

1400 Friday, April 14

Federal Room

IONOSPHERIC PROCESSES

T.A. Seliga, Chairman

5-1 MORPHOLOGICAL FEATURES OF AURORAL RADIO ABSORPTION: Kurt Toman, Air Force Cambridge Research Laboratories, Bedford, Mass.

The development of auroral cosmic noise absorption during five days in March and April 1965 was deduced from observations made at more than eight locations in the northern hemisphere. One-day sample sizes of the absorption time series were correlated using the lag technique. The peak values of the correlation coefficients were found to diminish slowly with distance up to hundreds of kilometers. For greater distances the correlation weakened at first only to be followed by an erratic recovery. This behavior was examined in terms of the magnetic shell values of the station ensemble. It was found that a relatively high correlation of auroral absorption can extend over thousands of kilometers if the corresponding pair of observing stations is located at the same invariant latitude.

5-2 EQUATORIAL IONOSPHERIC ABSORPTION DURING HALF A SOLAR CYCLE 1964-1970: S. Gnanalingam, Goddard Space Flight Center, National Aeronautics and Space Administration, Greenbelt, Md.

An extensive series of vertical-incidence absorption measurements made at Colombo, Ceylon (7°N , 80°E : Dip angle 5°S) is analyzed in detail to provide information on the principal characteristics of equatorial ionospheric absorption and, in particular, the causes of its temporal variations. It is shown that the dominant cause of variability during the solar maximum period 1968-1970 was solar x radiation. A quantitative empirical relationship between equatorial absorption and $1-8 \text{ \AA}$ solar flux in the range $0 - 2 \times 10^{-3} \text{ erg/cm}^2 \text{ sec}$ is presented demonstrating a linear increase of absorption with the square root of the flux for values in excess of $0.5 \times 10^{-3} \text{ erg/cm}^2 \text{ sec}$. Attention is drawn to the occurrence of days when the absorption was high even in the absence of x-ray activity. Available evidence points to an increase in solar Lyman- α radiation as the most probable cause of the enhanced electron density responsible for this high absorption.

5-3 HF RADIO WAVE ABSORPTION CALCULATIONS USING NEW IONOSPHERIC MODELS AND RECENT COLLISION FREQUENCY DATA: M.K. Lee and J.S. Nisbet, Pennsylvania State University, University Park, Pa.

More is now known about the behavior of the lower ionospheric densities and temperatures as a function of solar activity, solar zenith angle, season and geographical location. Recent models have been combined with collision frequency data of Itikawa (1971) and the neutral atmospheric models of Grove (1971) and Swartz *et al.* (1971) to calculate HF radio wave absorption under a variety of conditions. These calculations are compared with previous empirical and analytic studies.

COMMISSION 3

5-4 HIGH-LATITUDE SPREAD-F AND IONOSPHERIC TROUGHS: J.R. Herman, Analytical Systems Corporation, Burlington, Mass.

The occurrence of high-latitude spread-F exhibits a decided oval pattern when mapped in coordinates of geomagnetic latitude and local time. The nighttime maximum occurrence region (corresponding to Pennendorf's "travelling maximum") is centered at about 0200 GLT; latitudinally it extends both poleward and equatorward of the Feldstein auroral oval. Spread-F contours of constant occurrence frequency have been generated without regard to the level of magnetic activity, whereas the main ionospheric trough position was mapped by Muldrew (J. Geophys. Res. 70: 2635, 1965) as a function of K_p . Utilization of cumulative probability distributions of average daily K_p allows statistical determination of the K_p level (and trough position) corresponding to each spread-F contour level. The results lead to the conclusion that the main ionospheric trough constitutes the equatorward boundary of spread-F occurrence, and both trough and boundary move equatorward in concert with increasing magnetic activity.

5-5 ROCKET OBSERVATIONS OF SPORADIC-E LAYERS: L.G. Smith, GCA Technology Division, Bedford, Mass.; and E.A. Mechtly, Aeronomy Laboratory, Department of Electrical Engineering, University of Illinois, Urbana, Ill.

The characteristics of midlatitude sporadic-E layers have been observed using rocket payloads incorporating a probe and a propagation experiment. Layers below 120 km show evidence of preferred altitudes. The slopes of layers are within one degree of horizontal. The horizontal dimensions are deduced to be several hundred kilometers. Individual profiles of daytime layers show a range of shapes ranging from triangular to rectangular. The plasma frequency derived from the peak electron density in the layer is found to agree with the blanketing frequency given by the local ionosphere sounder.

5-6 ONE-TO-ONE COMPARISON OF TOPSIDE AND BOTTOMSIDE SPREAD-F OVER OTTAWA, CANADA: R.W. Jenkins, Communications Research Center, Ottawa, Ontario.

Topside ionograms taken by Alouette 1 over Ottawa are compared with coincident bottomside ionograms in an attempt to resolve more completely the sources of spread-F traces both top and bottomside. A check on the presence of horizontal gradients which yield multiple paths for top and bottomside reflection is provided by the topside soundings. As well, determination of the presence of mechanisms such as aspect-sensitive scattering and ducts or holes is facilitated by a one-to-one comparison of top- and bottomside features. Results will be discussed.

5-7 A COMPUTER-PRODUCED MOVIE ILLUSTRATING IONOSPHERE PROCESSES: L.H. Brace, H.G. Mayr, and R.F. Theis, Goddard Space Flight Center, National Aeronautics and Space Administration, Greenbelt, Md.

A movie produced on a computer-plotter illustrates the effects of variations in the neutral atmosphere and the solar ultraviolet flux upon the photochemistry and heat balance of the E and F regions. Vertical profiles of the ion composition and electron and ion temperatures

COMMISSION 3

between 120 and 300 km are calculated for the full range of solar activity, independently varying the magnitude of the euv flux and its spectrum as well as the thermospheric temperature of the model. This presentation illustrates the sensitivity of the chemical and heat balance of the ionosphere to the euv spectrum and the neutral concentrations and therefore places bounds on the accuracies with which these parameters should be measured to resolve a given uncertainty in the rates of specific processes.

5-8 ELECTRON VELOCITY DISTRIBUTION FROM CYLINDER PROBE CHARACTERISTICS: W.R. Hoegy, Goddard Space Flight Center, NASA, Greenbelt, Md.

The electron velocity distribution contains detailed information on the physics of the ionosphere and its measurement would provide a valuable diagnostic tool. An example of the importance of a knowledge of the velocity distribution is provided by the discrepancy in electron temperature between probes and radar backscatter. A distortion in the velocity distribution at energies less than or equal to several kT will result in distinct probe and radar temperatures, therefore a measurement at low energies would settle this aspect of the temperature discrepancy. Cylinder probe volt-ampere curves from rocket and satellite borne instruments are examined to extract information on the electron velocity distribution and its deviation from a Maxwell distribution. A polynomial fit to the data points is used to generate the second derivative of the probe current which is proportional to the electron velocity distribution. The apparent distortion of the velocity distribution may be caused by: (1) a real non-Maxwellian distribution function; (2) surface variations (patchiness) in the probe contact potential; or (3) real deviations from the idealized Langmuir probe theory.

5-9 A MODIFIED MONTE CARLO MODEL FOR THE IONOSPHERIC HEATING RATES: H.G. Mayr, Goddard Space Flight Center, NASA, Greenbelt, Md.; and S.C. Robertson, Consultants and Designers, Inc., Greenbelt, Md.

Following Cicerone and Bowhill (1971) a Monte Carlo method is adopted as a basis to derive the photoelectron heat input into the ionospheric plasma. Considering that the size of the source elements must be small compared with the range over which photoelectrons dissipate their energy, a great number of Monte Carlo runs are required normally to compute the heating rates. This approach is modified in an attempt to minimize the computation time. The heat input distributions are computed for arbitrarily small source elements that are spaced at distances apart corresponding to the photoelectron dissipation range. By means of a nonlinear interpolation procedure their individual heating rate distributions are utilized to produce synthetic ones that fill the gaps between the Monte Carlo generated distributions. By varying these gaps and the corresponding number of Monte Carlo runs the accuracy of the results is tested to verify the validity of this procedure. It is concluded that with this model the computation time can be reduced by more than a factor of three, thus improving the feasibility of including Monte Carlo calculations in self-consistent ionosphere models.

COMMISSION 3, Session 6

1400 Friday, April 14

New York Room

IRREGULARITIES AND MOTIONS

J. Kelso, Chairman

6-1 SIMULTANEOUS L-BAND AND VHF IONOSPHERIC FADING EFFECTS AT THE GEOMAGNETIC EQUATOR: T.S. Golden, Goddard Space Flight Center, NASA, Greenbelt, Md.; and W.B. Sessions, Westinghouse Corporation, Baltimore, Md.

Using signals received from ATS-5 and Intelsat 1 simultaneous observations of ionospheric fading at 1550 MHz and 136 MHz were recorded at the NASA site at Lima, Peru. Observations over an equinox period have shown fades as great as 27 dB at 136 MHz and as great as 6 dB at 1550 MHz. Future system design of earth-space or aircraft-satellite links in the equatorial regions may well be influenced by the magnitude of the observed scintillations. The general characteristics of the scintillation signatures at the two frequencies are discussed with emphasis on comparison of two frequencies with respect to rates and depths of fades. The statistical distributions of signal levels are also presented, from which time availabilities of the signals relative to the median levels can be derived.

6-2 VHF IONOSPHERIC SCINTILLATION FADING MEASUREMENTS AT LIMA, PERU: H.A. Blank and T.S. Golden, Goddard Space Flight Center, National Aeronautics and Space Administration, Greenbelt, Md.

During the spring equinox of 1970, scintillating signals at VHF (136.4 MHz) were observed at Lima, Peru. The transmission originated from ATS-3 and was observed through a pair of antennas spaced 1200 ft apart on an east-west baseline. The empirical data have been digitized, reduced, and analyzed utilizing the computer center at NASA/GSFC. The results of that analysis are presented in this paper. They include amplitude probability density and distribution functions, time auto-correlation functions, cross-correlation functions for the spaced antennas, fade duration probability functions, and appropriate spectral density functions. The presentation of the results of the analysis will include estimates of the statistics of the ionospheric irregularities causing the scintillation such as gross irregularity size (east-west), and irregularity velocity (east-west).

6-3 ESTIMATION OF THE CUMULATIVE AMPLITUDE PROBABILITY DISTRIBUTION FUNCTION OF IONOSPHERIC SCINTILLATIONS: H.E. Whitney, J. Aarons, and D.R. Seemann, Air Force Cambridge Research Laboratories, Bedford, Mass.

The fading characteristics of ionospheric scintillations are described by experimental measurements of the cumulative amplitude probability distribution function (cdf). The cdf expresses the probability or percentage of time that the signal amplitude will equal or exceed a given amplitude. Signal strength recordings at 136 MHz from synchronous satellites were processed to give 324 cumulative distributions for various levels of ionospheric scintillations. The distributions were divided into five groups corresponding to ranges of scintillation index, the predominant measure in scintillation studies. A mean or model distribution was obtained for each of the five ranges of scintil-

COMMISSION 3

lation index and then, by weighting the models according to the occurrence of each range, cumulative amplitude probability distribution functions were produced which represent long-term observations from auroral, midlatitude, and equatorial regions. Short-term, 15-min, distributions are shown to agree extremely well with Nakagami's m -distribution for various values of m . A spectral index can be obtained from the measurement of m at two frequencies and used to interpolate amplitude distributions to other frequencies. The data allows a fading margin to be estimated for satellite communication systems in the VHF range.

6-4 DIURNAL VARIATIONS OF F-REGION MOTIONS: T.J. Herron, Lamont-Doherty Geological Observatory, Columbia University, Palisades, N.Y.

A cross-spectrum analysis technique was used to determine hour-by-hour changes in horizontal phase velocity and direction of continuous "background" motions in the ionosphere crossing an array of 4 CW Doppler sounders (50-km spacings) operating at 4.35 MHz near New York. Continuous tracking over many days of 10-100 min period waves showed daytime velocities of 50-250 m/sec increasing at night to 500-2500 m/sec. The waves were dispersed with short periods fastest. Directions of phase propagation vary smoothly from southerly during the day through west, into the north at night. Phase velocities, at any one period, increase to a maximum just before sunrise when ionospheric electrical conductivities are a minimum. Observed velocities are those of long-period electromagnetic waves in the ionosphere where phase velocity varies as the inverse square root of conductivity and period ($c=1/\sqrt{\sigma T}$). Diurnal changes in velocity are those predicted by diurnal changes in conductivity. The equation above predicts group velocity of twice the phase velocity with short periods arriving first, as has been observed. A hypothesis of downcoming hydromagnetic waves, attenuating and refracting into the zone of low electromagnetic wave velocity in the lower ionosphere will explain most observed characteristics of mesoscale ionospheric waves.

6-5 SIMULTANEOUS VERTICAL-INCIDENCE AND DIRECTION-OF-ARRIVAL OBSERVATION OF IONOSPHERIC PERTURBATION DUE TO A TRAVELING DISTURBANCE: N.N. Rao, Radiolocation Research Laboratory, University of Illinois, Urbana, Ill.

Variations in the azimuthal and elevation angles of arrival of an 8-MHz signal caused by ionospheric perturbations due to a traveling disturbance were measured for a propagation path consisting of transmitter near Houston, Texas, and receiver near Urbana, Illinois. Vertical-incidence ionograms were recorded simultaneously by a network of four ionosondes located around the midpoint of the propagation path. Parameters of an analytical model for the disturbance are obtained by fitting the model to constant electron-density contours obtained from true-height analysis of the ionograms. The model parameters are then used in conjunction with a three-dimensional ray-tracing program to compute the direction of arrival variations of the 8-MHz signal. The results indicate the computed variations to be in good agreement with the measured variations for the elevation angle of arrival but not for the azimuthal angle of arrival. The discrepancy is explained in terms of the direction of propagation for the deduced analytical dis-

COMMISSION 3

turbance model relative to the propagation path of the 8-MHz signal.

6-6 OBSERVATIONS OF QUASI-PERIODIC WAVELIKE TRAVELING IONOSPHERIC DISTURBANCES: E.K. Walton, Radiolocation Research Laboratory, University of Illinois, Urbana, Ill.

Quasi-periodic wavelike traveling ionospheric disturbances (TID's) consistent with the gravity wave theory have been studied using a radio direction finding (RDF) system. Three HF transmitters at the vertices of an equilateral triangle were used. Each transmitter was placed approximately 30 km from a centrally located interferometer RDF site and ionosonde. The RDF system measured the azimuthal and incidence angles of arrival and the amplitude of the received signals. The three CW transmitters were operated sequentially, switching every 20 seconds. Deviations in the received signal due to TID's were studied. Measurements of the direction of arrival of the signals provided information on the ionospheric tilt at the three reflection points as a function of time. Autocorrelation and spectral density curves of the individual time series records yielded information on the random and periodic structure of the wavelike disturbances. Cross-correlation curves of these records were used to calculate their direction and speed. Six months of data were compiled on these wavelike disturbances. Histograms and/or typical values of the wavelength, period, amplitude, speed, and direction of the TID's are given. Techniques for observing these parameters using a single radio source (perhaps the ionosonde pulses) are developed. Methods of using these data to improve the accuracy of short-range radio direction finding measurements are discussed.

6-7 AMPLITUDE PROBABILITY DISTRIBUTION FOR IONOSPHERE DIFFRACTED VHF-UHF SIGNALS: C.L. Rino and E.J. Fremouw, Stanford Research Institute, Menlo Park, Calif.

The probability distribution for ionosphere-diffracted VHF-UHF signals is of interest to geophysicists as well as communication system designers. Under the assumption of gaussian first-order statistics for the complex signal at the receiver, the statistical specification of the signal is complete when the intensity of the in-phase and phase-quadrature components and their covariance are determined. These quantities were computed assuming weak single scatter and a layered ionosphere with correlation between layers. The results show that Briggs and Parkin's formula for the scintillation index S_4 neglects terms of second order which can be important in certain cases, and that some caution must be exercised in applying the Nakagami distribution for the probability density of amplitude. A precise definition of the near and far zones is given in terms of a single parameter. The computed amplitude probability is very sensitive to the transverse scale size in the near zone (as defined above), but much less so in the far zone. This sensitivity can be used to infer scale sizes from amplitude data recorded at a single receiver. An excellent fit to data from ATS-3 recorded at Lima, Peru, was obtained for a transverse scale size of 300 m. As this is approaching the far zone it must be interpreted as an upper bound from these data alone. The work complements and extends a worldwide scintillation model that has been recently developed. The scintillation model estimates the rms value of the F-region electron-

COMMISSION 3

density fluctuation and predicts average scintillation levels to better than an order of magnitude at subionospheric latitudes lower than 70° geomagnetic.

6-8 FADE-RATE CORRELATION: M.R. Epstein, Page Communications Engineers, Inc., Vienna, Va.

The limits were measured of both frequency separation and physical separation within which two transmitted HF signals exhibit similar received fade-rate characteristics. The experiment, which was fundamentally different from conventional diversity measurements, employed two mobile transmitters operating within several radio frequency bands between 9 and 23 MHz over paths varying from 500 to 4000 km. At each transmitting location two mobile transmitters were increasingly separated in range and subsequently in azimuth, with respect to the receiver site, until appreciable differences in the received fade-rate characteristics were observed. Similar tests were performed by separating the transmitted radio frequencies. The experiments indicate that there is a region surrounding any HF transmitter, such that signals from transmitters operating on nearby radio frequencies within the region exhibit similar remotely received signal strength fade rates. The size of this fade-rate region is on the order of 60 to 100 mi, if the signals being compared are separated by less than 350 kHz for frequencies near 15 MHz and about 1 MHz for frequencies near 25 MHz. These results have application to the design of long baseline antenna arrays for high-resolution ionospheric investigations.

6-9 DIFFERENTIAL-PHASE MEASUREMENTS OF FINE-SCALE IONOSPHERIC IRREGULARITIES: J.L. Auterman and L.J. Porcello, Radar Land Optics Laboratory, University of Michigan, Ann Arbor, Mich.

Wide-bandwidth, differential-phase measurements on harmonically related 162 and 324 MHz emissions from the Explorer 22 and Explorer 29 satellites were made simultaneously at ground-based sites about one km apart. Measurements were made in February 1967 at College, Alaska, and in April 1967 at Fort Huachuca, Arizona. Such phase records yield the integrated electron density (IED), to within an unknown additive constant, along the ray path extending from the satellite to each receiver site, with a temporal bandwidth of about 230 Hz in the phase structure. The fine time resolution, available as a consequence of maintaining such a large bandwidth, provides, in principle, a unique method of observing small ionospheric irregularities, with lateral dimension on the order of ten meters. Both a spectral analysis and a cross-correlation analysis were performed on the phase records. The power spectra of the differential phase records could be approximated by the form $Af^{-n}(\text{rad}^2/\text{Hz})$ where, for 9 data samples, A was in the range 6×10^{-3} to 0.8 and n varied from 1.8 to 2.7. The mean value of n was 2.4. Simultaneous phase records from the two sites yielded essentially similar power spectra. Earlier data collected using the same technique indicated even smaller values for the lower range of A. Cross-correlation analysis of the two-site spaced-receiver data indicated the presence of F-region ionospheric irregularities during some of the observations. These observations are unique in that correlated perturbations in the differential phase are used to detect the irregularities, in contrast with the usual case in which signal amplitude

COMMISSION 3

scintillations are analyzed to yield irregularity structures. The correlation analysis yielded evidence of irregularities for the College observations, at heights ranging from 350 to 800 km. The same method did not yield well-defined evidence of irregularity structure for the Fort Huachuca observations. Coherency spectra, obtained from cross-spectral analysis, yielded an estimate of the lateral scale of the irregularities. Detectable spectral contributions from the observed irregularities were found at spatial wavelengths as small as 360 m.

COMMISSION 3, Session 7

0830 April 15, Saturday

Congressional Room

IONOSPHERIC PERTURBATION I

R.S. Cohen, Chairman

7-1 IONOSPHERIC MODIFICATION PRODUCED BY VERY POWERFUL RADIO TRANSMITTERS; EXPERIMENTAL RESULTS: J.A. Fejer, Department of Applied Physics and Information Science, University of California, San Diego, La Jolla, Calif.

The results of modification experiments in Boulder and Arecibo are reviewed. The modification effects include the production of artificial spread-F, the distortion of the F_2 layer, the modification of radio wave absorption, the modulation of the 6300 Å oxygen line of the airglow, and the enormous enhancement of the "plasma line" of incoherent backscatter.

7-2 IONOSPHERIC MODIFICATION AS VIEWED BY A THEORIST: F.W. Perkins, Plasma Physics Laboratory, Princeton University, Princeton, N.J.

The principal theoretical results concerning ionospheric modification experiments have been concerned with the amount of heating the ionosphere will undergo and the role of parametric instabilities. The theory will be reviewed in both these areas, and a comparison of the data with theory will be made. Particular emphasis will be placed on the comparison with the recently developed nonlinear theory of the saturation of parametric instabilities.

7-3 VLF AND LF OBSERVATIONS OF D-REGION MODIFICATION: T.B. Jones, Environmental Research Laboratories, National Oceanic and Atmospheric Administration, Boulder, Colo.

The phase and amplitude of WWVL (20 kHz) and WWVB (60 kHz) signals reflected above the high-power HF transmitter at Platteville, Colorado, have been monitored during periods of ionospheric heating. Amplitude changes of about 1% and phase changes of around 0.5° were observed on both these frequencies for modifying frequencies of 5.1 and 7.6 MHz. On the assumption that the electron collision frequency is a linear function of the electron temperature and that the cooling factor $G = 1.3 \cdot 10^{-3}$, the fractional increase in collision frequency is 0.3 for a radiated power of 20 MW. Full wave calculations show that the phase and amplitude variations produced by an increase in v of this magnitude are appreciably greater than those observed experimentally. The phase and amplitude changes have been investigated as a function of the power and frequency of the disturbing transmissions in an attempt to determine the dependence of the electron collision frequency on the electron energy.

7-4 TEMPERATURE AND ELECTRON DENSITY RESULTS IN THE ARECIBO HEATING EXPERIMENTS: R.L. Showen, University of Puerto Rico, Mayaguez, P.R.; and L.A. Dias, Rice University, Houston, Texas.

Modification of the F region over Arecibo is accomplished with a 100-kW transmitter operating between 5 and 10 MHz. The effects on the electron temperature and incoherent-scatter electron-density profiles are presented. The electrons are heated as much as 400 K at night with ordinary

COMMISSION 3

mode transmission. The observed spatial extent and magnitude of heating is consistent with the deviative absorption theory. The electrons relax to their ambient temperature in less than one minute. When the heater frequency is well matched to the f_{F2} , the ionograms show a splitting, and the incoherent-scatter electron-density profiles are detectably changed.

7-5 RADIATION VOLUMETRIC FORCE ON AN ANISOTROPIC IONOSPHERE: P.J. Moser and J.J. Gibbons, Ionosphere Research Laboratory, Pennsylvania State University, University Park, Pa.

The volumetric force of a high-frequency radio wave on an ionospheric plasma has been computed including the earth's magnetic field. The first-order particle equation of motion was solved for the high-frequency velocity. This velocity has a longitudinal component (parallel to wave propagation) as well as the usual transverse components found when the external magnetic field is absent. The longitudinal velocity yields high-frequency electron-density perturbations and a longitudinal electric field wave. A second-order current term results from the product of the high-frequency density perturbations and the high-frequency velocity. Therefore, in addition to the usual radiation pressure term from the cross product of the first-order current with the magnetic field of the wave one must include the cross product of the second-order current with the geomagnetic field and the electric force from the product of the first-order density perturbation and the longitudinal electric field to find the total nonlinear force on the electrons. Several calculations of this force have been made for simple slab and half-space models of the ionosphere.

7-6 KINESONDE OBSERVATIONS OF RF HEATING EFFECTS IN THE IONOSPHERE: L.S. Fedor, A.K. Paul, and J.W. Wright, Environmental Research Laboratories, National Oceanic and Atmospheric Administration, Boulder, Colo.

The coherent multifrequency, spaced-antenna measurement capabilities of the kinesonde are applied to observations of the ionosphere from a point 39 km west of the Platteville, Colorado, multimegawatt transmitter. Effects observed in the directly perturbed region include greatly increased scintillations of amplitude, phase path, and group-path following heater turn-on. Transient effects associated with turn-on are found, even at low F-region altitudes. The kinesonde is also employed passively to observe the ionospheric echo of the heating transmitter.

7-7 KINESONDE IONOSPHERIC OBSERVATIONS OF TURN-ON TRANSIENTS ASSOCIATED WITH INTENSE RADIO FREQUENCY TRANSMISSIONS: L.S. Fedor, Environmental Research Laboratories, National Oceanic and Atmospheric Administration, Boulder, Colo.

The time-delayed amplitude response of the ionosphere to intense radio transmissions from a transmitter located at Platteville, Colorado, is observed by the kinesonde located near the edge of the directly disturbed region. The difference between true heights of reflection of the kinesonde transmissions on several different frequencies, divided by the time delays, imply acoustic velocities. Ray-tracing and angle-of-arrival calculations are used to determine the horizontal extent of

COMMISSION 3

the region initially affected by the intense radio wave transmissions.

7-8 PRELIMINARY RESULTS FROM ARTIFICIAL RADIO SCINTILLATIONS OBSERVED DURING IONOSPHERIC MODIFICATION BY VERY HIGH POWER HF GROUND-BASED TRANSMISSIONS: C.L. Rufenach and C.A. Brink, National Oceanic and Atmospheric Administration, Boulder, Colo.

The radio sources Cygnus A and Cassiopeia A were observed near Boulder, Colorado, during six days of October and November 1971. Enhanced scintillations were observed at 26 MHz in the early evening hours when the ray path traversed the artificially produced small-scale irregularities near the peak of the F region. The ray path moved through the modified volume slowly allowing significant temporal changes in the scintillations to be correlated with the HF transmitter operation and ionograms taken at Erie, Colorado. These observations show strong correlation between the HF transmitter and ionogram features (broad-band attenuation and spread-F) and enhancement of scintillations (both amplitude and fading rate) on several days. On other days the correlation was not as pronounced. The spectral analysis of the artificial scintillations indicate that the spectrum of irregularities is a good approximation to the power-law variation reported for naturally occurring nighttime scintillations. The power-law spectrum is thought to be a better representation of both naturally occurring and artificially produced irregularities than the more common gaussian spectrum.

COMMISSION 3, Session 8

(Joint with COMMISSION 4, Session 4)

0830 Saturday, April 15

South American Room

CONJUGATE EFFECTS IN THE IONOSPHERE AND MAGNETOSPHERE I

W. Campbell, Chairman

8-1 THE EARTH'S FIELD LINES IN SPACE: J.G. Roederer, University of Denver, Denver, Colo.

Conjugate point experiments either assume the shape of a field line as known and focus on the study of a propagation phenomenon, or they use a propagation phenomenon to determine the shape experimentally, in particular, the location of the conjugate point. In both circumstances, a magnetic field model is employed and tested. For L -values less than 3-4 there is a trustworthy model, but beyond $L \sim 4$ external currents must be taken into account. This current system, as viewed from a fixed point on earth, has diurnal, seasonal, and nonperiodic variations. High-latitude conjugacy thus changes with time--and even may be disrupted--when the field line "opens" up into the tail or the dayside cusp. Magnetospheric models lead to numerical predictions for this "wandering" of conjugate points, provided the model parameters are known. A complicating factor is the role of ionospheric conductivity: To what extent and within what time scale are the "feet" of the field lines allowed to wander around? Diurnal and seasonal variations of conjugacy will be analyzed, and the effects of magnetospheric compression and neutral sheet current enhancements will be discussed.

8-2 FIELD-LINE IDENTIFICATION BY INJECTION OF BARIUM IONS: E.M. Wescott, Geophysical Institute, University of Alaska, Fairbanks, Alaska; M.H. Peek, Los Alamos Scientific Laboratories, Los Alamos, N.M.; and T.N. Davis, Geophysical Institute, University of Alaska, Fairbanks, Alaska

Two successful field-line tracing experiments were conducted on the $L = 1.26$ line over Kauai, Hawaii, in October 1971. Barium vapor was created in the detonation of a high explosive shaped-charge aligned along the earth's magnetic field at approximately 470-km altitude. The resulting ions travelled along the field line to the conjugate ionosphere with velocities up to 15 km/sec. The streak was visible over the entire 6900-km path length. The electric field (~ 1 mv/m) perpendicular to the magnetic field caused the ions to drift during transit away from the true conjugate, but extrapolation from subsequent drift rates allows the conjugate to be identified and compared with several field models. Differing ion drift rates and directions at the conjugate points indicates that the \vec{E} field is not transferred unattenuated along field lines. A similar field-line tracing experiment on the auroral zone field line from College, Alaska, is scheduled for March 1972.

8-3 HEMISPHERICAL AND LONGITUDINAL DIFFERENCES IN AURORAS: H.C. Stenbaek-Nielsen, Geophysical Institute, University of Alaska, Fairbanks, Alaska

The Alaskan and East Siberian sector of the auroral oval constitutes a magnetic well. The difference in magnetic field strength at 300 km

COMMISSION 3

over College, Alaska, and the conjugate is near 8000 gamma, giving a 7% difference in the loss cones between hemispheres. If effective, this will cause both hemispherical and longitudinal differences in the particle precipitation. Estimates are made of the ratio of the precipitation at conjugate points due to pitch-angle diffusion, a small hemispherical potential difference, and adiabatic acceleration (transverse and longitudinal). The observed intensity differences in the equatorward arcs (normally weak multiple arcs in the region of the hydrogen arc) as measured with all-sky cameras on conjugate aircraft are consistent with the estimated hemispherical intensity ratios of 1.1 to 1.3 due to pitch-angle diffusion. In the more spectacular poleward auroral forms, much larger deviations are often observed, with only a very few examples of the southern hemisphere auroras being the brighter. Although the adiabatic acceleration heavily favors precipitation in the Alaskan end of the field line, it does not appear to be capable of explaining certain morphological features in the data, notably the onset of the expansive phase in a substorm. The evidence of a magnetic field-controlled hemispherical difference in the particle precipitation adds to the evidence in favor of a longitudinal component in auroral morphology.

8-4 A NEWLY DEVELOPING PROGRAM OF GROUND-BASED CONJUGATE OBSERVATIONS: M.G. Morgan, Radiophysics Laboratory, Dartmouth College, Hanover, N.H.

Plasmapause studies by the ground-based VLF whistler technique require observation at locations of suitable L-value and whistler occurrence. In pursuit of these, the Dartmouth observing program which the British have accommodated on the Antarctic Peninsula since the beginning of the IGY, has been transferred to their Antarctic station at Halley Bay ($L = 4.2$). The 29° separation in longitude from the Stanford program at Siple (formerly Eights) Station will provide the opportunity for simultaneous observation at significantly different local times and the observation of east-west structure. A conjugate station has been installed at St. Anthony, Newfoundland. Equipment is under development for the supplementary observation of ULF whistlers (PCL micropulsations) at both stations, and a British program for placing three-component rubidium vapor magnetometers at both stations is planned. VLF observations at both stations have been underway since June 1971, and analysis will begin when the first data shipped from Halley Bay are received. A similar program is developing in a widely different longitude at the conjugate station pair, Farewell, Alaska ($L = 4.3$), and Campbell Island, New Zealand, where VLF observations were begun November 1971 and February 1972 respectively. The first year of data from Farewell has yielded suitable synoptic data covering more than 200 hours. The Campbell Island observations are a New Zealand program and so far have been on a relatively sparse observing schedule. As experience is gained with the ULF equipment at Halley Bay-St. Anthony, it is planned to add a ULF program at Farewell-Campbell Island. A New Zealand program to place magnetometers at both stations is planned. Thirdly, auroral hiss is being observed with wideband scanning equipment (up to 100 kHz), at Frobisher Bay, N.W.T. ($L = 14.5$), which is conjugate to the South Geographic Pole station and which is centered on the zone of maximum occurrence found by the Dartmouth experiment on OGO-6.

COMMISSION 3

8-5 SATELLITE OBSERVATIONS OF WHISTLER-MODE SIGNALS IN THE CONJUGATE REGION OF A 200-kHz STATION: Thomas Laaspere and S.C. Orphanoudakis, Radiophysics Laboratory, Dartmouth College, Hanover, N.H.

The payload of the polar-orbiting OGO-6 spacecraft included a narrow-band (≈ 200 -Hz) receiver at 200 kHz, connected to an electric dipole antenna. We have studied the signals received by this receiver both over the station and in the conjugate region of Achkhabad ($58^{\circ}23' E$, $37^{\circ}57' N$). The latitude of this station is nearly low enough ($\approx 30.5^{\circ}$ invariant) for propagation of a 200-kHz signal in the ducted whistler mode to the conjugate hemisphere along field lines terminating at the station. In the dawn-dusk orbital plane, signals are indeed relatively often observed in the conjugate region, but the source of the signals and their path of propagation is not completely clear. The pattern of observations is consistent with propagation over the long magneto-spheric path in field-aligned ducts spread in longitude near 22° invariant latitude, but we favor an interpretation involving nonducted propagation in which the occasionally high electric-field intensities encountered ($> 10 \mu V/m$) result from focusing effects or from propagation near the resonance angle.

8-6 ENERGETIC ELECTRON PRECIPITATION ON THE SIPLE-ROBERVAL FIELD LINE: T.J. Rosenberg, Institute for Fluid Dynamics and Applied Mathematics, University of Maryland, College Park, Md.

Energetic electron precipitation near the plasmapause has been examined at Siple Station by the University of Maryland. Measurements of bremsstrahlung x rays have been compared with Stanford University's conjugate observations of VLF activity. A detailed correlation has been found between x-ray bursts of short duration with energies greater than 30 keV and discrete VLF emissions in the 1-to 4-kHz band. Temporal features of this correlation indicate that electron precipitation accompanying the generation of discrete VLF emissions results from a cyclotron resonant interaction between energetic electrons and whistler-mode waves near the equatorial plane. This interaction is expected to lead to detailed conjugacy in electron precipitation. Plans for future investigations, which include conjugate x-ray measurements and artificial stimulation of electron precipitation with the Siple transmitter, will be discussed.

COMMISSION 3, Session 9

1330 Saturday, April 15

Congressional Room

IONOSPHERIC PERTURBATION II

R. S. Cohen, Chairman

9-1 SCINTILLATIONS PRODUCED BY ARTIFICIAL IONOSPHERIC MODIFICATION:

J.H.Pope and R.B.Fritz, Space Environment Laboratory, National Oceanic and Atmospheric Administration, Boulder, Colo.

In fall 1971, the ESSA-8 APT signals at 137 MHz were monitored on several occasions to determine if scintillations can be produced by operation of the ionospheric-heating transmitter located at Platteville, Colorado, and, if so, to determine their geographical extent. In the past ionograms taken during operation of the heater have shown that spread-F is produced. Scintillations were noted on a pass at about 1720 GMT on 15 October 1971, commencing when the satellite was north of Platteville at F-region heights of about 100 km in the north-south dimension shifted slightly southward from the location of the heating transmitter. The scintillation amplitude rose rapidly to an index of about 0.5, remaining somewhat constant during the transit of the active region. The scintillation period showed a systematic decrease during transit, starting with a period of about 3.5 sec in the north and ending with a period of about 1.5 sec in the south.

9-2 PLASMA RESONANCE RESPONSE ASSOCIATED WITH ARTIFICIAL IONOSPHERIC SPREAD-F: G.B.Goe, Environmental Research Laboratories, National Oceanic and Atmospheric Administration, Boulder, Colo.

The ionospheric F layer is modified by an incoming high-intensity wave in such a manner that spread-F appears on the sweep-frequency ionograms. At the same time, many wavelike echoes appear on the fixed-frequency virtual-height-amplitude records. The appearance of the wavelike echoes is explained by the plasma reaction to the incoming high-intensity wave in the vicinity of the ordinary reflection level. The electric field of the incoming wave oscillates parallel to the direction of the earth's magnetic field precisely at that height where the plasma frequency corresponds to the frequency of the incoming heating wave. We assert that the direction of the forced electron displacement is likewise parallel to the direction of the earth's magnetic field. When the speed of the displaced electron equals the speed of light in the medium, maximum energy goes into the plasma oscillation. As an electron travels at this characteristic velocity of the medium, the plasma oscillates at the natural resonant frequency of the plasma. One can compare the excitation of this resonance to the formation of a shock wave.

9-3 A MODEL OF ARTIFICIAL SPREAD-F PRODUCTION BY IONOSPHERIC HEATING: E.J.Valeo and F.W.Perkins, Plasma Physics Laboratory, Princeton University, Princeton, N.J.

We investigate the possibility that the artificial spread-F observed in recent ionospheric-heating experiments may be the result of a thermal instability induced by the modifier field. Our model consists of an electromagnetic wave vertically incident on a horizontally stratified ionosphere with parameters typical of the F₂ layer. Because of the large electron-thermal conductivity parallel to the background mag-

COMMISSION 3

netic field - assumed vertical for simplicity - the scale length for density perturbations is comparable with the plasma-density scale length. Thus, the problem is nonlocal, and the hydrodynamic motion of the plasma is an intrinsic part of the evolution.

9-4 PARAMETRIC EXCITATION OF ELECTROMAGNETIC WAVES: Egil Leer and J.A.Fejer, Department of Applied Physics and Information Science, University of California, San Diego La Jolla, Calif.

Parametric instabilities in which both the pump wave and the excited wave are electromagnetic in nature are discussed. Such instabilities can be excited by a pump wave of either ordinary or extraordinary polarization and the excited wave can be either in the same magnetoionic mode as the pump or in the opposite mode. The instability cannot be excited at the reflection level of a pump wave of extraordinary polarization, but it can be excited at lower levels. Excitation is strongly favored if the components of the propagation vectors of the pump and the excited waves along the magnetic field are equal; field-aligned irregularities in ionization are then produced. The effects of inhomogeneity are considered.

9-5 HF ENHANCEMENTS OF INCOHERENT-BACKSCATTER PLASMA LINES: I.J.Kantor, Rice University, Houston, Texas

Observations of enhancements of incoherent-backscatter plasma lines excited by strong HF radio waves are reported. Among the features described are: spectral shape and correlation between features, power dependence, rise and decay times, longer-term fading rates, comparison between up- and down-shifted plasma lines, and correlation with ion line enhancements.

9-6 IONOSPHERIC PROPAGATION OF ELECTRONIC SIDEBANDS GENERATED BY PARAMETRIC INSTABILITY: D. Arnush, TRW Systems, Redondo Beach, Calif.; and B.D.Fried and C.F.Kennel, University of California Los Angeles, Los Angeles, Calif.

Ionospheric propagation of parametrically generated electronic waves is studied to interpret backscatter spectral width measurements of the enhanced plasma line. From the dispersion relation for ionic and electronic modes parametrically coupled by an HF pump, we compute ray paths and path-integrated amplification. Both propagation and amplification are affected by pump amplitude and polarization near the parametric frequency matching altitude. Consequently, a realistic pump-amplitude height profile has been used. For a given frequency, parametric amplification typically occurs only over a few maxima of the pump amplitude; the wave then propagates out of parametric resonance and is collisionally damped thereafter. The electronic wave propagation, and pump polarization near reflection, depend upon the ionospheric magnetic field; both change the path-integrated gain. Backscatter techniques sample the spectrum at one k_f . Therefore, we follow waves of a single k_f but different frequencies backwards along their ray paths to the end of their resonant amplification regions and compute the integrated gain as a function of frequency. Propagation can explain a 30-kHz plasma-line spectral width. If only locally generated waves were de-

COMMISSION 3

tered in these studies suggest that the goal of using ground micro-pulsations as diagnostics is more distant than realized.

10-3 CHARACTERISTICS OF PC₁ FIELD-LINE PROPAGATION: Harold Liemohn, Boeing Company, Seattle, Wash.

Many types of geomagnetic micropulsation signals have been observed in the PC₁ band from 0.2 to 10 Hz, but only "pearl" or "ULF whistler" events have been investigated extensively. These events appear as a series of rising tones repeating at regular intervals. The characteristic dispersion inherent in the successive elements led to their interpretation as Alfvén-mode wave packets which propagate back and forth along field-line paths. The energy appears to be well collimated due to the phase velocity surfaces of the mode and amplification characteristics of the hot plasma medium. Thus these signals are a viable sensor of conjugate point locations in the geomagnetic field. Recent developments in the utilization of these signals as remote sensors of plasmapause dynamics will be described. Propagation properties in the ionospheric waveguide are also being actively investigated. Finally, the physical mechanisms responsible for their preponderant occurrence several days after the onset of major geomagnetic disturbances are being identified.

10-4 CONJUGATE GEOMAGNETIC STUDIES NEAR L ~ 4: L.J. Lanzerotti, Bell Laboratories, Murray Hill, N.J.

A program of conjugate magnetic field studies near L ~ 4 was begun during the 1970-71 austral summer. Measurements were taken at Siple, Antarctica, and at three stations spaced in latitude at ~70-km intervals near the conjugate point in Quebec: Girardville, St. Hedwidge, and Lac Rebours. The 1971-72 austral summer season saw data acquired at Siple and at three northern stations with a wider latitudinal spacing: Girardville, Lac Rebours, and Durham, New Hampshire. Strict selection criteria were imposed on the conjugate data in order to define well ULF plasma waves (period $\tau \sim 18-150$ sec) of magnetospheric origin. A significant local-time dependence is observed in the transmission properties of the ionosphere for these period waves. The tilt (with respect to the ionosphere) of the orientation plane of the waves at local noon is observed to be larger than at local night at the Antarctic station compared to the Lac Rebours station. The horizontal-plane polarization direction of these waves measured near L ~ 4 does not appear to change from predominately CCW to predominately CW around local noon at the northern stations (CW to CCW at Siple) as has frequently been reported using single hemisphere data. The hourly power spectra of the magnetic "noise" in all field components in the period band 8-512 sec has also been studied at the conjugate stations. The diurnal dependence observed in the conjugacy of the measured noise in this period band may be related to the S_d current system through field-aligned currents, even though the S_d fields at the conjugate stations are observed to be strongly nonconjugate.

COMMISSION 3

10-5 COMPARATIVE ANALYSIS OF THE RESULTS OF TWO RECENT EXPERIMENTS OF
HF MAGNETOCONJUGATE PROPAGATION: M.D. Grossi, Smithsonian
Astrophysical Observatory, Cambridge, Mass.

Two experiments of magnetoconjugate propagation in the band 7 to 12 MHz have been independently conducted in the recent past with basically similar instrumentation and almost identical measurement method. The results can therefore be combined and new relevant information obtained. The first experiment was performed in summer 1967 by SAO and the Argentinian laboratory LIARA between shell-conjugate sites ($L \approx 1.8$) located respectively, in Jupiter, Florida, and Ushuaia, Tierra del Fuego. The second was performed in Fall 1968 by the Soviet institute IZMIRAN between conjugate-point sites ($L \approx 2.8$) respectively, in Gorkiy and on board the Research Vessel Borovichi in the Indian Ocean. Comparison of the results of the two experiments permits, among other things, a first-order estimate of the effective area of conjugacy at HF. Although its extension in the north-south direction cannot be deduced reliably from the combined experimental results, a quantitative estimate of its extension in the east-west direction is possible. Its half-width is 1700 km between points at -23 dB. Path losses for the long-delay echoes that were observed and interpreted as due to magnetospheric guided propagation were, in fact, measured to be 63 dB worse than free space in receptions performed at the exact conjugate of the transmitter, and increased to only 86 dB for the listenings performed at a site 1700 km away toward east, along the L-surface intersect passing through the magnetoconjugate point.

COMMISSION 4

ON THE MAGNETOSPHERE

J. A. Fejer, Chairman

<u>Sessions</u>	<u>Page</u>
1. MAGNETOSPHERIC PHYSICS AND WAVES 1400 Thursday, April 13 Massachusetts Room Chairman: R. A. Helliwell Radioscience Laboratory Stanford University Stanford, Calif. 94305	79
BUSINESS MEETING 1700 Thursday, April 13 Massachusetts Room	
2. ARTIFICIAL PERTURBATION OF THE MAGNETOSPHERE I: VLF INJECTION 0900 Friday, April 14 South American Room Chairman: N. M. Brice School of Electrical Engineering Phillips Hall Cornell University Ithaca, N. Y. 14850	82
3. ARTIFICIAL PERTURBATION OF THE MAGNETOSPHERE II: PLASMA AND WAVE INJECTION 1400 Friday, April 14 South American Room Chairman: N. M. Brice School of Electrical Engineering Phillips Hall Cornell University Ithaca, N. Y. 14850	86
4. (Joint with COMMISSION 3: See Session 3-8)	
5. (Joint with COMMISSION 3: See Session 3-10)	

COMMISSION 4, Session 1

1400 Thursday, April 13

Massachusetts Room

MAGNETOSPHERIC PHYSICS AND WAVES

R.A. Helliwell, Chairman

1-1 INTERPRETATION OF JUPITER'S DECIMETRIC RADIATION IN TERMS OF
UPPER ATMOSPHERIC WINDS: N.M. Brice and T. McDonough, Cornell
University, Ithaca, New York

A mechanism is proposed for the diffusion of solar wind electrons and protons into the Jovian Van Allen belts. It is shown that the diffusion can be driven by electric fields generated by atmospheric winds which drag the ionized upper atmosphere across the Jovian magnetic field. The electric potential is conducted out to the magnetosphere along magnetic field lines. Fluctuations in the winds of Jupiter should then cause observable fluctuations in the decimetric radio emission. The observed dawn-dusk asymmetry of $\sim 10\%$ in the Jovian decimetric radiation is explained by the systematic behavior of the Jovian winds. We suggest the importance of monitoring of the dawn-dusk asymmetry of the Jovian radiation to give direct information on changes in the planetary wind systems in Jupiter's ionosphere.

1-2 VHF TECHNIQUE FOR THE STUDY OF THE UPPER PLASMAPAUSE: O.G.
Almeida, A.V. da Rosa, and C.G. Park, Radioscience Laboratory,
Stanford University, Stanford, Calif.

Simultaneous measurements of phase-path and Faraday rotation angle of VHF signals from geostationary satellites have been proposed as a means of studying the plasmasphere. In previous efforts, it was assumed that the Faraday rotation angle was a measure of electron content below a well-defined altitude so that the difference I_w between "total content" obtained from the phase-path measurements and the "Faraday content" is the content above that altitude. In this paper a more realistic interpretation of I_w is offered. Data taken at Stanford using ATS-3 satellite are presented and interpreted in terms of changes in electron content of the plasmasphere. The data during the storm of May 14, 1969, show a sudden increase in I_w immediately following the SSC at about 1900 UT (1400 LT at ATS-3). The increase lasts for some 3 hours, and then I_w decreases below the average level, followed by a slow recovery for several days. This behavior is consistent with a storm model in which the outer plasmasphere is "peeled" away by sunward convection and is subsequently replenished by slow filling from the underlying ionosphere. Studies of the local time dependence of such stormtime behavior may provide important clues on the magnetospheric convection.

1-3 WHISTLER WAVE-NORMAL VECTORS IN THE MAGNETOSPHERE: R.K. Burton,
K.W. Chan, R.E. Holzer, Institute of Geophysics and Planetary
Physics, University of California, Los Angeles; and E.J. Smith,
Jet Propulsion Laboratory, Pasadena, Calif.

The wave-normal vectors of lightning whistlers in the magnetosphere have been measured using the OGO-5 and -6 triaxial search coil magnetometer data. In the 400- to 1100-km range of altitudes accessible to OGO-6, the wave-normal vector deviates progressively from the vertical with increasing altitude. In this altitude range the angle between the

COMMISSION 4

wave normal and the geomagnetic field decreases with increasing magnetic latitude. Both results are consistent with propagation theory. Unducted whistlers were detected on OGO-5 inside the plasmasphere with in 30° of the magnetic equatorial plane. The angle between the wave normal and the geomagnetic field increased as expected from 40° to 90° as these whistlers propagated along the field line.

1-4 THE IONOSPHERIC CUTOFF OF EXTREMELY-LOW-FREQUENCY HISS: E.J. Smith, A.M.A. Frandsen, Jet Propulsion Laboratory, California Institute of Technology, Pasadena, Calif.; R.E. Holzer and R.M. Thorne, University of California, Los Angeles, Calif.

Intense hiss occupying a broad band of frequencies between several hundred Hz and 1-2 kHz is commonly observed in and above the ionosphere. The hiss appears to be generated at high altitudes in the plasmasphere and then to propagate downward. At altitudes between 400 and 1000 km, the hiss observed between L-shells of 2 and 5 typically exhibits a very sharp, low-frequency cutoff. The physical mechanism thought to be responsible for this cutoff is the reflection of the downcoming waves caused by a double ion cutoff in the index of refraction at low frequencies. An implicit feature of this explanation is a coupling of the right- and left-hand modes of propagation that can occur in a plasma containing several ions. Triaxial measurements of the magnetic field component of hiss, with and without a cutoff, have been obtained by the OGO-6 search coil magnetometer. These data have been subjected to a coherency analysis in order to study the sense of polarization and direction of propagation of the waves as a function of frequency. The results of this analysis will be presented and compared with the predictions of the double ion cutoff model.

1-5 BANDED WHISTLERS: E.M. Paymar, Lincoln Laboratory, MIT, Lexington, Mass.

Inspection of broadband VLF records from the Stanford University/Stanford Research Institute experiment aboard OGO-4 shows that some whistlers exhibit a banded structure in which one or more bands of frequencies are missing from the whistler's spectrum. The phenomenon is commonly observed by satellites on midlatitude field lines at all local times and at various longitudes around the world. The dispersion of banded whistlers (BW) is of several tens of $\text{sec}^{1/2}$, indicating that they originated in the opposite hemisphere and are propagating downward at the satellite. BW are generally spread in time (tenths of seconds) rather than sharply defined and tend to occur at random. The frequency spacing of the bands may be either uniform or irregular and may vary radically between successive events. Several possible explanations for BW are considered. In particular, an analysis of the interaction of plane electromagnetic waves traveling in an anisotropic plasma with a field-aligned slab of enhanced ionization is presented with promising results.

COMMISSION 4

1-6 POLARIZATION OF IONOSPHERIC-DUCT-PROPAGATED PCL MICROPULSATIONS AT LOW LATITUDES: B.J. Fraser, CIRES, University of Colorado, Boulder, Colo.; and W.R. Summers, Physics Department, University of Newcastle, NSW 2308, Australia

Observations have been made on hydromagnetic whistler-emission-type Pcl micropulsations at four low-latitude stations in Australia and New Zealand. Particular attention has been given to the polarization characteristics in the plane of the earth's surface. A consistent polarization pattern has been observed from the stations, and this is discussed in terms of temporal variations in the properties of the polarization ellipse. The effect of the ionospheric waveguide on signal polarization is considered, and the relationship of the ellipse major axis direction to a specific source region under stable ionospheric conditions is discussed.

1-7 CHARGE RADIATION IN WARM MAGNETOPLASMAS: D.J. Baker, Naval Research Laboratory, Washington, D.C.; and H. Weil, University of Michigan, Ann Arbor, Mich.

The power lost through radiation by a suprathermic electric charge as it spirals in a homogeneous magnetoplasma is calculated. Both electron and ion temperature effects are included via pressure terms in the basic equations from which the constitutive relations for the plasma are derived. Two plasma models were studied corresponding to the use of scalar or tensor pressures. Coherence effects are analyzed by studying Cerenkov radiation from a uniformly charged ellipsoid of revolution.

COMMISSION 4, Session 2

0900 Friday, April 14

South American Room

ARTIFICIAL PERTURBATION OF THE MAGNETOSPHERE I: VLF INJECTION

N.M. Brice, Chairman

2-1 VLF-WAVE INJECTION EXPERIMENTS: R.A. Helliwell, Radioscience Laboratory, Stanford University, Stanford, Calif.

VLF waves injected into the magnetosphere can interact strongly with energetic electrons over a wide range of energies. Some effects of this interaction are: (1) whistler-stimulated emissions, (2) artificially stimulated emissions (ASE), (3) whistler-triggered x-ray bursts, and (4) the recently discovered whistler-induced perturbations in VLF propagation. It is suggested that the time is ripe to carry out experiments based on these phenomena using a VLF transmitter on the ground or in a satellite. Such a facility is under construction at Siple Station, Antarctica, where a 13-mile long VLF transmitting antenna has just been installed on the one-mile thick ice cap. Experiments planned for this facility will be discussed.

2-2 COMPUTER SIMULATION OF DISCRETE VLF EMISSION GENERATION: R.A. Helliwell and T.L. Crystal, Radioscience Laboratory, Stanford University, Stanford, Calif.

Using a new computer model, a whistler-mode wave is coupled to a mono-energetic stream of cyclotron-resonant electrons at $L = 3$ in the equatorial plane. The magnetic field of the applied wave phase-bunches the electrons which then produce Doppler-shifted cyclotron radiation of nearly the same frequency. The total field is continually corrected to account for the addition of stimulated radiation. For a given interaction region length, self-oscillation of the system output occurs for stream densities above a certain threshold. When excited by a weak 10-m/sec pulse, the system output grows exponentially until it reaches a limiting or saturation value that depends on stream density. The delay to saturation can be made an appreciable fraction of a second, thus providing for the first time a simple explanation of the time gap often seen between a whistler and its triggered emission. In response to a step function input wave that is not too large the output tends to limit at a value that is independent of the input signal just as in the case of impulse triggering. This result may explain the observation that long-enduring whistler echo trains tend to exhibit a constant, or slowly decreasing, but never increasing, amplitude.

2-3 AMPLITUDE SPECTRA OF TRIGGERED VLF EMISSIONS: G.S. Stiles, Radioscience Laboratory, Stanford University, Stanford, Calif.

At present there does not exist a theory to adequately account for artificially stimulated VLF emissions. To better define the characteristics of this phenomenon, analog and digital amplitude spectra with frequency resolutions of approximately 30 Hz have been obtained for VLF emissions triggered by NAA (14.7 kHz) and received in the Antarctic. The spectra confirm previously reported triggering delays of 70 to 100 msec and positive frequency offsets of 50 to 400 Hz. A previously unreported characteristic is the presence of amplitude modulation in both the emission and the whistler-mode component of the transmitted signal.

COMMISSION 4

The period of this modulation varies from 70 to 110 msec for both signals; the trapping period of an electron in cyclotron resonance with a wave of reasonable amplitude at $L = 3$ falls in the same range. Many emissions also appear to have additional amplitude variations with periods from 5 to 10 msec. In the several case studies made thus far, the peak amplitude of the emissions varies from 50% to 200% of the peak amplitude of the NAA whistler-mode signal. The bandwidth of the few emissions that do not show the rapid amplitude variations appears to be less than 45 Hz.

2-4 NONLINEAR THEORY OF THE ONSET OF STIMULATED EMISSIONS: A.L. Brinca, Stanford University Institute for Plasma Research, Stanford, Calif.

It will be shown that a large-amplitude, parallel-propagating ($k \parallel B_0$) whistler causes distortion of the energetic component of the electron velocity distribution $f_0(v_{\parallel}, v_{\perp})$ in a predominantly cold magnetoplasma and gives rise to the creation of whistler sideband(s) if f_0 satisfies two conditions: f_0 must have a well-defined peak for some $v_{\perp} > 0$; and, f_0 must be either linearly unstable for the stimulating whistler or, if stable, satisfy

$2(\Omega/k_0) \int_0^{\infty} f_0 v_{\perp} dv_{\perp} \approx \left| \int_0^{\infty} v_{\perp}^3 (\partial f_0 / \partial v_{\parallel}) dv_{\perp} \right|$, where the integrals are evaluated at $v_{\parallel} = (\omega_0 - \Omega)/k_0$; Ω is the geomagnetic electron gyrofrequency, and ω_0 and k_0 are the frequency and wavenumber of the original whistler. In agreement with observations, the stimulated sideband(s) have a (positive or negative) frequency offset that increases with the original whistler amplitude B and a triggering delay that decreases with B . The underlying wave-particle mechanism can be extended to oblique whistlers ($k \times B_0 \neq 0$) and is thus relevant to VLF emissions stimulated by nondirected whistlers, i.e., of the type first observed with OGO-4.

2-5 RESONANCE CONES IN THE NEAR-FIELD PATTERN OF A SATELLITE-BORNE ELECTRIC DIPOLE ANTENNA: D.A. McPherson, J.H. Matsumoto, W.B. Harbridge, and H.C. Koons, Aerospace Corporation, El Segundo, Calif.

The near-field pattern of a short electric dipole antenna was measured by an instrument aboard the polar-orbiting satellite OVI-20S (1971-67B) at altitudes between 1500 and 1960 km. A 300-kHz signal exciting the dipole antenna was detected by a second dipole antenna fixed with respect to the first in spacecraft coordinates. The spacecraft spin provided the scanning function to map the near-field intensity as the angle between the antenna line of sight and the geomagnetic field direction varied. The pattern contains maxima which correspond to the group velocity resonance cones predicted to occur when the excitation frequency is less than both the electron gyrofrequency and the plasma frequency. The angle of the resonance cone with respect to the geomagnetic field direction was measured along the orbit. From this angle the electron density is determined. These measurements demonstrate that simple plasma dielectric theory is applicable to such satellite-borne antennas and represent a new technique for determining the ambient electron density in the magnetosphere.

COMMISSION 4

2-6 NONLINEAR IMPEDANCE AND NEAR FIELDS OF A VLF DIPOLE ANTENNA
MEASURED IN THE MAGNETOSPHERE: D.A. McPherson, W.B. Harbridge,
and H.C. Koons, Aerospace Corporation, El Segundo, Calif.

The nonlinear impedance and near-field intensities of a 120-ft dipole antenna were measured at very low frequencies by an instrument aboard the polar-orbiting satellite OV1-21S (1971-67A) at an altitude of \sim 900 km. The antenna is small compared to radiation wavelengths. At each of seven frequencies, the antenna was sinusoidally driven at seven voltage levels between 10 mV and 100 V peak-to-peak. The latter level is much greater than the plasma potential. The analog current and voltage waveforms were telemetered to ground together with broadband signals detected by two electric dipole antennas and a ferrite-core coil magnetic antenna located approximately two meters from the excited dipole. The resulting current waveforms are highly distorted with the harmonic content frequently exceeding the power in the fundamental. A consistent feature of the data is a decrease in the harmonic content at the higher voltage levels. The maximum harmonic content occurs at 10 or 30 V peak-to-peak. For excitation levels below 1 V peak-to-peak, the measured antenna impedance is in agreement with predictions of impedance appropriate to an ion sheath model. As the excitation voltage is increased, ion saturation current effects become apparent and the impedance increases approximately as the square root of the driving voltage.

2-7 ON RADIATION CHARACTERISTICS OF A LOOP ANTENNA WITH NONUNIFORM CURRENT DISTRIBUTION IN A MULTICOMPONENT MAGNETOPLASMA: T.N.C. Wang, Stanford Research Institute, Menlo Park, Calif.

The knowledge of radiation characteristics of a magnetic loop antenna in a multicomponent magnetoplasma is of current importance for the use of either a probe for the purpose of diagnostics, or a transmitting source for the satellite communication system in the space plasma. Most previous theoretical studies on this problem have assumed that the current distribution of the loop is uniform. This assumption is valid if the wavelengths in the medium of the major radiating modes are much greater than the loop circumference. As the driving frequency approaches any one of the resonance frequencies of the characteristic modes (e.g., electron or ion gyrofrequencies), the wavelengths of these modes will eventually become sufficiently small that this uniform current assumption is no longer valid. As the current becomes nonuniform, the loop antenna will develop an electric dipole moment in addition to its magnetic dipole moment; hence the interaction between the antenna and the magnetoplasma becomes a composite of both electric and magnetic sources. In the present paper, we have made a theoretical investigation of the radiation characteristics of a loop antenna with a nonuniform loop current distribution in a cold multicomponent magnetoplasma. A linear full-electromagnetic-wave theory is used for the analysis. In particular, the analytical expressions have been obtained for the loop radiation resistance and the input reactance for various frequency ranges. Numerical results relevant to ionospheric/magnetospheric plasma applications will be also presented.

COMMISSION 4

2-8 CYCLOTRON-HARMONIC RESONANCES IN THE TOPSIDE IONOSPHERE: D.B. Muldrew, Communications Research Center, Department of Communications, Ottawa, Ontario, Canada

Cyclotron-harmonic resonances can be studied by ray tracing using the dispersion relations for a hot plasma. The waves responsible for these resonances have a wave normal \underline{k} almost perpendicular to the magnetic field \underline{H} and a group velocity which is, except near reflection, almost parallel to \underline{H} . To determine the ray path, Snell's law is satisfied for inhomogeneous plane waves; the group path is determined from the real part of \underline{k} , and absorption is determined from the group direction and imaginary part of \underline{k} . Initially, the wave energy travels approximately along the field toward increasing \underline{H} and reflection occurs due to the gradient in \underline{H} . On a particular Alouette 2 ionogram, the third-harmonic-cyclotron resonance was observable for about 10 msec. It is found from ray tracing that for values of f/f_{H^*} (wave frequency/gyrofrequency) $\simeq 3.0001$ the rays returning to the antenna after about 1 msec or less are Landau-damped, and for $f/f_{H^*} \simeq 3.01$ the rays returning after 10 msec miss the antenna (78 m long). For $f/f_{H^*} \simeq 3.001$, rays can intercept the antenna without being damped for a period of about 10 msec. This agrees with the experimental results of different workers who found the resonance frequency to be within 0.2% of the harmonic gyrofrequency obtained from a model magnetic field.

COMMISSION 4, Session 3

1400 Friday, April 14

South American Room

ARTIFICIAL PERTURBATION OF THE MAGNETOSPHERE II:
PLASMA AND WAVE INJECTION

N. M. Brice, Chairman

3-1 A BARIUM CLOUD EXPERIMENT IN THE MAGNETOSPHERE: G. Haerendel,
Max-Planck-Institut für Physik und Astrophysik Institut für
extraterrestrische Physik, München, Germany

On September 21, 1971, a barium cloud was released from a Scout rocket at an altitude of 31,400 km. It could be observed by optical means for 1.5 h. The barium plasma, whose total mass was about 1.4 kg, formed a magnetic cavity with a radius of about 15 km transverse to the field and a steadily increasing length in the parallel direction. Inside the cavity the field strength was reduced by more than a factor of 50. The field recovery occurred over scale lengths much below the ion gyro-radius. The momentum transfer from the ambient plasma flow to the barium plasma proceeded from the dilute outskirts of the cloud to the interior whereby the cloud was progressively eroded. As a consequence, a plasma tail was formed with pronounced field-aligned structures. Acceleration times between 200 and 800 sec were observed for individual structures. The final drift velocities were directed to the southeast with variable magnitudes up to 4 km/sec (± 0.7 mV/m) in a rotating frame of reference. The experiment took place at $L = 6.8$ and $+19^\circ$ invariant latitude during a magnetically quiet time between 2200 and 2300 MLT.

3-2 HOW TO PRECIPITATE THE RING CURRENT WITH ARTIFICIAL PLASMA INJECTION: J.M. Cornwall, University of California, Los Angeles
(Present address: Space Physics Laboratory, Aerospace Corporation, El Segundo, Calif.)

The proton ring current, with single-particle energies from 1 to 50 keV, contains more energy than all other components of the magnetospherically trapped radiation. It may be possible to precipitate a large fraction of this energy into the ionosphere by injection of a light-ion plasma from a synchronous satellite, thereby rendering the ring-current protons unstable to a variety of plasma modes. Auroral-energy electrons can be precipitated by ions of any mass, but heavy (e.g., barium) ions will quench what may be the most important proton instability, which takes place in the electromagnetic ion cyclotron mode. This mode is unstable only if the ring-current protons have an average velocity greater than the wave phase velocity. The wave speed varies as $N^{-1/2}$, where N is the cold plasma density; under natural conditions N is too small for the ring current to be unstable outside the plasmapause. Injection of some tens of pounds of lithium ions at synchronous altitude will create an unstable region with a diameter of a few thousand kilometers; as a result of the instability, ring-current protons will precipitate into the ionosphere at a rate up to 1 erg/cm²sec. This should produce important effects in the upper E and F layers of the ionosphere. At the same time, precipitating auroral-energy electrons may create auroras and other effects usually associated with geomagnetic storms.

COMMISSION 4

3-3 ARC--A PROGRAM OF IONOSPHERIC MODIFICATION THROUGH ARTIFICIAL STIMULATION OF MAGNETOSPHERICALLY TRAPPED PARTICLE PRECIPITATION: D.J. Williams, Space Environment Laboratory, Environmental Research Laboratories, National Oceanic and Atmospheric Administration, Boulder, Colo.

The injection of cold plasma at geostationary altitudes under favorable ambient environmental conditions can lead to significant energy depositions in the ionosphere through the triggering of a naturally occurring magnetospheric plasma instability, the whistler-mode instability. The result of this instability is the scattering of the ambient magnetically trapped particle environment down the flux tube into the ionosphere. Nominal energy depositions of $\sim 28 \text{ erg/cm}^2 \text{ sec}$ ($2.8 \times 10^4 \text{ mW/m}^2$) are feasible over a $\sim 200 \text{ km}^2$ area in the ionosphere yielding a total energy deposition of $\sim 5.6 \times 10^6 \text{ W}$. By contrast, visible auroral occur at energy depositions of ~ 1 to $2 \text{ erg/cm}^2 \text{ sec}$. These results are discussed along with a satellite program (ARC) designed to measure quantitatively cause-effect magnitudes over a series of cold-plasma injections.

3-4 THE PRODUCTION OF MICROPULSATIONS USING VLF TRANSMITTERS: T. Bell, Radioscience Laboratory, Stanford University, Stanford, Calif.

A recent experiment at Siple Station in the Antarctic has shown that significant fluxes of energetic electrons can be precipitated into the lower ionosphere at times when VLF emissions are triggered in the magnetosphere by whistlers. It has been estimated that the peak fluxes observed in this experiment were of the order of $10^{-1} \text{ erg/m}^2 \text{ sec}$. If similar fluxes can be produced during the artificial triggering of VLF emissions by ground and/or satellite VLF transmitters, we would have available a powerful tool for studying not only the dynamics of wave-particle interactions in the magnetosphere but also the dynamics of the lower ionosphere. In the present paper we examine in greater detail a previous proposal to stimulate micropulsations. Periodic (period $> 1 \text{ min}$) transmissions from a VLF ground or satellite transmitter are used to trigger VLF emissions and precipitate energetic electrons. This periodic precipitated flux would modify the conductivity of the D and E regions, inducing periodic changes in current flow which could result in the radiation of micropulsations into the magnetosphere. Calculations indicate that micropulsation amplitudes of up to 1γ may be produced in the magnetosphere in this process. Furthermore, ground-level field perturbations may reach 100γ . Since both these amplitudes would be easily measurable with present techniques, the results lend plausibility to the idea of attempting to produce detectable micropulsations using VLF transmitters.

3-5 STUDIES OF THE MAGNETOSPHERE USING HIGH-POWERED ELECTRON BEAMS INJECTED FROM SOUNDING ROCKETS: J.R. Winckler, University of Minnesota, Minneapolis, Minn.

Success has been achieved in injecting electron beams of up to 1-amp current and 10- to 40-keV energy into the magnetic field in the upper ionosphere from sounding rockets. Some of these experiments are aimed at mapping field lines from the rocket into the atmosphere by observing the artificial auroral spots from the ground. Other experiments have different objectives. An Aerobee-350 rocket (Echo 1) launched from

COMMISSION 4

Wallops Island ($L = 2.6$) injected 40-keV electrons near the mirror pitch angle from the rocket. These electrons were reflected at the southern hemisphere conjugate point and were observed again at the rocket by particle detectors. The beams showed no evidence for catastrophic instabilities, and as many as three conjugate bounces were observed from a single injection. The motion of the particles is accurately in accord with advanced models of the geomagnetic field and Monte Carlo calculations of the multiple Coulomb scattering near the mirror points. The deduced quiet-time electric fields were less than 1 mV/m in these experiments. Electromagnetic emission was observed over a wide range of frequencies generated in space by the electron-gun pulses. Future experiments include Echo-type rockets in the auroral zone and at higher altitudes. Studies have been made of the application of these techniques to orbiting vehicles.

3-6 FIRST RESULTS OF RESONANCE OBSERVATIONS BY AN ADVANCED TOPSIDE RADIO SOUNDER: J.R. McAfee, Aeronomy Laboratory, National Oceanic and Atmospheric Administration, Boulder, Colo.

A radio sounder was carried to 660 km by a Javelin vehicle launched from Wallops Island at 0440 LT on June 25, 1971. The sounder was designed to provide frequency information with a precision of about 500 Hz at a few MHz, thus allowing the determination of the frequency characteristics of resonances observed near the plasma and upper-hybrid frequencies and harmonics of the electron gyrofrequency. The frequency vs. duration characteristics of the strong upper-hybrid resonance are consistent with the oblique electrostatic-wave echo model. The frequencies of resonances at the gyroharmonics are consistent with models of magnetic field strengths.

3-7 A DIFFUSION MODEL FOR THE ELECTRON-DENSITY DISTRIBUTION ALONG THE EARTH'S MAGNETIC FIELD IN AN F-REGION PLASMA CLOUD: P.B. Rao, Raytheon Company, Sudbury, Mass.

A diffusive equilibrium model for the electron-density distribution along the earth's magnetic field is presented for a plasma cloud generated in the F region of the ionosphere. The underlying analytic formulation is analogous to the one developed earlier by Bannister and Davis for the case of a neutral contaminant released in the upper atmosphere. The shape of the electron-density profile according to this model is characterized by an exponential form in the topside, a gaussian in the vicinity of the concentration maximum and a rather rapid cutoff due to diminishing effectiveness of the particle fall, and diffusion in the bottomside of the peak. The computed distributions are compared with those derived from the Thomson-scatter radar observations collected during a recent series of barium-release experiments conducted in Florida. The model and the measured profiles are found to be in good agreement.

COMMISSION 5
RADIO AND RADAR ASTRONOMY
M. H. Cohen, Chairman

<u>Sessions</u>	<u>Page</u>
1. PLANETS, SUN 1400 Thursday, April 13 California Room Chairman: G.A. Dulk Department of Astro-Geophysics University of Colorado Boulder, Colo. 80302	90
2. LONG BASE LINE INTERFEROMETRY I 0900 Friday, April 14 Galleries II Chairman: K.I. Kellermann National Radio Astronomy Observatory Edgemont Road Charlottesville, Va. 22901	94
3. LONG BASE LINE INTERFEROMETRY II 1400 Friday, April 14 Galleries II Chairman: S.H. Knowles Naval Research Laboratory Code 7132 Washington, D. C. 20390	97
BUSINESS MEETING 1700 Friday, April 14 Galleries II	
4. SPECTROSCOPIC INTERFEROMETRY 0830 Saturday, April 15 Galleries I and II Chairman: D.H. Rogstad Owens Valley Radio Observatory California Institute of Technology Pasadena, Calif. 91109	99
5. TECHNIQUES, PLANETS 1330 Saturday, April 15 New York Room Chairman: G.W. Swenson Department of Electrical Engineering University of Illinois Urbana, Ill. 61801	102

COMMISSION 5, Session 1

1400 Thursday, April 13

California Room

PLANETS, SUN

G.A. Dulk, Chairman

1-1 MILLIMETER SOLAR SYSTEM STUDIES AT THE UNIVERSITY OF TEXAS:
B.L.Ulich and J.R.Cogdell, Department of Electrical Engineering,
University of Texas, Austin, Texas

New absolute measurements of the sun, moon, Mercury, Venus, Mars, Jupiter, and Saturn have been made on the recalibrated 16 ft antenna at 3.1-mm wavelength to \approx 8% accuracy. Some new measurements at 8.6 mm and 2.14 mm are also presented. The solar and lunar results are in accord with established values, but the planetary values are higher than published values by about 20%. The calibration procedures and techniques will be discussed in detail. The new values show that the spectra of Mercury and Mars are in accord with simple, lunar-like models. On Venus, a discrepancy between calculated spectra and the new measured value appears, indicating that induced microwave absorption in CO₂ has perhaps not been treated correctly in the mm region. On Jupiter and Saturn, a rapid increase in disk temperature above the ammonia complex is seen indicating a window in the atmospheres between the ammonia and hydrogen infrared lines.

1-2 FURTHER EVIDENCE FOR MILLIMETER-WAVELENGTH SOLAR LIMB BRIGHTENING:
P.N.Swanson, F.L.Wefer, W.J.Decker, and J.P.Hagen, Pennsylvania State University, Department of Astronomy, University Park, Pa.

Observations of the 1970 total solar eclipse at wavelengths of 3.2 mm and 8.3 mm by The Pennsylvania State University indicated a complex limb brightening just inside the optical limb of the sun. Other observations of the eclipse by pencil beam antennas, using the limb of the moon to sharpen the antenna beam, were interpreted to show little or no limb brightening. These apparently contradictory results have been resolved by performing a computer-aided convolution of the antenna patterns of the pencil beam antennas with the complex limb brightening. The radial brightness distribution determined by The Pennsylvania State University was convoluted with the antenna patterns of the National Radio Astronomy Observatory 36-ft antenna operating at 3.6 mm and the Aerospace Corporation 15-ft antenna operating at 3.3 mm; both antenna beams being truncated by the limb of the moon. Initial results of the convolution agree well with the eclipse curves obtained with these antennas during the 1970 eclipse. It is concluded that the complex limb brightening determined by The Pennsylvania State University is compatible with the results obtained by these pencil beam antennas.

1-3 SPECTRAL CHARACTERISTICS OF ACTIVE CENTERS IN THE MILLIMETER WAVELENGTH RANGE: P.M. Kalaghan, Air Force Cambridge Research Laboratories, Bedford, Mass.

High-resolution spectroheliograms taken at radio wavelengths of 9.1 cm, 8.6 mm, and 3.4 mm in 1967-1969 by Stanford University, Air Force Cambridge Research Laboratories, and Aerospace Corporation, respectively, have been analyzed in order to extract the spectral characteristics of individual solar centers of activity. Antenna temperatures, areas, and

COMMISSION 5

fluxes of over 100 active regions observed simultaneously at each wavelength have been tabulated as a function of calendar date as each region migrated across the solar disc. Day-to-day variations in the brightnesses of selected regions are illustrated and employed to infer the corresponding variations of the temperature and electron-density profiles characterizing the gross altitude structure of the region, thereby allowing estimation of the physical conditions occurring within the disturbed region. Specific spectral classifications are suggested and the statistical association of these groupings with proton-flare-producing regions is presented.

1-4 POLARIZATION STRUCTURE OF A SOLAR FLARE REGION AT 9-MM WAVELENGTH: M.R.Kundu, Astronomy Program, University of Maryland, College Park, Md; and T.P.McCullough, U.S.Naval Research Laboratory, Washington, D.C.

Polarization structure of a solar-active region producing a flare around 1900 UT on September 28, 1971, has been measured at 9-mm wavelength using the 85-ft telescope of the NRL Maryland Point Observatory. The flare region underwent considerable changes in the degree of polarization during and after the flare. These changes in the degree of polarization will be discussed in terms of changes in chromospheric magnetic fields.

1-5 HIGH-SPEED OBSERVATIONS OF TYPE III SOLAR BURSTS: S.R.Mosier and J.Fainberg, Goddard Space Flight Center, National Aeronautics and Space Administration, Greenbelt, Md.

Solar-burst observations with time resolutions down to 20 msec have been made at frequencies from 30 to 70 MHz using a new multichannel digital spectrograph at the Clark Lake Radio Observatory in California. A high (8000 bit/sec) data rate and computerized processing have resulted in both high sensitivity and high frequency-time resolution. Of particular interest is the type IIIb burst, first identified by Boischot, which exhibits a highly irregular frequency-time structure within the normal type III frequency-time envelope. Observations of these bursts indicate that the narrow-band structure is due to a coupling or propagation effect rather than a source function and suggest that the source of the structure may be highly localized in the solar corona.

1-6 COMPARISON OF TYPE III SOLAR BURSTS OBSERVED BELOW 100 KHZ TO SIMULTANEOUS MEASUREMENTS OF ENERGETIC PARTICLES IN THE SOLAR WIND: N.Dunkel and R.A.Helliwell, Radioscience Laboratory, Stanford University, Stanford, Calif.

Type III solar bursts observed in the frequency range 20-100 kHz by the VLF experiment on OGO-3 have been compared to simultaneous measurements of solar flare electrons (≥ 45 keV) and protons (≥ 12 MeV) as reported by Lin. VLF data have been examined for 20 examples of prompt solar flare electron events. The fact that type III bursts were observed in all but 3 electron events, whether or not they were accompanied by proton events, suggests that electrons and not protons cause the emissions. The strength of the type III event is usually but not

COMMISSION 5

always related to the flux of solar flare electrons. No counterpart to the long decay (1-2 days) of the electron events has yet been observed in the type III emissions. These observations indicate that type III emission generation is in some way enhanced by the presence of the initial large gradient in the flux of energetic electrons.

1-7 OBSERVATIONS OF LOW-ENERGY SOLAR ELECTRONS ASSOCIATED WITH A TYPE III SOLAR RADIO NOISE BURST: L.A.Frank and D.A.Gurnett, University of Iowa, Iowa City, Iowa

This paper reports on the observation of low-energy solar electrons associated with a type III solar radio noise burst. These observations were made with the University of Iowa charged particle and low-frequency radio instrumentation on the IMP-1 spacecraft. The event discussed originated from an importance-B solar flare which occurred at 0940 UT, April 6, 1970. This event produced a type III radio noise burst which was observed over a period of about 6 hours at frequencies down to 31 kHz with the low-frequency radio receivers on IMP-1. This flare also produced a solar electron event which was observed with the LEPEDEA charged particle instrumentation on IMP-1. The peak intensity of the solar electron emission was about 10^2 electrons $(\text{cm}^2\text{-sec-sr-eV})^{-1}$ at an energy of few kilovolts. During the initial phase of the event, the electron flux is very anisotropic with the peak intensity in the direction of the expected spiral solar wind magnetic field. The observed time delays of the type III radio noise and the solar electrons indicate that the type III noise is produced by electrons with energies of about 3 keV if the radio emission is generated at the electron plasma frequency. From the relative duration of the various phenomena observed, it is believed that the type III radio noise generation is primarily associated with the anisotropic "leading edge" of the solar electron emission. No evidence was found of enhanced electron plasma oscillation intensities during this event as has been proposed in some theories of type III radio noise generation.

1-8 GYRO-SYNCHROTRON RADIATION BY A CHARGED PARTICLE IN A MAGNETO-PLASMA: H.C.Ko, H.S.King, and C.D.Chuang, Ohio State University, Columbus, Ohio

The expressions for the emissivity and the electromagnetic field generated by an electron spiralling in an ambient magnetoionic medium are derived using the Hamiltonian method and by the method of stationary phase. Dispersion effect is fully taken into account throughout the theoretical analysis. The errors in the previously published work by others are pointed out, and their reasons are given. The expression for the electromagnetic field also allows us to calculate the actual power flow in the ray direction instead of the wavenormal direction. A computer program has been developed to calculate the emission spectra for various physical models showing the Razin effect. The relevance of these results to the interpretation of the radio spectrum of the solar burst and other cosmic radio radiation is discussed.

COMMISSION 5

1-9 HIGH-POWER, HIGHLY DIRECTIONAL DECAMETRIC RADIATION FROM JUPITER:
N.Brice and T.McDonough, Cornell University, Ithaca, N.Y.

A means of producing high-power and highly directional decametric radiation from Jupiter is presented. The concept of a quasi-stable limit for plasma instabilities is introduced for waves near the ionosphere in magnetic flux tubes connected to the satellite Io. The outer boundary of these flux tubes meets the ionosphere in an ellipse, and the decametric radiation is beamed along the major axis of this ellipse and in the plane of constant magnetic fields. Large-amplitude waves are obtained through reflections at the edges of an amplifying region, so that waves pass many times through this region and are amplified on each pass.

1-10 FAST POLARIZED PULSE REVERSALS IN DECAMETER-WAVE RADIATION FROM THE SUN AND JUPITER: C.H. Barrow, Department of Physics, University of the West Indies, Kingston, Jamaica, W.I.

Solar Type III bursts have been observed at fixed frequencies close to 18 MHz (left- and right-hand polarization components) and 22 MHz (total power). Fast pulses, having durations of the order of 1 msec, have been detected superimposed on some of the Type III bursts by using techniques previously established for the study of similar phenomena in the radiation from Jupiter. The pulses are narrow band and may appear to be unpolarized unless examined with sufficient time resolution when they often display polarization reversals. These pulses are very similar to those which sometimes occur in the decametric radiation from Jupiter and the possible significance of this is discussed.

COMMISSION 5, Session 2

0900 Friday, April 14

Galleries II

LONG-BASELINE INTERFEROMETRY I

K.I. Kellermann, Chairman

2-1 THE NRAO MARK II TAPE RECORDER INTERFEROMETER SYSTEM: B.G. Clark, National Radio Astronomy Observatory, Green Bank, W.V.

The heart of the NRAO Mark II system is the Ampex VR 660C television-type tape recorder. The signals from the two interferometer elements are clipped (one bit digitized), sampled at a 4-MHz rate, and recorded on tape. At playback time, the data are recovered, buffered to recover time synchronism, and phase-rotated to remove the natural fringe rate of the interferometer. The two rectified data streams are multiplied in a multichannel correlator to produce the eventual interferometer output. The playback system includes an extensive system of software as well as the hardware. This system allows data to be processed in several modes; which is most efficient depends on the strength of the radio source being observed. As examples of the functioning of the instrument and of the various forms of data presentation, some results are presented of a three-element interferometer experiment of June 1971, involving the NASA 65-m telescope at the Goldstone Tracking Facility in California, the NRAO 43-m telescope at Green Bank, West Virginia, and the 22-m telescope of the Crimean Astrophysical Observatory. The long baselines, at the 3.5-cm wavelength, amount to about 2.7×10^8 wavelengths. The fact that fringes are seen at all, as they are on 11 sources, implies angular sizes smaller than about 0.0006 sec of arc. Various models will be discussed briefly with angular scales as small as 0.0004 sec of arc and brightness temperatures approaching 10^{13} K.

2-2 LONG-BASELINE SPECTRAL LINE INTERFEROMETRY: J.M. Moran, Smithsonian Astrophysical Observatory, Cambridge, Mass.

Interferometric observations of galactic OH and H₂O sources have been made using the Mark I and Mark II digital recording systems of the National Radio Astronomy Observatory. The observations of OH in the 18-cm ground state made between Haystack, NRAO, and Onsala, Sweden have yielded maps showing the distribution of emission features for the sources in W3 (OH), W49, and NML Cygnus. The observations of H₂O at 1.35 cm between Haystack, NRL and NRAO, and the Crimean Astrophysical Observatory have yielded maps of the emission features in W49, Orion, and W3 (OH). The smallest H₂O feature measured was the one at -1.8 km/sec in W49 which was 0.0003 in diameter. Among the OH sources the feature in W3 at -43.7 km/sec which was 0.005 was the smallest. There is a general similarity between the map of the right circularly polarized OH features in W3 (OH) and the map of the H₂O features which are unpolarized.

2-3 RECENT MICROWAVE OBSERVATIONS OF THE STRUCTURE OF COMPACT RADIO SOURCES: J.J. Broderick, Arecibo Observatory (NAIC), Arecibo, Puerto Rico

In the past year a series of transcontinental very-long-baseline experiments have been performed at wavelengths between 21 and 3 cm. The goal of these has been to determine the source structure of the stronger

compact extragalactic sources, although for the 21-cm experiment positional information was the prime interest. In this talk I will discuss the structure of some of the sources observed as a function of the observing wavelength and the epoch of observation. For some of the sources (e.g., 3C273 and 3C279) the structure is considerably variable in both respects. The variation of structure with wavelength can be interpreted as the result of different components dominating the brightness distribution at different wavelengths. The temporal variations are stronger at shorter wavelengths and can be interpreted as expansions (ultrarelativistic in some cases), but relatively simple models of component flux variation can also suffice.

2-4 HIGH-RESOLUTION OBSERVATIONS OF COMPACT RADIO SOURCES AT CENTIMETER WAVELENGTHS: G.E. Marandino, G.M. Resch, N.R. Vandenberg, University of Maryland, College Park, Md.; T.A. Clark, Goddard Space Flight Center, NASA, Greenbelt, Md.; H. Hinteregger, C. Knight, D. Robertson, A. Rogers, I. Shapiro, A. Whitney, MIT, Cambridge, Mass.; and R. Goldstein, D. Spitzmesser, Jet Propulsion Laboratory, Pasadena, Calif.

A number of compact radio sources have been obtained during the course of several experiments dating from July 1970 to the present. The bulk of these experiments were at 3.8 cm between the Haystack (120 ft) and the MARS (210-ft) antennas. Changes in the fine-scale structure of the quasars 3C273B and 3C279 (Knight *et al.*, *Science* 172: 52, 1971, and Whitney *et al.*, *Science* 173: 225, 1971) indicate that both sources are still evolving and now show evidence for changes in the relative amplitudes of components when interpreted as double source models. The changes in the visibility function of 3C279 from the most recent observations can no longer be modeled in terms of the simple expanding symmetrical double source which fit the earlier data. First epoch observations have been made on 3C345 and NRAO 512 with limited hour angle coverage. The 3C345 observations serve to distinguish between the two models presented by Cohen *et al.* (*Ap. J.* 170: 207, 1971). NRAO 512 shows structure at the millisecond of arc level. Extensive observations of other sources including 3C84, 4C39.25, 3C274, and VRO 42.22.01 are presented and compared with simple source models.

2-5 METER-WAVELENGTH SPECTRAL OBSERVATIONS OF COMPACT RADIO SOURCES BY VLBI: G.M. Resch and W.C. Erickson, University of Maryland, College Park, Md.; T.A. Clark, GSFC, NASA, Greenbelt, Md.; and S.H. Knowles, Naval Research Laboratory, Washington, D.C.

A program is under way utilizing VLBI techniques to measure the low-frequency spectra of radio sources, particularly those sources that show evidence of low-frequency cutoffs in their spectra. We have employed an interferometer consisting of the 300-ft antenna at Greenbank, W. Va., and the 150-ft antenna at Sugar Grove, W. Va. For most sources the resultant baseline of 50 km provides enough resolution to mask extended source components but not so much as to resolve the compact sources. Sensitivity depends on the frequency and recording system but typically ranges from 0.05 - 1.0 flux units. The initial experiments at frequencies of 111 and 196 MHz (with fringe spacings of $\sim 8''$ and $4.5''$) have yielded fluxes of compact components in sources such as 3C84, 3C273, 4C39.25, 0735 + 17, etc. In general these fluxes appear

COMMISSION 5

to be higher than one would predict from simple synchrotron self-absorption. Observations are continuing on a regular basis to ascertain the effects of interplanetary and interstellar scattering.

2-6 DECAMETRIC-WAVELENGTH VERY LONG BASELINE INTERFEROMETRY: S.D. Shawhan, University of Iowa, Iowa City, Iowa; T.A. Clark, GSFC, NASA, Greenbelt, Md.; W.M. Cronyn, National Oceanic and Atmospheric Administration, Boulder, Colo.; J.P. Basart, Iowa State University, Ames, Iowa

A series of three VLBI experiments at 26 MHz have been carried out. The October-November 1970 results from the 265-km Boulder-Haswell, Colorado, baseline will be reviewed. Definite fringes have been obtained on at least 19 3C sources: 2, 23, 43, 48, 55, 66, 71, 123, 144, 147, 153, 154, 186, 190, 191, 196, and 196.1, 456, and 459. New results from the August 1971 Boulder-Haswell and 950-km Boulder-Ames, Iowa, baselines will be presented and compared to the previous results. Boulder-Ames fringes have been obtained on 3C48, 3C144, and 3C459.

2-7 VLBI OBSERVATIONS OF PULSARS: T.A. Clark, GSFC, NASA, Greenbelt, Md.; J.J. Broderick, National Astronomy and Ionosphere Center, Arecibo, P.R.; W.C. Erickson and N.R. Vandenberg, Astronomy Program, University of Maryland, College Park, Md.; and S.H. Knowles, Naval Research Laboratory, Washington, D.C.

Beginning in November 1971, VLBI observations have been made at monthly intervals to monitor the apparent angular size of NPO532. The Arecibo 1000-ft antenna, the NRAO 300-ft antenna, and the NRL Sugar Grove 150-ft antenna were used at 196 and 111 MHz. The purpose of this experiment is to correlate changes in the apparent size of the source with the changes in the scattering in the intervening media which are being observed by Counselman and Rankin (BAAS 3:383, 1971, and Ap. J. 166: 513, 1971), and extends our previous observations of NPO532 (Erickson *et al.*, BAAS 3:463, 1971, and Ap. J., in press). Observations of several of the pulsars have been made utilizing the MK-I system and a gated cross-correlation reduction program. PSR 0950 appeared to be partially resolved on the longer baseline, yielding an apparent angular diameter of about 0.05-0.1 sec of arc. This must be a result of scattering in the interstellar and/or interplanetary media. No large fringe phase perturbations of this type reported by the Canadian VLBI group on PSR 0329 have been observed.

2-8 LBI STUDIES OF A PULSAR: J.A. Galt, Dominion Radioastrophysical Observatory, Penticton, British Columbia; N.W. Brotan, T.H. Legg, and J.L. Locke, National Research Council, Ottawa, and J.L. Yen, University of Toronto, Toronto, Ontario, Canada

Pulsar PSR 0329 + 54 has been observed interferometrically between Algonquin and Penticton using video tape recordings of up to an hour in length. The RF band 408-412 MHz was recorded and later played back repeatedly through narrowband (200-KHz) filters to produce a set of fringe patterns at adjacent frequencies. Fluctuations in fringe phase can be seen between adjacent frequencies in the video band, indicating a rather larger scattering angle than would be predicted either from the decorrelation bandwidth or from the diffraction-pattern scale size.

COMMISSION 5, Session 3

1400 Friday, April 14

Galleries II

LONG-BASELINE INTERFEROMETRY II

S.H. Knowles, Chairman

3-1 ASTROMETRIC RESULTS FROM VLBI OBSERVATIONS OF EXTRAGALACTIC RADIO SOURCES: A.R. Whitney, H.F. Hinteregger, C.A. Knight, D.S. Robertson, A.E.E. Rogers, I.I. Shapiro, Massachusetts Institute of Technology, Cambridge, Mass.; T.A. Clark, Goddard Space Flight Center, NASA, Greenbelt, Md.; G.E. Marandino, N.R. Vandenberg, University of Maryland, College Park, Md.; and R.M. Goldstein, Jet Propulsion Laboratory, Pasadena, Calif.

Three techniques have been used to determine source positions from VLBI observations. These are based on fringe-rate, fringe-phase, and differential (wideband) group-delay measurements. The accuracies achieved from these different approaches range from ~ 0.5 down to ~ 0.05 sec of arc. Substantially higher accuracy is anticipated with further development of the techniques. Recent results will be presented along with a description of the electronic systems and data-reduction methods employed.

3-2 INTERFEROMETRIC OBSERVATIONS OF AN ARTIFICIAL SATELLITE: R.A. Preston, R. Ergas, H.F. Hinteregger, C.A. Knight, D.S. Robertson, I.I. Shapiro and A.R. Whitney, Massachusetts Institute of Technology, Cambridge, Mass.; A.E.E. Rogers, Haystack Observatory, NEROC, Westford, Mass.; and T.A. Clark, Goddard Space Flight Center, NASA, Greenbelt, Md.

Very-long-baseline interferometric observations of radio signals from the TACSAT synchronous satellite were made at 7.3 GHz between Haystack, NRAO (140 ft) and Owens Valley (90 ft) in October 1969. Even though extending over only seven hours, these observations have enabled an excellent orbit to be deduced. Precision in differential delay and delay-rate measurements reached 0.15 nanosec and 0.05 picosec/sec, respectively, in this initial experiment, thus demonstrating the feasibility of VLBI satellite geodesy.

3-3 A METRIC PROGRAM OF VERY-LONG-BASELINE ASTRONOMY: P.D. Hemenway, University of Virginia and National Radio Astronomy Observatory, Charlottesville, Va.

A VLBI program is under way to gather astrometric and geodetic information using the interferometers at Green Bank, West Virginia, and Owens Valley, California. The "four-antenna" technique is used to eliminate clock phase variations. The current status of the program, its application to various astronomical and geodetic problems, and the expected accuracy will be briefly discussed.

3-4 RADIO INTERFEROMETRIC MEASUREMENTS OF UNIVERSAL TIME VARIATIONS AND EQUATORIAL COMPONENTS OF AN INTERCONTINENTAL BASELINE: J.L. Fanselow, P.F. MacDoran, J.B. Thomas, J.G. Williams, and D.J. Spitzmesser, Jet Propulsion Laboratory, Pasadena, Calif.; L. Skjerve, Philco-Ford Corporation, Barstow, Calif.; and J. Urech, Instituto Nacional de Tecnica Aeroespacial, Madrid, Spain

During the summer 1971, a series of independent station radio interferometric observations were conducted between two stations of the Deep Space Network (DSN), the 64-m station at Goldstone, California, and the 26-m station at Madrid, Spain. Using a 24-kHz bandwidth and hydrogen-maser frequency systems, ten or more extragalactic radio sources were observed at S-band over a period of several weeks. Simultaneous solutions are being performed in order to determine the variations in UT1, the positions of the sources, and the equatorial components of the Goldstone/Madrid baseline. This baseline has been directly compared with DSN station locations derived from spacecraft tracking. Preliminary results of these experiments will be presented.

3-5 SOURCE POSITIONS AND BASELINE FROM GOLDSTACK OBSERVATIONS: M.H. Cohen, California Institute of Technology, Pasadena, Calif.

Observations were made in February 1971 on the Goldstack interferometer at $\lambda = 3.8$ cm, using Mark I VLB terminals with a bandwidth of 330 kHz and an integration time of 160 sec. The fringe-rate residuals have been analyzed for the baseline and the positions of the radio sources. A number of positions are determined to $\pm 0''.2$. Independent determinations of the equatorial projection of the baseline give values differing by 1 part in 10^6 .

3-6 HIGH-FREQUENCY OBSERVATIONS OF THE OMEGA NEBULA: K.J. Johnston, E.O. Hulbert Center for Space Research, Naval Research Laboratory, Washington, D.C.; and R.W. Hobbs, Laboratory for Solar Physics, Goddard Space Flight Center, NASA, Greenbelt, Md.

Observations of the very complex M17 (NGC 6618) region, which covers an area of nearly one square degree, show that it is composed entirely of thermal sources. Contour maps made with the 85-ft Maryland Point antenna were integrated to yield flux densities of 610, 624, and 644 f.u., with standard deviations of 10%, at wavelengths of 0.955, 1.65 and 2.73 cm, respectively.

3-7 21-CM OBSERVATIONS IN THE DIRECTIONS OF GLOBULAR CLUSTERS: F.J. Kerr and G.R. Knapp, Astronomy Program, University of Maryland, College Park, Md.

Globular clusters are not usually considered to be interesting objects in radio astronomy. However, we have used 21-cm observations in the direction of globular clusters for three purposes: (i) Some high-velocity calcium lines have been seen in the optical spectra of several globulars. We have looked for 21-cm lines at the same velocities in an attempt to obtain new evidence on the distance or character of the high-velocity hydrogen clouds. (ii) Globular clusters are convenient objects outside the galactic interstellar layer for obtaining the ratio of the column densities of gas and dust over the same line of sight. We have done this for the hydrogen-to-dust ratio, and plan similar measurements for several molecular species. (iii) Observations at the optical velocities of the clusters themselves have enabled us to set new lower limits for the amount of neutral hydrogen in several globulars, which are valuable for theories of mass loss from stars.

COMMISSION 5, Session 4

0830 Saturday, April 15

Galleries I and II

SPECTROSCOPIC INTERFEROMETRY

D.H. Rogstad, Chairman

4-1 A COMPARISON OF THE H I PROPERTIES OF FIVE SCD GALAXIES:

D.H. Rogstad and G.S. Shostak, Owens Valley Radio Observatory, Pasadena, Calif.

Neutral hydrogen studies of the five Scd galaxies M33, NGC 2403, IC342, M101, and NGC6946 have revealed substantial similarities in their radial hydrogen distributions and rotation curves. If we define the extent of the galaxy by its Holmberg diameter, we find that 80% of the observable H I lies within this boundary. The fractional H I mass contained therein is a constant, with a mean value of 8.8%. The central H I surface density is also a constant within this classification. We find that all the H I global properties and ratios are constant or scale with the Holmberg radius and/or the mass. Because of the very flat rotation curves observed for all these Scd objects, total masses are not known. Surface mass-luminosity ratios must reach values of ~ 20 at the Holmberg radius.

4-2 HYDROGEN-LINE APERTURE SYNTHESIS OF AN EXTERNAL GALAXY: M.C.H.

Wright, National Radio Astronomy Observatory, Charlottesville, Va.

Aperture-synthesis techniques are now enabling us to resolve the spiral structure of nearby late-type galaxies. Observations in the neutral hydrogen line provide us with a map of the brightness distribution which is usually interpreted as a map of the H I surface density distribution. Detailed comparisons between the gas and stellar distributions can be made on the scale of the spiral arms. Recent H I observations of M33 show a neutral hydrogen feature which follows the line of the optical spiral arm but whose brightest concentrations do not correspond one-to-one with the optical features. Spectral line observations also yield radial velocity information which enable maps of the isovelocity and velocity dispersion to be constructed. A velocity resolution commensurate with the angular resolution gives us the details of the kinematics of the galaxy and, in particular, a test of the predictions of the density-wave theory of spiral structure. It is to be expected that the present epoch of observations should provide us with a new understanding of late-type galaxies and the process of star formation.

4-3 21-CM H I OBSERVATIONS OF A PECULIAR DARK CLOUD: S. C. Simonson, III, Astronomy Program, University of Maryland, College Park, Md.

The Sharp-edged dust cloud, Khavtassi 713, whose densest part is Lynds 379, at $\ell = 17^\circ, b = -3^\circ$, has been noted for its association with filamentary H α emission nebulae and radio continuum sources. The Dwingeloo 21-cm line survey reveals a neutral hydrogen feature at a mean velocity $V = 21$ km/sec conforming in shape and position to Kh 713 and possessing a velocity gradient in latitude $dV/db = -2.7$ dm/sec/deg. Stellar data indicate the distance to Kh 713 is about 1 kpc, which would make its size 25×50 pc, its neutral hydrogen mass $3400 M_{\odot}$, its kinetic energy associated with the velocity gradient 2×10^{47} sec 2 erg, and its expansion age $6 \times 10^6 \cot \theta$ years, where θ is the angle between the line

COMMISSION 5

of sight and the velocity vector. The resemblance of Kh 713 to certain bright-rimmed dark clouds near H II regions suggests that the velocity gradient resulted from interaction with an H II region whose exciting stars are no longer visible. The apparent involvement with H α filaments and continuum sources suggests that at least two early-type stars equivalent to O9V are now present in the nebula.

4-4 APERTURE SYNTHESIS OF INTERSTELLAR NEUTRAL HYDROGEN IN ABSORPTION:
E.W. Greisen, California Institute of Technology, Pasadena, Calif.

The Owens Valley Radio Observatory interferometer has been used to carry out a program of aperture synthesis in the interstellar neutral hydrogen absorption line. Maps having resolutions of 1 kHz and about 1.3 arc min have been produced using a novel Fourier inversion procedure. The Perseus Arm feature in the spectrum of Cassiopeia A shows a very large amount of hydrogen and a complicated structure. For example, at one frequency the optical depths range from greater than 7.0 on one side of the source to around 1.0 on the other side. About 3 km/sec from this frequency, a similar range of optical depths is found, but with the direction of the spatial variation reversed. The hydrogen appears to occur partly in small condensations within large clouds. The Perseus Arm feature in the spectrum of Cygnus A contains little hydrogen but shows considerable structure. The largest optical depths are greater than 0.5, but over much of the source the peak optical depths are only about 0.1. The absorption features in the spectra of the Crab Nebula and 3C353 both contain considerable amounts of hydrogen, but only that of the Crab Nebula shows any significant structure. The results of the program point out the importance, in observations of this sort, of extremely careful calibration.

4-5 INTERFEROMETRIC SPECTRAL LINE OBSERVATIONS OF CONTINUUM SOURCES NEAR THE GALACTIC PLANE: D.A. Elliott, S. Gottesman, C. Heiles, K.W. Riegel, and M.C.H. Wright, Department of Astronomy, University of California, Los Angeles, Calif.

We have observed 11 continuum sources, mostly close to the galactic plane, in the 21-cm spectral line using the NRAO 3-element interferometer. For the two northerly sources Cas A and Cyg A we can do a complete two-dimensional aperture synthesis to a resolution of ~ 1 min with some information in small structure to a resolution of about 20 sec. For the rest of the sources on the program, including W49, W51, M8, M17, Ori A, Ori B, Taurus A, 3C353 and 3C358, coverage of the uv plane was only sufficiently complete to allow a one-dimensional synthesis to the same resolution. Velocity resolution varies from source to source depending on the breadth of the H I line profile, from a maximum resolution of $\sim 1/6$ km/sec to a minimum of 1.3 km/sec. There is sufficient angular resolution to show structure at the maximum distance of the Orion continuum sources as small as 30,000 AU, with correspondingly lower sizes for material which is along the line of sight but closer. Even for the most distant galactic sources, structure as small as 3 pc at the sources W49 and 3C358 is resolvable. Physical properties of the interstellar medium between us and the sources, and associated with the discrete sources themselves, are discussed.

4-6 INTERFEROMETRIC OBSERVATIONS OF FORMALDEHYDE ABSORPTION IN FRONT OF STRONG GALACTIC SOURCES: E.B. Fomalont, National Radio Astronomy Observatory, Greenbank, W.Va.; and L.N. Weliachew, Owens Valley Radio Observatory, Pasadena, Calif.

Observations have been made of formaldehyde absorption at 4830 MHz in front of Sgr A, Sgr B2, W3, NGC 2024, W31, W33, W43, W49, and W51. The Caltech interferometer, consisting of two 90-ft paraboloids, was used to synthesize a beam of 40×60 sec in position angle 90° . The main absorption features show variations of optical depth over the sources, but there is no significant clumping. The isotopic ratio C^{12}/C^{13} of 10 for Sgr A and Sgr B2 should be increased to $\sim 25 \pm 5$ for Sgr A and ≥ 25 for Sgr B2 because of the high optical depths at the center of the absorbing clouds; $\tau_{\max} \sim 2.0$ for Sgr A, $\tau_{\max} \gtrsim 4$ for Sgr B2. The $+40$ km/sec cloud associated with Sgr A appears to be rotating as a solid body. The mass of the cloud is calculated to be $\sim 3 \times 10^5 M_\odot$. From hydrogen absorption data only a small proportion of the cloud is composed of atomic hydrogen, hence the cloud consists mainly of molecular hydrogen with a density $\sim 10^5 \text{ cm}^{-3}$.

4-7 H₂O INTERFEROMETRY AT BERKELEY: R. Hills, M. Janssen, D.D. Thornton, and W.J. Welch, Radio Astronomy Laboratory, University of California, Berkeley, Calif.

A high-frequency spectral-line interferometer has recently begun operation at the Hat Creek Observatory of the University of California. The instrument consists of a 6-m reflector and a 3-m reflector with a fixed separation of 265 m. Operation is in the frequency range 20-26 GHz, either in the continuum or with a multichannel receiver with up to 128 channels. The interferometer is intended primarily for position measurements. In particular, it is being used to study the absolute positions of the principal interstellar water vapor sources, the water line frequency being 22.2 GHz. The baseline calibration is based on continuum observations of about 10 compact extra galactic radio sources. The lobe width of the interferometer is approximately 10 sec of arc at the instrumental meridian, and both the available signal/noise and the position accuracy of the calibrators permit measurement of the water vapor source positions with about 1 sec of arc uncertainty.

4-8 GALACTIC SPECTRAL LINE INTERFEROMETRY: Carl Heiles, Astronomy Department, University of California, Berkeley, Calif.

Spectral line interferometry is producing new, exciting results which are interesting in themselves. However, our ultimate goal is to contribute to astronomical and astrophysical knowledge. Given existing and anticipated instruments, we see three general areas in which the high angular resolution is particularly important; they tend to be associated with different observational techniques. These three areas include interstellar chemistry and organic chemistry; the study of protoplanetary systems; and the study of pre-protoplanetary systems. The study of chemistry is highly complementary to the others, since it can yield information on physical conditions prevailing not only at present but also in the past. However, presenting such complete physical pictures will require time-consuming studies in many chemical species and sometimes in several transitions of a given molecule.

COMMISSION 5, Session 5

1330 Saturday, April 15

New York Room

TECHNIQUES, PLANETS

G. W. Swenson, Chairman

5-1 THE MICROWAVE SPECTRUM OF MARS: J.N.Cuzzi and D.O.Muhleman,
California Institute of Technology, Pasadena, Calif.

A thermophysical model of Mars refined from that of Leighton and Murray is used to make numerical calculations of expected microwave spectra. It is found that the observable spectra of Mars, calculated for the last four oppositions, are flat from a few mm to 21 cm to within the accuracy of present data. An average value of observed temperature is obtained for each opposition by averaging all the observations over wavelength and is found to match computed spectra quite well without adjustment of the independently determined model parameters. This result is primarily due to subsurface temperature effects existing near polar regions and varies slightly due to varying polar cap extent and geocentric aspect from one opposition to the next. In addition, the model reproduces the infrared temperature-versus-latitude data of Sinton and Strong to within experimental error. We suggest that the agreement of observables calculated from this lunar-type model with the data is sufficiently good to minimize the likelihood of the existence of liquid water near the Martian surface. The electrical loss tangent was varied over a range of .005 to .015, chosen as limits for dry, particulate geological materials and the entire range is found to be consistent with the microwave data. Final values of our parameters are: thermal inertia = .006 effective dielectric constant = 2.5 ± 0.25 , Band albedo = 0.25, infrared emissivity = 0.90.

5-2 LINEARLY POLARIZED RADIATION FROM VENUS AND MARS AT 8 GHS: E.T. Olsen and H.D. Aller, University of Michigan, Ann Arbor, Mich.

The polarizations and flux densities of Venus and Mars were observed during the 1969 inferior conjunction and 1971 opposition, respectively. Polarized radiation was detected from both planets. The instrumental polarization of the University of Michigan 85-ft paraboloid was determined from observations of galactic H II regions; Cassiopeia A was used as the primary flux density standard. Venus had a measured disk temperature $T_D = 676 \text{ K} \pm 34 \text{ K}$ and a degree of polarization $P = 0.228\% \pm 0.052\%$ at a position angle of $4^\circ \pm 7^\circ$ measured eastward from the Venusian pole. Mars, at an average distance of 1.385 AU from the sun, had a disk temperature of $T_D = 197 \text{ K} \pm 10 \text{ K}$ and $P = 1.41\% \pm 0.32\%$ at a position angle of $110^\circ \pm 6^\circ$ relative to the Martian pole. All uncertainties are standard errors and include a 5% uncertainty in the telescope gain calibration and the uncertainty in the instrumental polarization of less than 0.02%. Possible implications of these results will be discussed.

5-3 ON APERTURE SYNTHESIS WITH WAVELENGTHS AS SHORT AS 10 MICRONS;
David Cudaback, Radio Astronomy Laboratory, University of California, Berkeley, Calif.

Information gathered from the literature has been combined with new measurements of interferometer phase fluctuations at Hat Creek and

COMMISSION 5

water vapor fluctuations at White Mountain to calculate the differential phase paths for proposed interferometers. The calculations are presented with altitude and wave length as parameters. When the differential paths are greater than are tolerable for conventional interferometry, as defined by Hinder and Ryle, Jennison's technique of 1958 can be used to determine relative phases of different spatial frequencies. Jennison's technique will permit determination of brightness distributions but not absolute positions. When using that technique the bandwidth must be limited so the beams come together within their region of coherence. We specify this maximum bandwidth as a function of altitude and wavelength.

5-4 A NEW HIGH-POWER, DUAL-POLARIZED LINE FEED FOR THE ARECIBO SPHERICAL REFLECTOR: L.M.LaLonde, Cornell University, Ithaca, N.Y.; and A.W.Love, North American Rockwell Corporation, Downey, Calif.

A high-power, dual-polarized, 430-MHz line feed for the 1000-ft. diameter spherical reflector has been constructed following a design by Love. The feed was installed in January 1972, and the performance of the antenna illuminated by the full-scale feed is identical to that predicted from computed performance using an aperture distribution measured from a model scaled at a factor of 6.5. The new feed provides an increase in aperture efficiency over the previous square line feed by 3.8 dB. The on-axis gain at the zenith is 60 dB with an aperture efficiency of 53%. Sidelobe levels are 3-4% of the peak gain, and the feed bandwidth is in excess of 8 MHz at 1-dB points. The vignetting loss at maximum zenith angle (20°) is approximately 4 dB. The feed handles full-peak and average powers of 2.5 MW and 150 kW respectively, transmitting on either circular or linear polarizations and receiving the orthogonal polarization. Isolation between receive and transmit ports is in excess of 30 dB.

5-5 THE ITAPETINGA MILLIMETER-WAVE RADIO TELESCOPE IN BRAZIL: Pierre Kaufmann, Universidade Mackenzie, São Paulo, Brazil; R.D'Amado, ESSCO, Concord, Mass.; and M.L.Meeks, NEROC Haystack Observatory, Westford, Mass.

The 45-ft diameter (13.7-m) precision radio telescope at the Itepetinga Radio Observatory, Atibaia, Brazil, was completed December 1971 and is operated by Centro de Rádio Astronomia e Astrofísica, Mackenzie University, São Paulo. The antenna (constructed by ESSCO) consists of a paraboloidal reflector with a Cassegrain subreflector, supported on an azimuth mount and enclosed in a spaceframe radome, 22 m in diameter. The total aperture blockage, space frame plus subreflector and quadripod, amounts to about 7%. The radome membrane, 0.75 mm in thickness, reduces the signal by less than 0.5 dB up to a frequency of 20 GHz and has resonant peaks with 2-dB loss at 60, 170 and 280 GHz. These losses are primarily reflective, and the maxima fall in frequency regions where the atmosphere is opaque. The telescope is situated about 40 miles north of São Paulo in a bowl, 800 m above sea level, in a comparatively dry climate, the mean content of precipitable water averaging 20 mm in winter (July) and 40 mm in summer (January). The telescope is currently undergoing calibration and is expected to be effective down to 3-mm wavelengths. A program involving VLBI measurements of 22-GHz water-vapor

COMMISSION 5

sources is planned with Haystack Observatory, the baseline being 7294 km in length with the approximate direction LHA = -5^h and declination $\delta = -70^\circ$.

5-6 A 65-METER TELESCOPE FOR MILLIMETER-WAVE RADIO ASTRONOMY: S.von Hoerner and J.W.Findlay, National Radio Astronomy Observatory, Green Bank, W.Va.

The design of a 65-m (213-ft) diameter fully steerable radio telescope is described. The instrument is intended to work satisfactorily at wavelengths as short as 3.5 mm (86 GHz) under benign atmospheric conditions. It is an azimuth-elevation instrument, designed to work in the open air. The principle of homologous deformation is applied to minimize the effects of gravitational deflections; a novel pointing system is used, and considerable care has been taken to analyze the effects of wind and temperature on the telescope performance. The telescope can be used with either Cassegrain or prime-focus optics. The methods by which the design can provide the high surface accuracy and the precise pointing precision required of such an instrument are described in some detail, and the expected effects of the environment on these characteristics are discussed. The requirements that a site for such a telescope must meet are stated, and present-day cost estimates are given. The work discussed has been carried out by a group of scientists and engineers associated with NRAO; two only from this group have been selected as authors.

5-7 ESTIMATING THE CONFUSION LIMIT OF A RADIO TELESCOPE WITH HIGH SIDELobe LEVELS: J.R.Fisher, Astronomy Program, University of Maryland, College Park, Md.

Most methods for the estimation of the confusion limit of a radio telescope have only been concerned with the effect of unresolved sources in the main beam. Development of the Clark Lake array has demanded that the contribution of sidelobes to the confusion problem be studied in detail. This array is a thin-armed "Tee" where main beam area is very small but it suffers from high sidelobe levels due to an incremental phasing scheme. An analytical method for calculating the "confusion noise" will be outlined with an arbitrary antenna pattern and a random spacial distribution of sources having a known number-versus-intensity relationship. A specific example will be demonstrated using Clark Lake array and the log N-log S curve from the 5C catalog.

5-8 THE HARVARD MINICORRELATOR: J.A.Ball, Harvard College Observatory, Harvard, Mass.

A one-bit digital cross-correlator for use in radio astronomy was designed and built at Harvard. Only 16 channels (lags) were built in hardware, however a recycling scheme allows the incoming bits to be processed through the correlator several times over to multiply the number of hardware channels by a factor which may be quite large at low sample rates. For example, for a spectral window of 400 kHz, 112 lags can be computed and for 125 kHz, 400 lags. To do this the correlator is connected to a minicomputer (Supernova) for both input and output and so is treated as a peripheral processor. The same computer performs the Fourier transforms and displays the spectra.

COMMISSION 5

5-9 CROSS SPECTRUM INTERFEROMETRY: J.L.Yen, University of Toronto, Toronto, Ontario, Canada

The correlation spectrometer and the filter spectrometer have been the two main instruments for radio spectral line observations. In spectral line interferometry the correlation spectrometer is more commonly employed. With the rapid development of high-speed digital integrated circuits in recent years, it has become possible to build special-purpose computers for computation of the Fourier spectrum of signals at real-time data rates sufficiently fast for radio spectral line observations. This approach is particularly attractive for spectral line interferometry because one can evaluate the complex Fourier spectra of each of the signals, multiply to obtain the cross spectrum and the integrate. Thus the complex visibility of a source distribution is obtained. Important aspects of the use of Fast Fourier Transform computer in spectral line observations and cross-spectrum interferometry are discussed. Comparison with spectrometers of other types, in particular for use in interferometry, is also given. The variety and flexibility possible in the design and possible applications in both spectral line and continuum long baseline interferometry and in multi-element interferometry are emphasized. Finally, we describe an example of a cross-spectrum interferometer.

COMMISSION 6

RADIO WAVES AND TRANSMISSION INFORMATION

L. B. Felsen, Chairman

<u>Sessions</u>	<u>Page</u>
1. TRANSIENT PHENOMENA 1345 Thursday, April 13 Pan American Room Chairman: T.B.A. Senior 2216 Space Research Building 2455 Hayward Street Ann Arbor, Mich. 48105	108
BUSINESS MEETING 1700 Thursday, April 13 Pan American Room	
2. BEAMS AND OPEN RESONATORS 0900 Friday, April 14 Pan American Room Chairman: G.A. Deschamps Electrical Engineering Department University of Illinois Urbana, Ill. 61801	112
3a. NONLINEAR AND STOCHASTIC PHENOMENA 1020 Friday, April 14 Pan American Room Chairman: N. Marcuvitz School of Electrical Engineering New York University 181st & University Avenue New York, N.Y. 10453	114
3b. STOCHASTIC ASPECTS OF WAVE PROPAGATION 1400 Friday, April 14 (till 1800) Pan American Room Chairman: N. Marcuvitz School of Electrical Engineering New York University 181st & University Avenue New York, N.Y. 10453	117
4. NUMERICAL METHODS 1400 Friday, April 14 Massachusetts Room Chairman: K.K. Mei Department of Electrical Engineering and Computer Science University of California Berkeley, Calif. 94720	121

COMMISSION 6

<u>Sessions</u>	<u>Page</u>
5. ADAPTIVE ARRAYS 0830 Saturday, April 15 Pan American Room Chairman: A.A. Ksieinski ElectroScience Laboratory Ohio State University 1320 Kinnear Road Columbus, Ohio 43212	125
6. DIFFRACTION 0830 Saturday, April 15 New York Room Chairman: L.B. Felsen Polytechnic Institute of Brooklyn Graduate Center/Route 110 Farmingdale, N.Y. 11735	129
7. ANTENNAS AND ARRAYS 1330 Saturday, April 15 Pan American Room Chairman: D.K. Cheng Electrical Engineering Department Syracuse University Syracuse, N.Y. 13210	134

COMMISSION 6, Session 1

1345 Thursday, April 13

Pan American Room

TRANSIENT PHENOMENA

T.B.A. Senior, Chairman

1-1 ELECTROMAGNETIC TRANSIENT INTERACTION WITH OBJECTS WITH EMPHASIS ON FINITE SIZE OBJECTS, AND SOME ASPECTS OF TRANSIENT PULSE PRODUCTION: C.E. Baum, Air Force Weapons Laboratory, Kirtland Air Force Base, Albuquerque, N.M.

This paper first considers some of the techniques involved in the production of transient electromagnetic fields with fast rise times, large pulse widths for nonoscillatory pulses, and smooth characteristics in the frequency domain. Some examples considered include conical and cylindrical TEM transmission lines, the surface transmission line where a wave is guided between a conducting sheet and a lossy half space, and radiating electric and magnetic dipole antennas. Some proximity effects of objects under illumination to the wave "radiating" or guiding structure are also considered. The second and major portion of this paper deals with the transient interaction of electromagnetic waves with objects, primarily objects of finite size in free space. We briefly review some of the older techniques such as solution in the frequency domain together with inverse Fourier transforms as well as the application of high and low frequency asymptotic forms to time domain waveforms. Then one of the most important topics of the paper is discussed; this is the singularity expansion method. This method utilizes the analyticity properties of the solution of the interaction (or scattering) problem to make an expansion in terms of natural frequencies, natural modes, coupling coefficients, and the singularities of the Laplace transform of the incident wave. This expansion can be written in both frequency and time domains. It is particularly useful in describing transient waveforms in cases where only a few terms are needed. Some numerical procedures are described and some specific examples are discussed.

1-2 PULSE SCATTERING FROM A SPHERE COATED WITH AN INHOMOGENEOUS SHEATH: N.G. Alexopoulos, Electrical Sciences and Engineering Department, University of California, Los Angeles, Calif.; and D.A. Huebner, Hughes Aircraft Company, Canoga Park, Calif.

In this paper the backscattered waveform caused by a short electromagnetic pulse incident upon a metallic sphere clad with a radially stratified dielectric or plasma layer is investigated. The effect of the sheath on both the specular and creeping wave returns is examined in detail. In particular, the specular return is found to increase in width for inhomogeneous coatings of both the converging and diverging kind. Such behavior is explained in terms of geometric optics. The total energy in the specular return and its relation to the optical cross section of the coated sphere is also considered. The creeping wave return is found to depend in both amplitude and position on the sheath thickness, permittivity gradient, and dielectric constant. A sheath whose permittivity decreases with radius enhances the creeping wave, while one whose permittivity increases with radius attenuates the wave. This characteristic is discussed in terms of surface wave theory. The value of the permittivity at the surface of the sphere is found to affect the group velocity of the creeping wave and thus its

COMMISSION 6

position in the wave form. A dielectric constant less than unity at the surface increases the propagation velocity of the creeping wave, while a value greater than unity slows the wave down. Plots of the various backscattered waveforms are presented.

1-3 WAVEFORMS RADIATED BY CONTINUOUSLY LOADED LINEAR ANTENNAS EXCITED BY GAUSSIAN PULSE: D.L. Sengupta and Yu-Ping Liu, Radiation Laboratory, University of Michigan, Ann Arbor, Mich.

The far-field waveforms radiated by a continuously loaded linear antenna excited symmetrically by gaussian pulse-type slice generators are investigated by numerical techniques. The loading is assumed to be symmetrical and increases continuously towards the end of the antenna. The antenna is considered to be a thin cylinder of finite length. The far field produced by the antenna is at first obtained as a function of frequency by numerically solving the appropriate Hallen's integral equation for the time harmonic case. The radiated waveforms for the gaussian pulse input case are then obtained numerically by using the fast Fourier inversion technique. Numerical results for the radiated waveforms in different directions are obtained as functions of the loading and the ratio of the input pulse width to the transit time on the antenna.

1-4 GENERALIZED APERIODIC EXCITATION IN TRANSIENT FIELD PROBLEMS: E.M. Kennaugh and J.H. Richmond, ElectroScience Laboratory, Ohio State University, Columbus, Ohio.

The impulse response waveform is a useful descriptor in transient scattering or radiation problems. Numerical computation of response waveforms is complicated in those cases where slow decay or oscillatory ringing occurs. A generalization of impulse excitation to a class of input-output waveforms of finite duration is presented. It is shown how the requisite input waveform may be determined so as to greatly reduce duration of the response in many cases. The technique is illustrated for thin-wire scatterers and radiators using new results obtained by the reaction principle. Since the input waveforms used are influenced by the shape, size, and composition of scatterers, potential applications to target recognition are discussed.

1-5 SOME COMPUTATIONAL ASPECTS OF TRANSIENT ELECTROMAGNETICS: C.L. Bennett, Sperry Rand Research Center, Sudbury, Mass.; and E.K. Miller, Lawrence Livermore Laboratory, Livermore, Calif.

A critical examination of transient electromagnetic computational techniques is the topic of this paper. The historical development of and reasons for the current interest in transient electromagnetic effects will be given. In particular, the time domain magnetic field integral equation applied to surfaces and the time domain electric field integral equation specialized to thin wires will be considered. The relative advantages, disadvantages, limitations, and potential capabilities of each of these time domain integral equations will be considered with those of its frequency domain counterpart to place their relative roles in mutual perspective. Special attention will be devoted to the computational features of the time domain versus frequency domain approaches, including computer storage and time

COMMISSION 6

requirements and relative accuracies of their respective algorithms, and such less easily evaluated topics as ease of use and scope of applicability. Some representative, numerical results and experimental verification will be presented. Finally, brief consideration will be devoted to various nonintegral equation transient computational techniques.

1-6 E-FIELD INTEGRAL EQUATION APPROACH TO TIME DOMAIN SCATTERING FROM CYLINDRICAL BODIES: W.A. Davis, T. Itoh, and R. Mittra, University of Illinois, Urbana, Ill.

Many workers have investigated the problems of electromagnetic pulse scattering from various shapes of scatterers. To date, most of the work has been based on the H-field integral equation (HFIE) approach, and the E-field integral equation (EFIE) was used only in modified forms for such special cases as that of thin wires. In this paper, a direct and more rigorous form of the time domain EFIE was developed and applied to problem of scattering from a large semi-infinite hollow cylinder with near axis incidence of a gaussian pulse. The integral equation was discretized in time and space and was solved stepwise rather than by the inversion of the matrix which is commonly employed in the frequency domain solution. It was found that the solution was highly dependent on the realization of the edge condition. A stable solution was obtained only if the current components and their derivatives at the edge of the cylinder were expressed in a discretized form in such a way that they reasonably represent the physical phenomena. As one way of checking the accuracy of this algorithm, the following procedure was taken: first, the EFIE for a half plane was derived from the EFIE for a semi-infinite hollow cylinder by taking a limiting procedure analytically. Then the numerical solution for the half plane problem was compared with the Fourier transform of the exact solution found in Born and Wolf. Similar comparisons were made for the solution of the hollow cylinder problem and agreement was found to be good in both cases.

1-7 ANGLE SAMPLING IN TIME DOMAIN SCATTERING CALCULATIONS AND MEASUREMENTS: R.S. Smith, C.L. Bennett, and J.D. DeLorenzo, Sperry Rand Research Center, Sudbury, Mass.

Recent development of the space-time integral equation technique, together with the development of a time domain scattering range, have enabled both the numerical solution and the experimental verification of transient electromagnetic scattering problems directly in the time domain. These solutions are computed at discrete time points by simply marching along in time with the space-time integral equation, and similarly, on the scattering range the responses are measured at discrete time points. In order to fully characterize the target response, the data (either computed or measured) must be obtained for many angles of incidence. Since the data-gathering process is time-consuming it is important to determine the minimum number of incidence angles over which the scattering data must be obtained in order to characterize the target. In this paper the temporal sampling theorem is used to derive an angular sampling rule for rotationally symmetric bodies. The analysis is carried out using a simple time domain scattering model. The minimum number of incident angles is obtained as a function of the

COMMISSION 6

temporal sample rate required to represent the incident pulse. The analytical results are compared with data obtained from time domain scattering range measurements and found to be in good agreement.

1-8 UNDERGROUND IMPULSE RESPONSE MEASUREMENTS: J.D. Young, D.L. Moffatt, and R. Caldecott, ElectroScience Laboratory, Ohio State University, Columbus, Ohio.

This paper discusses an experimental program to apply time domain reflectivity techniques to the identification of buried metallic and nonmetallic objects by means of their scattering signature. An automated time domain measurement system is described. The RF portion consists of an impulse generator, a series of probes, and a sampling oscilloscope. The oscilloscope is interfaced to an instrumentation computer, which controls a measurement trial, stores the data in disk memory, and facilitates analysis of the data. Range-gating, fast Fourier transform, and digital filtering are among the manipulation steps which may be used. Experimental data presented include transmission from a buried dipole antenna to several surface-mounted receiving probes, and scattering signatures of several 4-in. diameter cylinders at depths of 1, 3, and 5 ft.

COMMISSION 6, Session 2

0900 Friday, April 14

Pan American Room

BEAMS AND OPEN RESONATORS

G.A. Deschamps, Chairman

2-1 GAUSSIAN BEAMS AND OPEN RESONATORS: William Streifer, Electrical Engineering Department, University of Rochester, Rochester, N.Y.

This paper discusses the theory of Gaussian beams and open resonators. The various mathematical formulations are reviewed including those based upon scalar diffraction theory, the parabolic wave equation, and complex rays. The last two are particularly suitable for studying stable configurations in the lossless approximation, and the principal results of these calculations are presented. Various methods of computing losses for both stable and unstable resonators are compared. Current problems relating to the effects of misalignment, unstable configurations, inhomogeneous wave guiding structures, and the presence of time-varying, inhomogeneous, anisotropic, and/or nonlinear media in the cavity will be discussed.

2-2 REFLECTION AND TRANSMISSION OF BEAMS AT A DIELECTRIC INTERFACE: H.L. Bertoni, L.B. Felsen, and J.W. Ra, Department of Electrical Engineering and Electrophysics, Polytechnic Institute of Brooklyn, N.Y.

When complex values are assigned to the source coordinates in the expressions for the fields radiated by a point source in a homogeneous medium, the resulting fields have the form of a gaussian beam. This fact may be utilized to develop results for beam propagation and scattering in inhomogeneous regions by analytic continuation of corresponding results for point source fields. The analytic continuation procedure is investigated for two-dimensional beam fields reflected from and transmitted through a planar dielectric interface. Interpretation of the reflected fields reveals that they incorporate directly the lateral beam shift, a phenomenon usually regarded as a diffraction effect. When the beam is incident from the denser medium at an angle greater than the critical angle for total reflection, calculation of the evanescent transmitted fields requires special care since the corresponding results for an ordinary line source have not been well developed. A "local inhomogeneous plane-wave" approximation is derived for the transmitted field in this case, together with physically meaningful restrictions on the range of validity of the approximation. These restrictions, and their interpretation, are of importance in approximating the evanescent fields produced by total reflection in more general configurations not amenable to rigorous analysis.

2-3 QUASIOPTICAL ANALYSIS OF HOLOGRAPHIC IMAGES: G.A. Deschamps, Department of Electrical Engineering, University of Illinois, Urbana, Ill.

The usual description of the holographic process is based on a Fourier analysis in the plane of the hologram of the various fields involved. It does not readily tell how images of three-dimensional objects are related in space nor how they are distorted when the reference wave used in viewing the images is changed in position or in frequency.

COMMISSION 6

A representation of the field as a sum of spherical waves will be described that can be used to answer some of these questions. The central role is played by a geometric construction which to a pair of points (p_1, p_2) associates a third point $p = p_1 \oplus p_2$. Within the Fresnel approximation the product of fields with centers at p_1 and p_2 is a field with center p . The operation \oplus organizes the space into an Abelian group. Transformations of projective geometry relate the object, its images, and a representation of the hologram. They can be applied to points having complex locations hence to the holography of gaussian beams.

COMMISSION 6, Session 3a

1020 Friday, April 14

Pan American Room

NONLINEAR AND STOCHASTIC PHENOMENA

N. Marcuvitz, Chairman

3-1 CANONICAL EQUATIONS IN THE THEORY OF NONLINEAR DISPERSIVE WAVE PROPAGATION IN ONE DIMENSION: Frederick Tappert, Bell Telephone Laboratories, Whippany, N.J.

Nonlinear wave propagation phenomena in dispersive media are described, in general, by a complicated set of primitive equations which depend on the particular types of waves and media under consideration. By means of systematic asymptotic expansions valid for weakly nonlinear and weakly dispersive systems, one may reduce a large class of primitive equations to relatively simple canonical equations which have a universal form and are amenable to detailed theoretical-numerical analysis. Two such canonical equations which have proven to be a great value are the Korteweg-deVries (KdV) equation and the nonlinear parabolic (NP) equation. The KdV equation and its generalizations represent canonical descriptions of low-frequency, long-wavelength, acoustic-type nonlinear waves in dispersive media. The salient features of solutions of the KdV equation, as elucidated by computer simulations, are the formation of "solitons" via spontaneous and induced fission processes, the remarkable stability of solitons when interacting with one another, and the recurrence of initial states in periodic systems (nonequipartition of energy). Theoretical analysis has yielded a rather complete understanding of the first two features, but the third remains a challenge to theoretical investigation.

The NP equation represents a canonical description of high frequency, quasi-monochromatic nonlinear waves in dispersive media. The salient features of solutions of the NP equation are the "self-trapping" of wave packets and the formation of "envelope solitons" from general initial states, the growth and saturation of modulations imposed on a periodic wave train ("side-band" or "modulational" instability), and the recurrence of initial states in periodic systems. Theoretical understanding of the behavior of solitons of the NP equation is still relatively undeveloped, and one hopes that further computer simulations will soon lead to major advances in this area.

3-2 NONLINEARITY IN ELECTROMAGNETICS: J.B. Keller, Department of Mathematics, University Heights; and Courant Institute of Mathematical Sciences, New York University, N.Y.

At large field strengths all materials exhibit a nonlinear response to electromagnetic fields. The fields in laser beams are strong enough to make this nonlinear response experimentally observable and significant. Therefore methods for the theoretical analysis of electromagnetic waves in nonlinear media have become important. Some of the main causes and effects of nonlinearity will be described, and some of the methods for analyzing them will be explained. These methods include the method of characteristics, regular perturbation theory, two time methods, singular perturbation theory, etc. The methods will be illustrated by applications to typical problems.

COMMISSION 6

3-3 REFLECTION AND TRANSMISSION OF WAVES IN AN ELECTRON-HEATED NON-LINEAR PLASMA: T.S. Wang and Y.T. Lo, University of Illinois, Urbana, Ill.

There are various types of nonlinear phenomena in plasma. Tsytovich considered the nonlinearity due to $(\vec{V} \cdot \vec{V}) \vec{V}$ and $\vec{V} \times \vec{B}$ in fluid equations whereas Whitmer and Barrett, based on the same set of equations, determined the reflected and transmitted waves through a plasma layer. Keller and Millman developed a general theory with no particular reference to physical processes. Ginzburg studied the nonlinear phenomenon due to electron heating, in particular its application to the cross-modulation of waves in ionosphere, the so-called Luxemburg effect. In this paper we consider the nonlinear effects on the reflected and transmitted waves in an electron-heated plasma of semi-infinite extent first and of conducting-plate-backed layer next, based on the Ginzburg's theory. In this theory the plasma is characterized by two variables, the average electron velocity \bar{U} and the effective electron temperature T_e . Ginzburg showed that if the applied field strength is smaller than the "plasma field" E_p , the state of the plasma changes slightly under the influence of the field. On the other hand, if the applied field is much greater than E_p , the plasma parameters will be altered significantly. By matching the fields at the air-plasma interface and solving some nonlinear equations, we have computed the transmitted field and the reflection coefficient as functions of the incident field strength for various cases. The results show the interesting nonlinear effect, in particular the existence of minimum reflection for some particular values of the incident field. As the incident field strength becomes very strong the transmitted field reaches a saturated value as predicted by Ginzburg.

3-4 NUMERICAL CALCULATIONS OF A WAVE PROPAGATING IN A NONLINEAR MEDIUM IN THE PRESENCE OF TURBULENCE: A.J. Glass and I.W. Kay, Wayne State University, Detroit, Mich.

The objective of the work described in this paper is to show how an existing computer program for calculating the amplitude and phase distribution of a scalar wave propagating in a nonlinear medium can be modified to accommodate the presence of homogeneous isotropic turbulence. The original computer program is designed to compute the propagation of an intense beam of light, with an arbitrary variation of intensity and phase defined on an initial reference plane, through a weakly absorbing medium, in the presence of transverse convective flow. By using what is essentially the bilocal approximation of Keller it is possible to modify the differential equation for the field propagating under these conditions to include the effect of weak turbulence in the medium. It can be shown that the resulting equation has the same form as that of Keller with the addition of a source term which depends nonlinearly upon the average field. The numerical method employed in the original computer program relies on an alternating-direction, implicit, finite difference scheme of the Crank-Nicholson type. This provides a fast and accurate computational scheme. In modifying the calculation to include the effect of turbulence according to the bilocal model of Keller, a problem arises due to the nonlocal nature of the scattering kernel in the Keller formulation. What was formerly a differential equation becomes a differentio-integral equation in the presence of

COMMISSION 6

turbulence. The integral term destroys the effectiveness of the algorithm which is based on a local difference relation. It is shown that the field produced by the nonlinear interaction can be expressed as a sum of propagating modes which depend upon the location and residues of the poles of a function defined by the dispersion relation inherent in Keller's model. Each of the modes satisfies a nonlinear but entirely local equation. Thus, it is possible to apply the available computing technique by generalizing it to a system of equations of the type for which it was originally developed.

1400 Friday, April 14

Pan American Room

STOCHASTIC ASPECTS OF WAVE PROPAGATION

N. Marcuvitz, Chairman

3-5 THE FLUCTUATION SPECTRUM AND EQUIVALENT ELECTRICAL CIRCUIT OF A SIMULATED AURORAL ARC: J.T. Coleman, Battelle, Columbus Laboratories, Columbus, Ohio

Laboratory simulations of an E-layer auroral electrojet system have permitted the direct measurement of the electron fluctuation spectrum of the stationary state of this instability. A number of spectra have been generated and the structure function of the turbulence $S(\omega)$ measured. Evidence is presented for the buildup and enhancement of this spectrum as a function of the electrojet drive level. The frequency dependence of this spectrum is estimated and related to radar observations of the backscatter properties of auroral arcs. The frequency dependence observed by rocket probes flown through auroral arc formations is also correlated with the laboratory observations, and the results to date are found to be reasonable and encouraging. The equivalent electrical circuit of the simulated auroral arc has also been measured as a function of the strength of turbulence. The impedance to the current is shown to be frequency-dependent, with a considerably different dc impedance than that presented to the higher-frequency fluctuating currents. Evidence for the presence of anomalous resistivity is also discussed.

3-6 WAVE PROPAGATION IN A SLAB OF ONE-DIMENSIONAL RANDOM MEDIA: R.H. Lang, George Washington University, Washington, D.C.

The problem of a plane wave normally incident on a slab of random medium, where the medium has refractive index variations only in the longitudinal direction, has been considered. The mean and the correlation of the field are obtained approximately by solving certain integral equations. These equations have been derived in the past literature by perturbation techniques or resummation procedures. The results of a previous author who solved the integral equation for the mean are used in the paper. These results are simplified and his method is used to find the mean Green's function for the slab. The correlation of the field is then found by solving the correlation equation in conjunction with the mean field and the mean Green's function. It is shown that this result is energetically self-consistent, and the average reflected and transmitted power is calculated. This calculation shows that as the slab width is increased the average power reflected from the slab also increases. The above investigations are carried out for media with delta function and exponential correlations.

3-7 ON THE INFLUENCE OF LOCALLY CORRELATED IRREGULARITIES IN MULTIPLE SCATTERING: J.C. Hassab, Naval Underwater Systems Center, Newport, R.I.; and J. Jarem, Drexel University, Philadelphia, Pa.

The scattering of an incident wave by random irregularities of non-uniform intensity has been studied in the limit of small-scale fluctuations (Hassab and Jarem, 1971 URSI Spring Meeting). In the present paper, we consider the influence of locally correlated fluctuations

COMMISSION 6

possessing a slowly varying gaussian intensity. The coherent wave is described by the bilocal Dyson equation set in wave-number space; this formulation leads to an approximate solution for the coherent wave through use of strong local properties exhibited by the turbulent intensity. The incoherent power is obtained from the Born approximation, with the coherent field acting as the source function. With the above results, we calculate the scattering pattern of a turbulent sphere with a locally exponential correlation function. It is found that the mean-square fluctuations influence only the magnitude of the incoherent directivity pattern, while its angular distribution depends solely on the local correlation function. Furthermore, the magnitude of the scattered coherent wave depends strongly on the turbulent intensity, whereas the phase is mainly a function of the local correlation length. Other related effects, such as medium's anisotropy, will be presented and discussed.

3-8 BACKSCATTER FROM GATED FLUCTUATING REGIONS: A BREMMER SERIES APPROACH: Shalom Rosenbaum, Polytechnic Institute of Brooklyn, Farmingdale, N.Y.

In many monostatic configurations, the effective scattering volume is defined longitudinally by the radar gating and transversely, by either the antenna beamwidth or the finite extent of the scattering region. Often the radar signal must traverse fluctuating transmission regions on its way to and from the range cell. Consequently, the return signal is perturbed not only by events within the range cell but contains statistical characteristics ascribable to the fluctuating transmission path as well. The limit of large-scale fluctuations (which is of interest in the current context) is dominated by strong incoherent small-angle scattering. A systematic analytic sequence resembling that pursued by Bremmer (though significantly complicated by the three-dimensionality and temporal dependence of the fluctuations) constitutes the main subject matter of this study. The proposed iterative scheme, while properly accounting for multiple small-angle scatter, orders successive iterates by the number of large-angle scattering events they represent. While the discussion is carried within the physical framework of an electromagnetic (radar) application an extension to the acoustical (sonar) analog is simple. Furthermore, the extension of the presently investigated monostatic configuration to bistatic ones is possible but is by no means trivial. The reported work has initially been motivated by an attempt to interpret on-board radar cross-section and spectral measurements associated with an ionized wake.

3-9 FOURTH MOMENT OF A WAVE PROPAGATING IN A RANDOM MEDIUM: W.P. Brown, Jr., Hughes Research Laboratories, Malibu, Calif.

We shall discuss some recent work on the fourth moment of a scalar wave propagating in a random medium. Starting with a partial differential equation obtained by various authors in a multiple scattering approximation, we shall discuss the general properties of the fourth moment of an initially plane wave and then present numerical results for a two-dimensional plane wave. Results will be given for the variance and covariance of irradiance scintillations. Both results agree with experiment. In particular, the variance exhibits the experimentally observed saturation phenomenon, and the covariance results indicate that the

COMMISSION 6

correlation length for irradiance scintillations is not proportional to $(\lambda z)^{\frac{1}{2}}$ in the saturation region.

3-10 INTENSITY FLUCTUATIONS OF STOCHASTIC FIELDS: L.S. Taylor,
University of Maryland, College Park, Md.

A variety of phenomena of current interest involve the propagation of fields which have been randomized by previous passage through stochastic regions. Examples include the radio-astronomical observations of the solar plasma and the contribution of the turbulent upper layers of the atmosphere to the twinkling of starlight. These phenomena and others may be crudely understood on a ray basis, when it is recognized that even small phase variations introduced by the stochastic element are converted into intensity fluctuations during passage through the uniform medium by focusing. This is the principle used in shadowgraph photography of turbulent (and uniform) flows. Although the ray-optical theory has been well known, a general electromagnetic solution using the Helmholtz-Kirchhoff integral has been lacking. The difficulty has been that eighth-order integrations are involved. In this paper, we reduce the integrals to lower orders to obtain compact general expressions for the auto-correlation and spectrum of intensity fluctuations in terms of the fourth-order coherence function on an initial plane. From these general expressions the restricted formulas previously obtained for various special cases can be readily deduced, and a number of new results are made available.

3-11 WAVE FLUCTUATIONS IN LOCALIZED SMOOTHLY VARYING TURBULENCE:
Akira Ishimaru, Department of Electrical Engineering, University
of Washington, Seattle, Wash.

In the past, smoothly varying turbulence has been studied by changing the structure constant to the function $C_n^2(\bar{r})$. The purpose of this paper is to show that the above approach is insufficient, and that a random process developed by Silverman can be successfully used to describe the wave fluctuations in localized smoothly varying turbulence. The localized turbulence is characterized by a correlation function which is a product of a function of the average coordinate and a function of the difference coordinate. The corresponding spectrum is also given by a product of a function of the difference wave number and a function of the average wave number. They are related to each other through two Fourier transform pairs. Making use of the above spectrum, the fluctuations of waves propagating through such a turbulence can be given by a convolution integral of the structure constant $C_n^2(\bar{r})$ and a function involving the outer scale of the turbulence L_o . It is shown that for a plane wave case, if the distance L is within (L_o^2/λ) , then the usual formula given by Tatarski is valid. But if the distance is between L_o^2/λ and $(bL_o)/\lambda$ where b is the total size of the turbulence, the variance of the wave is nearly constant, and if $L \gg (bL_o)/\lambda$, the variance decays as L^{-2} . Similar conclusions are shown for a spherical wave case.

COMMISSION 6

3-12 REMOTE DETERMINATION OF THE WIND VELOCITY AND STRUCTURE CONSTANT USING NARROW BEAM WAVES: J.M. Heneghan and Akira Ishimaru, Department of Electrical Engineering, University of Washington, Seattle, Wash.

A method is developed for remotely determining the average transverse wind velocity and the atmospheric structure constant (strength of turbulence) at N points along a line-of-sight path. The technique avoids the basic instability problem that was encountered in previous work, limiting calculations to one or two points. The method involves the inversion of an integral equation that has been developed for a focused beam wave. The measured data, the amplitude correlation function, and the amplitude and phase structure functions are related linearly to the unknown structure constant. A linear equation can be obtained for the wind velocity by a differentiation scheme. In the resulting linear integral equations a small measurement error may produce a large variation in the computed wind velocity and structure constant; thus, the problem is ill-posed, and the solution is dependent upon the statistical nature of the unknown and the data. The inversion procedure consists of minimizing the errors in the unknown. The method also gives an indication of the final error in the solution. For example, with an input error of one percent it is predicted that the RMS error of the unknown will be on the order of ten percent.

3-13 TRANSMISSION OF PULSED-CARRIER SIGNALS OVER A RANDOMLY DISPER-
SIVE STRIPLINE: R.E. McIntosh, J.M. Wilk, and L.W. Pickering, University of Massachusetts, Amherst, Mass.

The results of an experiment designed to measure the effects of a random plasma transmission medium on the envelopes of RF pulses are reported. The experiment utilizes a strip transmission line in which the region separating the two conducting planes contains a randomly inhomogeneous gaseous discharge during the transit time of the RF pulse along the line. This arrangement allows control of the random refractive index fluctuations through variation of several physical parameters of the gas discharge. At the output of the line the envelopes of the randomly disturbed pulses are sampled and processed with a probability analyzer which determines the probability density function of the average amplitude of the received pulses. The coefficient of variation of these amplitudes, which is calculated numerically, is then compared with theory, which predicts the predominance of dispersive effects. It is found that the experimentally determined dependence of the pulse statistics on carrier frequency agrees well with the theory for small medium fluctuations. It is also found that the pressure dependence of the measurements agrees with simple arguments that relate the background air pressure and the electron number density of the medium.

COMMISSION 6, Session 4

1400 Friday, April 14

Massachusetts Room

NUMERICAL METHODS

K.K. Mei, Chairman

4-1 ON THE FUNDAMENTAL LIMITATION OF NUMERICAL SOLUTION OF INTEGRAL EQUATIONS: R. Mittra, Laboratory for Electromagnetic Theory, Technical University of Denmark, Lyngby, Denmark

The numerical solution of an integral equation typically entails its conversion into a matrix equation. It is necessary in this process to approximate the kernel of the integral equation and to express the unknown in this equation in terms of a suitable set of basic functions. The purpose of this paper is to demonstrate that the accuracy of the final solution depends critically on how well the kernel has been approximated. The paper begins by considering an analytical model of an integral equation with a truncated kernel. The above equation is inverted both for the noise-free and noisy case, and it is found that when the matrix size is increased beyond a certain point a nonunique solution results for the ideal noise-free case, whereas the solution is unstable for the practical case where round-off errors are always present in the numerical processing of the equation. This behavior is attributable to the smoothing of the kernel and is responsible for imposing a fundamental limitation on the accuracy of the numerical solution of integral equations. The theoretical considerations are illustrated in the paper by some examples involving waveguide and antenna problems.

4-2 HORIZONTAL ARRAY OVER A LOSSY GROUND: W.C. Kuo and K.K. Mei, Department of Electrical Engineering and Computer Sciences, and Electronics Research Laboratory, University of California, Berkeley, Calif.

The Sommerfeld's formulas for a dipole over a lossy ground provide the necessary Green's functions for numerical solutions to the antenna integral equation. However, when it comes to evaluate those formulas in actual applications we found that they are too time-consuming to be useful. In this paper, an approximated boundary condition is used to solve the dipole problem so that a fast converging integral is obtained. The approximate boundary condition approach which was first used by Feynberg on vertical dipoles is now modified to solve horizontal dipoles. The results computed from the approximate formulas are compared to those obtained directly from the Sommerfeld's formulas and are found to be accurate even when both the source and observation points are close to the ground. Due to the fast-converging nature of the approximate integrals, we are now able to apply the integral equation technique to the horizontal dipole arrays over a lossy ground economically. The integral equation of Hallen's type is derived for dipole antennas over the ground, and results are presented for the dipole arrays series-connected by transmission lines. The field penetration into the lossy ground is also investigated.

COMMISSION 6

4-3 ELECTROMAGNETIC FIELDS OF A SUBTERRANEAN CYLINDRICAL INHOMOGENEITY EXCITED BY A LINE SOURCE: A.Q. Howard, Jr. and J.R. Wait, Office of Telecommunications, Institute for Telecommunication Sciences, Boulder, Colo.

The anomalous fields from a buried cylindrical inhomogeneity in an otherwise uniform half-space are analyzed. The problem is rendered two-dimensional by assuming that the uniform line source of current is parallel to the subsurface cylinder. The multipole scattered field coefficients are obtained from the numerical solution to the associated singular Fredholm integral equation of the second kind. The horizontal magnetic field amplitude, the vertical magnetic field phase, and the amplitude and phase of the ratio of horizontal to vertical magnetic fields are shown to be diagnostic of the location of the inhomogeneity. The results have possible applications to electromagnetic location in mine rescue operations and to geophysical prospecting.

4-4 HOW TO USE THE H-INTEGRAL EQUATION FOR ELECTRICALLY THIN ANTENNAS AND SCATTERERS: R. Mittra, Laboratory for Electromagnetic Theory, Technical University of Denmark, Lyngby, Denmark

It is well known that the H-integral equation is preferable for numerical solution of the problem of scattering from solid surface structures since this equation has several features that make it more attractive than the E-equation. First of all, the H-integral equation is of the second kind whereas the E-equation is of the first kind; and second, the kernel of the E-equation involves a second partial derivative whereas only the first derivative appears in the corresponding place of the H-equation. Nevertheless, it has been found that the use of the H-equation is fraught with numerical difficulties when it is applied to thin wire, or thin plate, antennas, and scatterers. It is the purpose of this paper to investigate the cause of these difficulties and to find a representation of the H-equation which is useful for dealing with electrically thin structures. The three types of problem considered are: (i) scattering from a strip with small but finite thickness; (ii) scattering from a thin cylinder; (iii) the thin wire antenna problem. It is indicated in the paper how the H-equation could be used for each of the above problems.

4-5 SCATTERING BY FINITE CONDUCTING WIRES IN DISSIPATIVE MEDIA: J.C. Lin and A.W. Guy, Department of Rehabilitation Medicine, School of Medicine, University of Washington, Seattle, Wash.

The problem of electromagnetic scattering by a thin wire of finite length and conductivity embedded in a lossy medium is considered. An internal impedance per unit length of wire is assumed. The integral equation formulation reveals, as in the corresponding free space case, that for a plane wave incident at an arbitrary angle on a thin wire, a current is induced on the wire only if the incident radiation has a component polarized in the same direction as the wire axis and this current is in the axial direction. Numerical solutions for the current induced on, and field scattered by a straight wire are obtained using the point-matching techniques whereby the boundary conditions are satisfied exactly at a finite number of discrete points along the wire. The basis functions used are piecewise linear ones. For fine carbon, tungsten, and copper wires, the computed E-plane power patterns are

COMMISSION 6

compared with experimental results obtained through a thermographic technique. The technique involves the use of an infrared camera for recording temperature distributions produced by energy absorption in materials of known thermal conductivity and complex dielectric constants. The power patterns may then be obtained as a function of the calculated heating pattern.

4-6 NUMERICAL ANALYSIS OF RADIATION FROM WIRE ANTENNAS ON CONDUCTING BODIES: N.C. Albertsen, J.E. Hansen, and N.E. Jensen, Laboratory for Electromagnetic Theory, Technical University of Denmark, Lyngby, Denmark

Current interest in the effect of alternative mountings of wire antennas on European scientific and application satellites has motivated the development of a general numerical technique for the computation of radiation patterns of monopole antennas on conducting bodies. The technique uses a combination of two different types of integral equations for the determination of the unknown current distributions. An electric-field integral equation in its thin wire approximation is applied to the monopole antennas as well as to any other wire-like structure that may be connected to the conducting body. On the body itself, which is supposed to consist of smooth surfaces, a magnetic-field integral equation is used. In this way the electromagnetic problem is formulated in terms of two coupled integral equations which may be solved numerically by the method of moments. Several examples of numerical results obtained by this technique will be presented. These include radiation patterns for monopole antennas which are mounted on the curved surface or end surface of a perfectly conducting circular cylinder of which the maximum dimension is of the order of one wavelength. The influence of the addition at various positions on the body of a passive metallic rod of varying length is also studied. In all cases the results compare well with experimentally obtained radiation patterns.

4-7 CALCULATION OF CURRENTS INDUCED ON A L-WIRE SCATTERER WITH END CAPS: C.M. Butler and M.R. Long, University of Mississippi, University, Miss.

A set of Pocklington-type integral equations for currents on a thin-wire scatterer in the shape of an L is presented for the case of a structure in free space as well as above a perfectly conducting ground plane. The development of the integral equations is based upon the so-called extended boundary condition first introduced by Waterman rather than upon $E_{tan} = 0$ on the scatterer surface. The cylindrical wire elements are considered solid in contrast to the usual assumption of tubes, and the end caps are accounted for by a quasistatic approximation technique. The unknown currents are expanded in a particular basis set which, within the framework of the method of moments, leads to a very efficient numerical procedure for solving the integral equations. Numerical results are presented.

COMMISSION 6

4-8 RADAR BACKSCATTER FROM A PLASMA-CLAD STRIP: G.E. Stewart and K.E. Golden, Aerospace Corporation, El Segundo, Calif.

The scattering of normally incident electromagnetic waves polarized parallel to the plane of incidence is analyzed for a plasma-clad strip by application of the method of moments. The mutual impedances between the current elements on the strip are computed for an assumed plasma layer by transforming the integral expressions to Fourier transform space and numerically evaluating the resulting integrals. The plasma layer is assumed to vary only in the direction normal to the surface of the strip, and the variation in electron density and collision frequency is approximated by a series of homogeneous slabs. For an incident plane wave, the voltage excitation of each of the elemental strips can be computed using the voltage transmission characteristics of the plasma slab. The vector defining the current distribution is expressed in terms of the product of the inverse of the impedance matrix and the voltage distribution vector. The scattered field is then expressed in terms of the induced current distribution, and the effective scattering width of the strip can be determined. For tenuous plasma layers the mutual impedance between the elemental strips is only slightly modified, and the resulting effective scattering width of the strip can be interpreted in terms of the plane wave transmission characteristics of the plasma sheath. If the mutual impedances are significantly altered by the plasma sheath, the current distribution is modified and no such simple interpretation is possible.

COMMISSION 6, Session 5

0830 Saturday, April 15

Pan American Room

ADAPTIVE ARRAYS

A. Ksieinski, Chairman

5-1 ADAPTIVE ARRAYS FOR COMMUNICATION SYSTEMS: R.T.Compton, Jr.,
ElectroScience Laboratory, Ohio State University, Columbus, Ohio

This talk will review the adaptive array research currently under way at Ohio State University. First, an experimental four-element adaptive array processor constructed under Navy contract, will be described. This processor has been used to study the patterns obtained from a conformal array on an aircraft mockup. The results show that this type of system operates properly with almost arbitrary element placement or mutual impedances, a fact of considerable practical importance to the antenna designer. Typical patterns obtained with and without interfering signals will be shown. The effects of signal power, angular separation of desired and interfering signals, and element patterns will be discussed. Secondly, methods for combining the adaptive array concept with practical communication systems will be discussed. Some early experiments involving simple modulated waveforms will be described, and then newer techniques for reference signal generation with coded communication systems will be discussed. Methods for obtaining code timing lockup and tracking will be described.

5-2 ADAPTIVE RF BEAM FORMATION FOR PHASED ARRAYS: A.E. Zeger, General
Atronics Corporation, Philadelphia, Pa.

Adaptive phased-array antennas control their radiation patterns by employing beam formation algorithms which utilize measurements of the wavefront (WF) at the antenna. Attention is more often focused upon the adaptive processor and the array beamformer than it is upon the WF measurement subsystem. The different and often competing requirements of the beamformer and the array WF sampler are discussed. The competition is for access to the signal energy received by the antenna array. Limited by available components, the designer of an adaptive array must compromise and accommodate the needs of the beamformer and the WF sampler. In large phased arrays, beam formation at RF can reduce hardware cost, but measurement of the unamplified, unfiltered WF at each element is a challenge. Techniques for determining the WF incident upon an RF beamforming adaptive array are examined. The design of an adaptive array employing RF phase shifters and RF combiner is presented. This array uses a single time-shared processor to sequentially sample the WF at each array element. This design is applicable to a large, flush-mounted, conformal array for SHF satellite communications. Element spacings are randomized to reduce the effects of mutual coupling. The expected pattern, angular tracking rate, and noise figure of the system are calculated.

5-3 DECISION-THEORETIC ADAPTIVE ARRAYS: G.O.Young, J.E.Howard, and
R.A.Birgenheier, Hughes Aircraft Company, Culver City, Calif.

A new class of adaptive antennas has been conceived that makes use of a digital processor following a set of antenna elements. The processor develops source (e.g.,targets, multipath) location estimates. It also

COMMISSION 6

develops amplitude and phase weightings suitable for synthesis of a controlled pattern. The system consists of a direction finder that locates sources and determines weightings, followed by a controlled array that may be any antenna for which a pattern is to be synthesized. Note that in this scheme, the estimation and control aspects of the adaptive problem are separated, so that location estimation can take place independently of the desired pattern synthesis. The source locations are found from a sufficient statistic determined by decision-theoretic estimation techniques. Mathematically, this statistic is determined by decision-theoretic estimation techniques. Mathematically, this statistic is a multimodal N -dimensional surface for N sources and must be searched for a global maximum. Possible methods for reducing the time required for performing the corresponding N -dimensional search are being investigated. In order to improve estimation accuracy, an adaptive technique has been developed that updates as a function of time the probability distributions from which the estimates are made. By so doing, the estimates and control are improved with time so as to compensate for initial parameter value uncertainty and to adapt to a changing environment. The feasibility of the processing has been demonstrated by numerous computer simulations in which the actual software to be used in an eventual system was used to provide a realistic assessment of expected performance. The simulations demonstrated the ability to accurately locate multiple, closely-spaced (within a beamwidth) sources.

5-4 ADAPTIVE ARRAY RECEIVING ANTENNAS: L.E.Brennan, Technology Service Corporation, Santa Monica, Calif.

In an adaptive receiving array, the weight applied to each array element is generated by a separate adaptive control loop. An adaptive array configuration will be described which maximizes the output signal-to-noise ratio in a nonuniform external noise environment. These adaptive systems reduce antenna sidelobes selectively in the directions of greatest interference. An adaptive receiving array also senses the presence of near-field scatterers, such as aircraft structures near an airborne antenna, and adjusts the antenna illumination function to restore a low sidelobe antenna pattern. When one element of a receiving array fails, the excitation applied to the remaining elements is adjusted to restore low sidelobes. This technique can be applied to conformal array antennas mounted on a curved surface. The theory of maximum S/N adaptive arrays, based on earlier side-lobe canceller and adaptive array work by S. Applebaum and P. Howells, will be reviewed. Examples of steady-state and transient array response will be presented to illustrate these advantages of adaptive receiving arrays. A technique for adaptively controlling both the array illumination function and filter response in an airborne array radar will also be described. This technique for adaptively controlling the system response in both space and time compensates for platform motion in a coherent airborne radar and provides excellent MTI (moving target indication) performance.

5-5 ADAPTIVE ARRAYS WITH SIMPLIFIED WEIGHTING STRUCTURES: A.L. McGuffin Aircraft Equipment Division, General Electric Company, Utica, N.Y.

Adaptive array processing is a potential means of providing improved receive antenna phase center control for AMTI motion compensation.

Since the complex weight applied to each antenna element approaches the optimal weight for that element, the phase center can be displaced farther than is practical with conventional techniques. Certain results of an investigation of simplified adaptive array techniques are presented to illustrate phase center displacement weighting as the number of degrees of freedom of the system is reduced. One simplification, the use of subarray weighting of delayed clutter and full array weighting of undelayed clutter, provides examples of how the processor adapts to changes in the weighting structure. The performance attainable when conventional AMTI is employed downstream from the adaptive array processor to compensate for a second type of array simplification is also discussed. A compatibility problem which arises under certain conditions is described briefly. The computed performance of this configuration is compared with those attainable when the adaptive processor parameters are altered to partially account for the presence of the downstream AMTI.

5-6 COHERENT OPTICAL ADAPTIVE ARRAYS: T.R.O'Meara, Hughes Research Laboratories, Malibu, Calif.

We will survey all known types of coherent optical adaptive arrays and relate them to their microwave predecessors. The versatility of the optical art has in some cases progressed beyond the microwave art, and we will illustrate this point via some new classes of systems not previously discussed in the literature. The driving needs for adaptive optical phased arrays are probably greater than for adaptive microwave phased arrays, and this will be illustrated by discussion of two application areas: (1) partial compensation for atmospheric turbulence, and (2) adaptive lock-on a single reflector, or glint, in a multi-glint environment.

5-7 ANTENNA ARRAYS WITH LOW REDUNDANCY: W.K. Klemperer, National Oceanic and Atmospheric Administration, Boulder, Colo.

A number of eminently sensible designs for "super synthesis" antenna arrays have been proposed, and a few large instruments incorporating these ideas have been built or are under construction. There remains a large class of objects (particularly those exhibiting short-term variability) for which the technique of earth's rotation synthesis is unsuitable for improving either observational sensitivity or resolution. This paper outlines some useful properties of two-dimensional antenna arrays with low redundancy. Such arrays exhibit interelement spacings which are generally unique (in the sense that they occur only once) and are uniformly distributed. Low-redundancy design can significantly reduce the cost of large arrays for radio and radar investigations while providing greatly improved resolution and operational flexibility.

5-8 COMPARISON BETWEEN THE PEAK SIDELOBE OF THE RANDOM ARRAY AND THE ALGORITHMICALLY DESIGNED APERIODIC ARRAY: B.D. Steinberg, Moore School of Electrical Engineering, University of Pennsylvania, Philadelphia, Pa.

Thinned arrays (mean interelement spacing greater than one-half wavelength) are made aperiodic to suppress grating lobes. Many thinning

COMMISSION 6

algorithms were created in the 1960's and tested by computer simulation. Several years ago, while examining the published patterns of such arrays, Y. T. Lo noted that their sidelobe properties did not appear to be superior to what would be expected of random arrays. A test of that observation with respect to the peak sidelobe is made in this paper. Seventy-five algorithmically designed aperiodic arrays are examined and the distribution of their peak sidelobes, relative to the expected values for random arrays having the same parameters is obtained. The distribution is compared to that of a set of 180 random arrays. Lo's conjecture is well vindicated in both the average and the median values, each being within a few tenths of a dB of the theoretical values. Both distributions are found to be log normal. They differ markedly in their standard deviations, however; the standard deviation of the random array distribution (1.3 dB) is approximately half that of the algorithmic set. Among the several algorithms examined, the method of dynamic programming produces the lowest peak sidelobe. The paper concludes with a discussion of the relative merits of the random versus the algorithmic approach to the design of large, thin antenna arrays.

COMMISSION 6, Session 6

0830 Saturday, April 15

New York Room

DIFFRACTION

L.B. Felsen, Chairman

6-1 HIGH-FREQUENCY BACKSCATTERING FROM AN ELLIPTIC METAL PLATE:

P.L.E. Uslenghi, Department of Information Engineering, University of Illinois at Chicago Circle, Chicago, Ill.; and S.W. Lee, Antenna Laboratory, Department of Electrical Engineering, University of Illinois, Urbana, Ill.

The high-frequency backscattered field produced by a time-harmonic, arbitrarily polarized, plane electromagnetic wave obliquely incident on a perfectly conducting plate of elliptical shape is determined by means of the geometrical theory of diffraction. For oblique incidence, the first two terms of the asymptotic expansion of the far field are obtained. At axial incidence, the backscattering behavior is complicated by the presence of an astigmatic cylinder with four cusps; however, the leading term of the field expansion is trivially obtained by physical optics. A matching between the dominant terms of the on-axis and off-axis expansions is effected via Bessel functions. The resulting formula is uniform in the angular variables and yields a previously known result for the particular case of a circular disk. On the basis of this formula, the radar cross sections corresponding to the direct and cross-polarized returns are computed as functions of the aspect angles, for various values of the wavelength and of the axes ratio.

6-2 DETERMINATION OF THE NEAR FIELD OF A DIELECTRIC WEDGE BY QUASI-OPTIC METHODS: Stewart Maurer, Department of EE/EP, Polytechnic Institute of Brooklyn, Brooklyn, N.Y.; and Kazimierz Siwiak, Raytheon Corporation, Bedford, Mass.

A quasi-optical description of the fields within a dielectric wedge (2-5 λ long) excited by a surface wave from an abutting dielectric slab is given in this paper. It is demonstrated that the field at the junction may be approximated by a local mode characteristic of the dielectric wedge. This mode, described asymptotically by a ray field characterized by a circular caustic is then considered as incident on the remainder of the wedge. There are three regions of interest within the wedge: (1) before critical angle reflection where geometric-optics suffices, (2) between the critical angle and the caustic, and (3) beyond the caustic where a geometric optical shadow region exists and diffraction effects related to lateral waves serve as the major illumination. All three regions, the last in particular--beyond the caustic, in which the maximum amplitude is observed--are determined by approximate integral formulations which are numerically evaluated. A comparison with actual amplitude measurements is given.

6-3 A THEORETICAL INVESTIGATION OF RADAR TARGET RETURN: P.D. Crout, Massachusetts Institute of Technology, Cambridge, Mass., and U.S. Naval Weapons Center, China Lake, Calif.

In this paper a reciprocity theorem is applied to derive a mathematical expression for radar target return, this being expressed as the voltage obtained at a specified point in the RF network of a radar receiver. The expression obtained consists of a surface integral which extends

over the illuminated portions of the target surface. The integrand of this integral involves data which pertain to the geometry of the system, the physical nature of the target surfaces, and the nature of the antenna patterns (including kinds of polarization) used under transmitting and receiving conditions, the two not necessarily being the same. An examination of this integrand is sufficient to indicate the relative effectiveness of different combinations of transmitting and receiving antenna patterns in distinguishing between natural and man-made targets, and hence in reducing the effect of clutter. The integral itself can be evaluated using Fresnel zones as in optics, the result being that most of the target surfaces may be omitted and the desired results obtained by considering only the contributions of certain "Fresnel parts," which pertain to edges, corners, near points, etc. Various specific results are discussed.

6-4 THE TIME HARMONIC AND TRANSIENT RESPONSE OF AN OBLATE SPHEROID:
D.A. Hill and R.H. Ott, Office of Telecommunications, Institute for Telecommunication Sciences, Boulder, Colo.

The backscatter response of a perfectly conducting oblate spheroid of arbitrary axial ratio is examined for the case of broadside incidence. The major axis is assumed large in terms of a wavelength, and physical optics is used to obtain the time harmonic response. The result is instructive because the transition of the scattered field from a curvature dependence (as predicted by geometrical optics) to an electrical size dependence (as in the case of a flat plate) is shown as the axial ratio is varied from one to zero. Curves of echo area versus axial ratio show that geometrical optics is valid if the minor axis is at least a half-wavelength or, equivalently, if at least one Fresnel zone is contained on the body. The impulse response (valid for short times) is obtained by an inverse Fourier transform. The expression is shown to agree exactly with the direct time-domain result obtained from the second derivative of the area function. Responses to a pulsed sinusoid are obtained by convolution to illustrate the pulse distortion as a function of axial ratio.

6-5 THE RADIATION CONDITION AND THE RECIPROCITY THEOREM FOR FIELDS IN MOVING MEDIA: C-T. Tai and C.F. Stubenrauch, Radiation Laboratory, University of Michigan, Ann Arbor, Mich.

The mathematical form for the radiation condition for fields in a moving medium has been derived. Such a condition may be assumed to exist from physical reasoning; however, it has not been explicitly stated for the moving medium case. The expression for the electric field due to sources in a moving medium may be expressed in terms of an appropriate dyadic Green's function which satisfies a modified vector wave equation derived from the Maxwell-Minkowski theory. This expression involves both a volume and a surface integral. Investigation of the conditions necessary for the surface integral to vanish leads to the radiation condition in moving media. It has been found that this condition is dyadic in nature having different factors for the $\hat{\theta}$ and $\hat{\phi}$ components. For stationary media the expression derived reduces to the well-known Sommerfeld radiation condition. The Lorentz reciprocity theorem has been investigated for boundary value problems involving an interface between a stationary medium and one moving with velocity

parallel to the interface. Expressions are derived by using symmetry properties of the dyadic Green's functions. It is found that the direction of the velocity must be reversed when source and field positions are interchanged.

6-6 ANALYSIS AND SEPARABILITY OF COORDINATES FOR ELECTROMAGNETIC FIELD PROBLEMS IN INHOMOGENEOUS ANISOTROPIC MEDIA: A. Mohsen, Department of Electrical Engineering, University of Manitoba, Winnipeg, Manitoba, Canada

Analysis of electromagnetic fields in inhomogeneous anisotropic media is of practical interest in antenna, scattering, and propagation problems. The Whittaker and Debye-Bromwich types of representation, which split the field into so-called transverse electric (TE) and transverse magnetic (TM) parts, have had a considerable and fruitful applications for homogeneous media. The search for situations giving rise to uncoupled TE and TM fields is justified by the fact that, in such cases, the calculations involved can be considerably simplified. A general solution of the Maxwell equations for source-free anisotropic inhomogeneous media is presented in terms of general orthogonal coordinates. The dielectric constant $\bar{\epsilon}$ and permeability $\bar{\mu}$ are tensor functions of position, assumed nonsingular so that their reciprocals $\bar{\epsilon}^{-1}$ and $\bar{\mu}^{-1}$ exist. The gauge transformations allow for field representation in terms of only two scalars (components of Hetzian potentials) satisfying certain differential equations. These differential equations are in general of higher order than the second, but under certain conditions they reduce to second order. These conditions are considered in detail when the dielectric constant and permeability have their principal axes in the direction of the coordinate axes. The previous works of Bromwich, Nisbet, Wexler, Uslenghi, and Friedman are special cases of the present analysis. Since the method of separation of variables is of such wide usefulness in the solution of problems in homogeneous media, it is important to investigate just how far this method can be extended in the more complex problems involving inhomogeneous media. Separability conditions are obtained for the resultant equations using Stäckel determinant. An auxiliary function of coordinates is also introduced in order to further simplify the solutions.

6-7 DIFFRACTION, CERENKOV, AND TRANSITION RADIATION: S.R. Seshadri, Department of Electrical Engineering, University of Wisconsin, Madison, Wisc.

The subject of diffraction, Cerenkov, and transition radiation is reviewed by considering the problem of radiation from a point charge moving with uniform velocity along a straight line under various situations. When the medium is unbounded and the particle velocity is subluminal, the diffraction effects due to the finite path length give rise to what is called diffraction radiation. For an unbounded medium and superluminal velocities, there is Cerenkov radiation. If the interaction length is sufficiently long, Cerenkov radiation manifests itself as a peak in the radiation pattern in a direction that can be obtained in accordance with the usual synchronism condition. If the path length is infinite, the radiation occurs only in a particular direction with respect to the motion of the charge, and the diffraction effects due to the finite length spill the radiation in other directions

COMMISSION 6

as well. Half of the path is then considered to be in Medium 1 and the other half in Medium 2, the two media being separated by a plane interface normal to the path length. Even when the particle velocity is subluminal for both media, radiation occurs when the charge traverses the interface. The characteristics of this radiation are summarized. Transition radiation occurs for all particle velocities and for infinite path length and cannot be distinguished from the diffraction radiation resulting from the finite path length. When the particle velocity is superluminal, Cerenkov radiation occurs and manifests itself as a peak or peaks in the radiation pattern depending on whether the particle velocity is superluminal corresponding to Medium 2 or Medium 1. The peaks in the radiation pattern can be explained in simple terms. Numerical results of radiation pattern for various types of Media 1 and 2 will be presented.

6-8 GREEN'S DYADIC FOR A WARM PLASMA SLAB: R.E. Collin, Case Western Reserve University, Cleveland, Ohio

In a warm plasma slab of finite thickness the field can be found in terms of the transverse electric field and the AC electron density which satisfy the vector and scalar Helmholtz equation with the current and charge as source functions, respectively. The two fields are coupled together by the boundary conditions at the slab-vacuum boundary. It will be shown that by introducing a four-dimensional field vector with the electric field for the first three components and the AC electron density multiplied by a suitable constant for the fourth component that a self-adjoint system is obtained. The Green's dyadic becomes a four-dimensional dyadic. The reciprocity and symmetry properties of this dyadic are determined and lead to corresponding properties for the fields. The solution for the Green's dyadic will be given. It also will be shown that the solution procedure is simplified by using the reciprocity properties of the Green's dyadic as determined by the self-adjoint properties of the overall system.

6-9 MOMENT EXPANSION FOR IONOSPHERIC RANGE ERROR: A. Mallinckrodt, Communications Research Laboratories, Tustin, Calif.; R. Reich and H. Parker, Radio Corporation of America, Lanham, Md.; and J.H. Berbert, Goddard Space Flight Center, National Aeronautics and Space Administration, Greenbelt, Md.

On a plane earth the ionospheric or tropospheric range error depends only on the total refractivity content or zeroth moment of the refracting layer and the elevation angle. On a spherical earth, however, the dependence is more complex, so for most accurate results it has been necessary to resort to complex ray-tracing calculation. This report offers a simpler high accuracy alternative to the ray-tracing calculation. By appropriate expansion of the angular dependence in the ray-tracing integral in a power series in height, an expression is obtained for the range error in the form

$$\Delta R = \sum_{m=0}^N G_m(E) M_m, \text{ where } G_m(E) \text{ is a simple function of elevation}$$

angle at the expansion height and M_m is the m^{th} moment of the refractivity distribution about the expansion height h_c . The rapidity of

COMMISSION 6

convergence is heavily dependent on the choice of expansion height. For expansion heights in the neighborhood of the centroid of the layer (300-490 km), the expansion to $N = 2$ (three terms) gives results accurate to about 0.4% at $E = 10^\circ$, which is considered quite good in view of the simplicity of the formulation. As an analytic tool the expansion affords some valuable insight on the influence of layer shape on range errors in special problems.

COMMISSION 6, Session 7

1330 Saturday, April 15

Pan American Room

ANTENNAS AND ARRAYS

D.K. Cheng, Chairman

7-1 ANALYSIS OF A PARALLEL ARRAY OF WAVEGUIDE OR CAVITY BACKED RECTANGULAR SLOT ANTENNAS: D.P. Nyquist and S.P. Mathur, Department of Electrical Engineering and Systems Science, Michigan State University, East Lansing, Mich.

The circuit and radiation properties of a parallel array of transverse, rectangular slots cut in the broad side of a rectangular waveguide are investigated analytically. It is assumed that the ends of the waveguide on either side of the slot array are terminated by arbitrary reflection coefficients; if these coefficients are appropriately adjusted, the effects of traveling and standing waves in the backing waveguide (or cavity) upon the characteristics of the slot antenna array can be studied. Based on a rigorous integral equation approach (earlier studies were based mostly on an approximate variational approach with assumed slot fields), the slot field (or voltage) distributions excited in the apertures of each of the elements of the slot array by impressed currents at the centers of any number of the elements are calculated. In terms of these slot fields, the electrical properties of the array are studied by computing the self and mutual impedances of the slots and the radiation field maintained by them. A coupled system of integral equations for the slot fields in each element of the array is formulated (using the appropriate Green's function for the arbitrarily terminated backing waveguide) based on the boundary condition for the tangential magnetic fields in the slot apertures. This system of equations is solved both by the method of moments and by an extension of the King-Sandler theory for cylindrical antenna arrays. Particular emphasis is placed on the study of a Yagi-Uda type parasitic slot array consisting of a driven element, a parasitic reflector element, and a number of parasitic director elements. The effects of the element lengths and spacings as well as the waveguide dimensions and reflection coefficients upon the radiation patterns of the array and the input impedance to its driven element are investigated. The phase velocity of the wave along the array aperture is determined; by changing this velocity either endfire or broadside radiation can be achieved. It may be possible to vary this velocity and sweep the radiation beam by varying the cutoff frequency of the backing waveguide.

7-2 NUMERICAL TECHNIQUES FOR SOLVING COUPLED LOG-PERIODIC DIPOLE ANTENNAS: W.A. Imbriale, TRW Systems Group, Redondo Beach, Calif

Numerical techniques are used in the analysis of coupled log-periodic dipole antennas. The analysis is formulated in terms of impedance and admittance matrices for the dipole and transmission line networks. The impedance matrix for the dipoles is calculated using moment techniques where the method of subsectional basis is applied with both the expansion and testing functions being sinusoidal distributions. Sinusoidal basis functions are extremely useful for this analysis since the use of one segment per dipole is equivalent to the induced EMF method of calculating mutual impedances and gives a good "first-order" solution which is shown to be quite accurate in predicting midband general performance such as bound on VSWR, impedance, beamwidth, and

directivity. Comparisons are made between this first-order solution and the more exact treatment. Also, other approximations to reduce the size of the impedance matrix are discussed which make the solution of an otherwise intractable problem practical with the existing generation of computers.

In the coupled array problem not only is there mutual interaction between the dipole elements but also through the transmission line feeder boom since the feeder boom of one antenna is a perturbing object in the field of the other antennas. This is not the case in a single LPD antenna since the boom is decoupled by virtue of being located on the bisector of the dipole elements. Calculations were carried out for systems on one, two, and four log-periodic antennas and comparisons are made to experimental data.

7-3 WIDE-ANGLE IMPEDANCE MATCH OF AN INFINITE LINEAR ARRAY OF DIPOLES:
H.D. Jaeger and W.K. Kahn, George Washington University, Washington, D.C.

A method for impedance matching of a phased-array antenna over wide scan angles by means of circuits connecting the various array elements has been described by Hannan, Lerner and Knittel. This approach was expanded by Hannan (Radio Sci. 2:361, 1967) into a constructive proof that match at all scan angles was possible. However no concrete application of the technique to a particular array of antennas specifying the details of choice in matching circuits and illustrating the nature of convergence of the result has been presented. For a variety of reasons an infinite array of inclined dipoles lends itself to the required calculations. These calculations, which will be discussed, have been carried out for several values of antenna element spacing.

7-4 APPROXIMATION OF A CONFORMAL ARRAY WITH MULTIPLE, SIMULTANEOUSLY EXCITED PLANAR ARRAYS: J.K. Hsiao, Radar Division, Naval Research Laboratory, Washington, D.C.

Considerable interest has been shown in the last few years in conformal arrays. This type of array has a variety of potential uses. However, it also has some problems which are not readily solvable. A conformal array on a surface of small curvature can be approximated by a number of planar arrays, several of which may be excited simultaneously so as to achieve performance similar to that of a conformal array. Since the main beam of a planar array can be steered to any direction in real space, several planar arrays, each oriented in a different direction, can be steered cooperatively to form a single beam in a desired direction. With such an arrangement, the problem of array phasing is greatly eased. Within each array, the conventional row and column phase setting can be used, although each array requires an additional phase shift to compensate the phase difference due to its position on the curved surface. However, this correction is much simpler than that required for a conventional conformal array in which each element requires this compensating phase setting. Furthermore, the switching is greatly simplified as it involves only a few planar arrays as compared to the usual conformal array, in which one must switch radiating power among a large number of elements. One might expect the performance of this composite array to be comparable to that of a

COMMISSION 6

single conformal array in the main beam region, since the radiating power of each array is added in phase in this direction. However, the interference that occurs in the sidelobe region is entirely different from that which occurs in a conventional conformal array. The effect on main beam shape, sidelobe level, and directivity gain requires careful examination. Some results of an investigation of these effects are presented in this paper.

7-5 MUTUAL COUPLING BETWEEN CIRCUMFERENTIAL SLOTS ON METALLIC CONES: K.E. Golden, G.E. Stewart and D.C. Pridmore-Brown, Aerospace Corporation, El Segundo, Calif.

The effect of tip scattering on mutual coupling is investigated for circumferential slots on a semi-infinite metallic cone. Mutual coupling measurements as a function frequency and angular separation are presented and compared with numerical calculations. The results illustrate interference effects between the direct coupling from slot-to-slot via the geodesic path over the conical surface and the backscattered ray from the tip. The analysis utilizes a computer calculation of mutual coupling between circumferential slots on an equivalent cylinder to predict the direct coupling contribution and utilizes the tip cross section for calculating the tip diffracted component. The tip cross section is derived from asymptotic expression for the tip scattering component of the surface magnetic field excited on a semi-infinite conical surface by circumferential slot. The experimental apparatus is an 11° half-angle cone-sphere 35 in. long. The two X-band slots are located 10.16 and 10.64 in. from the tip respectively. The cone is terminated in a sphere to minimize scattering from the base region. For small angular separations, the comparison between theory and experiment illustrates that the mutual coupling is determined by the shortest wave path. For angular separations near 180°, the mutual coupling is dominated by backscattering from the tip. For the intermediate angular separations, the direct and tip scattering components interfere resulting in near cancellation of the coupled signal.

7-6 ON DOUBLY ORTHOGONAL FUNCTIONS: Y.L. Chow, University of Waterloo, Waterloo, Ontario Canada

As an extension of the prolate spheroidal functions, doubly orthogonal functions generated from the truncated Fourier transforms are studied in this paper. The Fourier transforms can be in multidimensional spaces. The truncated spaces in both Fourier domains can be of two different and arbitrary shapes, either singly or multiply connected. The fundamental eigenfunction, thus generated, exhibits doubly orthogonal and maximum energy concentration properties, similar to those of the prolate spheroidal functions. Such eigenfunctions are analytically extremely difficult. On the other hand, they are simple in terms of symbolic mathematical operators and numerical analyses. Hence, the mathematical properties of such eigenfunctions are studied in symbolic forms and their numerical values are computed through an iterative procedure. The symbolic mathematics are based on three theorems: namely, the Fourier transform and its inverse, the Parceval's theorem, and the completeness theorem of eigenfunctions from a homogeneous Fredholm's equation of the second kind. The kernel of the Fredholm's equation is assumed to be real and 180° symmetrical across the origin.

COMMISSION 6

At the end, three examples of such doubly orthogonal functions are given. These include the applications to circular antenna aperture with center blockage, spatial frequency coverage of a supersynthesis array, as well as a comparison of energy concentration with the Taylor aperture distribution.

7-7 FAR-FIELD RADIATION RESISTANCE AS A TERM IN AN ANTENNA'S IMPEDANCE:
W.S. Ament, Naval Research Laboratory, Washington, D.C.

In a homogeneous medium with dyadic Green's function G , the electric field $E(p)$ at p , due to current-density $j(q)$ at q on an antenna A , is

$E(p) = \int_A G(p-q) \cdot j(q) dq$. Let $j_t(q)$ be the current density on A in the "transposed" medium, and I , I_t be the corresponding driving currents across the infinitesimal antenna gap in a necked-down part of A . Then $I_t I Z_{emf} = \int_A j_t(q) \cdot E(q) dq$ is a variational "impedance" form helpful in finding accurate j , j_t . This can be extended to allow for ohmic losses in A . $I^* I Z_{cp} = \int_A j^*(q) \cdot E(q) dq$ gives an impedance Z_{cp} through a complex-

power integral related by Poynting's theorem to total far-field power flux. In some lossless free space circumstances, Z_{cp} and Z_{emf} are identical, whence their confusion in textbooks. In the collisionless magnetoionic medium, one must use a Fourier-represented G : If an ideally flat A lies in a general x,y plane, and u,v,w are x,y,z components in k -space, the Z_{cp} calculation reduces to a u,v integral. Here the dispersion relation gives $w(u,v)$ real only for certain regions R in the u,v plane. The u,v integral for $\text{Re}(Z_{cp})$ restricted to regions R gives the "far-field radiation resistance" justified by Poynting's theorem. Other terms in $\text{Re}(Z_{cp})$ give power dumped into gyrating local charged particles. These statements are generalized and justified.

7-8 SMALL ANTENNAS IN DISPERSIVE MEDIA: Giorgio Franceschetti,
University of Naples, Italy

For a complete description of the communication channel in dispersive media, e.g., subsurface propagation by using pulse techniques, a knowledge of the frequency response of the antenna is necessary. In this note, a network representation is given for the input admittance (or impedance) of the following antennas: oblate (parallel-plate antenna), prolate (linear antenna), spherical, metal antennas of dimensions small with respect to the local wavelength, and fed at small finite equatorial gap. The input admittance (or impedance) is given in terms of physically realizable inductances, capacitances, resistances, conductances, and a reciprocal gyrator. The value of each network component is given as the product of a geometrical factor that depends on the particular antenna considered, and a second factor that depends only on the external medium. This fact highlights the possibility of using the antenna as a probe, which can be exactly calibrated in a known medium, e.g., free space. The transient response of the antenna can be inferred from the singularities of the input impedance (or admittance) in the complex frequency plane: complex poles (response at

COMMISSION 6

small observation times), and branch-cuts (response at large observation times). The effective height is also computed for the antennas under consideration. As a check, the radiation resistance and effective height of the prolate antenna are considered versus the same parameters for an elementary electric dipole. The expressions are identical except for correction factors that account for the finite gap and the frequency dependence.

7-9 RADIATION PATTERNS AND DIRECTIVITY OF SMALL HOMOGENEOUS DIELECTRIC SPHERES EXCITED BY SIMPLE SOURCES: V.B. Mason and C-T. Tai, University of Michigan, Ann Arbor, Mich.

In this theoretical study the field distribution over a waveguide aperture placed against the surface of a homogeneous dielectric sphere is modeled using a superposition of electric and magnetic dipole currents. Expressions for the far-zone field and directivity are then derived and numerically evaluated by means of a digital computer for spheres ranging from about 0.5 to 5 wavelengths in diameter. Subsequently the field patterns are plotted for various combinations of sphere size and dielectric constants. These curves are then compared to experimental data measured by W.F. Croswell and J.S. Chatterjee (NASA Langley Research Center) for plexiglas spheres ranging from 2 to 5 in. in diameter. Our calculation confirms their finding that a small dielectric sphere may be used to produce field patterns which are superior to that of an optimized circular horn of the same cross-sectional area. The theoretical curves show, however, that at certain frequencies the sphere exhibits a resonance effect in which an appreciable sidelobe level is produced with a commensurate decrease in directivity. The effect of dielectric loss is studied, and it is noted that with spheres constructed of a material such as plexiglas the resonance effect and pattern degradation are almost completely obliterated.

7-10 THE ORTHOGONALIZATION OF TWO ELLIPTICAL POLARIZATIONS: T.S. Chu, Bell Telephone Laboratories, Holmdel, N.J.

Two orthogonal polarizations can be used to double the capacity of a communication system. However, the transmission medium or the radiating system may fail to maintain orthogonality between the two polarizations. One can recover the orthogonality if the polarization characteristics are reasonably constant over the operating bandwidth. Two nonorthogonal elliptically polarized waves can be simultaneously transformed into two orthogonal polarizations by combining a differential phase shifter and a differential attenuator. To minimize the amount of differential attenuation required to remove a given amount of non-orthogonality, a differential phase shifter should first be used to transform the two arbitrary elliptical polarizations into two oppositely rotating elliptical polarizations with the same axial ratio. Since the two orthogonal polarizations in a dual polarization communication system will be either linear or circular, the orthogonalization will proceed via two nonorthogonal linear polarizations for the linear case or via two oppositely rotating elliptical polarizations having parallel axes and equal axial ratios for the circular case. Explicit analytical solutions are presented with the aid of the Poincare sphere. The analysis also suggests experimental techniques for determining the required differential phase shift and differential attenuation. System

COMMISSION 6

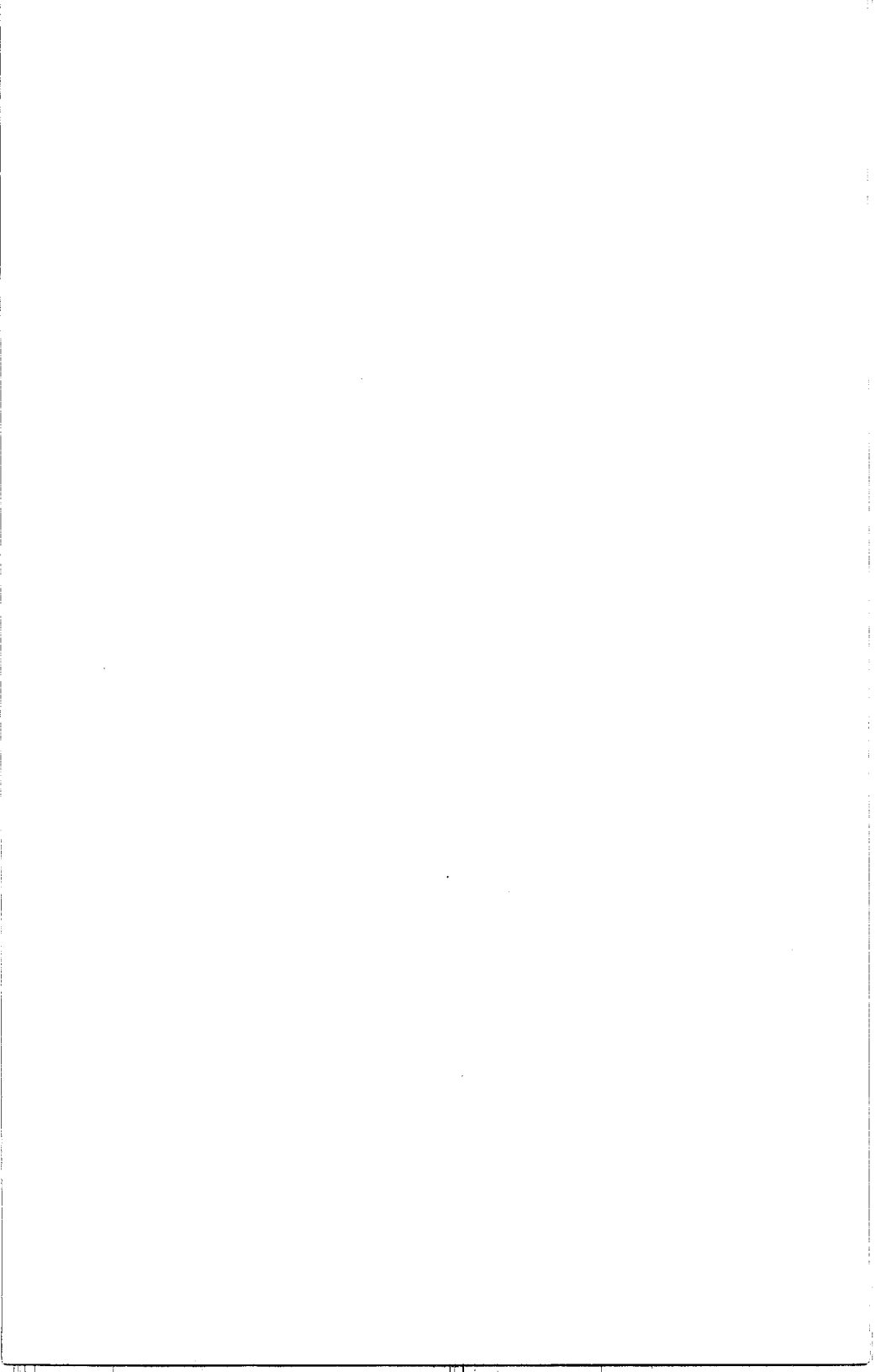
applications will be discussed. If the polarization distortions are time-varying, the above scheme requires two beacon signals for adaptive control of the differential elements.

AUTHOR INDEX

Aarons, J. 61
 Ajmera, R.C. 13
 Albertsen, N.C. 123
 Alexopoulos, N.G. 108
 Allan, L.E. 34
 Aller, H.D. 102
 Almeida, O.G. 79
 Ament, W.S. 137
 Arnush, D. 73
 Auterman, J.L. 64
 Axline, R. 37
 Baker, D.J. 81
 Ball, J.A. 104
 Bannister, P.R. 26
 Baron, M.J. 43,44
 Barrick, D.E. 29
 Barrow, C.H. 93
 Basart, J.P. 96
 Batcheior, D.B. 13
 Bates, H.F. 43,45
 Baum, C.E. 108
 Behnke, R.A. 52
 Bell, T. 87
 Bennett, C.L. 109,110
 Bennett, J.A. 49
 Berbert, J.H. 132
 Bertoni, H.L. 112
 Birgenheimer, R.A. 125
 Blank, H.A. 61
 Bostian, C.W. 34
 Brace, L.H. 59
 Brennan, L.E. 126
 Brice, N.M. 79,93
 Brinca, A.L. 83
 Brink, C.A. 68
 Broderick, J.J. 94,96
 Brotan, N.W. 96
 Brown, G.S. 37
 Brown, W.P., Jr. 118
 Burton, R.K. 79
 Butler, C.M. 123
 Caldecott, R. 111
 Carpenter, D.L. 75
 Caruso, J.A. 7
 Chan, K.W. 79
 Chesnut, W.G. 47,54
 Chow, Y.L. 136
 Chu, T.S. 138
 Chuang, C.D. 92
 Clark, B.G. 94
 Clark, T.A. 95,96,97
 Clifford, S.F. 32
 Cogdell, J.R. 12,90
 Cohen, M.H. 98
 Coleman, J.T. 117
 Collin, R.E. 132
 Collis, R.T.H. 17
 Compton, R.T., Jr. 125
 Corbin, V.L. 49
 Cornwall, J.M. 86
 Cox, D.C. 25
 Cronyn, W.M. 96
 Crout, P.D. 129
 Crystal, T.L. 82
 Cudaback, D.C. 102
 Cuzzi, J.N. 102
 D'Amado, R. 103
 da Rosa, A.W. 110
 Davis, J.H. 12
 Davis, R.M., Jr. 47
 Davis, T.N. 69
 Davis, W.A. 110
 deBettencourt, J.T. 34
 Decker, W.J. 90
 DeLorenzo, J.D. 110
 Derr, V.E. 18
 Deschamps, G.A. 112
 Dias, L.A. 66
 Dillingham, J.H. 47
 Doherty, R.H. 57
 Dunckel, N. 91
 Ellingboe, A. 28
 Elliott, D.A. 100
 Epstein, M.R. 64
 Ergas, R. 97
 Erickson, W.C. 8,95,96
 Evans, J.V. 51
 Evenson, K.M. 7
 Fainberg, J. 91
 Falcone, V.J., Jr. 39
 Fang, D.J. 38
 Fanselow, J.L. 97
 Farley, D.T. 52
 Fedor, L.S. 67
 Fejer, J.A. 66,73
 Felsen, L.B. 112
 Findlay, J.W. 104
 Fisher, J.R. 104
 Flock, W.L. 39
 Fomalont, E.B. 101
 Franceschetti, G. 137
 Francis, S.H. 48
 Frandsen, A.M.A. 80
 Frank, L.A. 92
 Fraser, B.J. 81
 Fremouw, E.J. 56,63
 Fried, B.D. 73
 Fritz, R.B. 72
 Fung, A.K. 37
 Galt, J.A. 96
 George, R.L. 57
 Gibbons, J.J. 67
 Gieraltowski, G.F. 74
 Glass, A.J. 115
 Gnanalingam, S. 58
 Goe, G.B. 56,72
 Golden, K.E. 124,136
 Golden, T.S. 61
 Goldstein, R.M. 95,97
 Gottesman, S. 100
 Gray, D.A. 22,33
 Green, J.L. 39
 Greisen, E.W. 100
 Grossi, M.D. 77
 Gruner, R.W. 11
 Gurnett, D.A. 92
 Gustafsson, S.G. 25
 Guy, A.W. 122
 Haerendel, G. 86
 Hagen, J.P. 90
 Hagfors, T. 74
 Hall, F.G. 29
 Hansen, J.E. 123
 Harbridge, W.B. 83,84
 Hardy, K.R. 17
 Hassab, J.C. 117
 Hayne, G.S. 37
 Hearn, J.R. 13
 Heiles, C. 100,101
 Helliwell, R.A. 55,75,82,91
 Helms, W.J. 55
 Hemerway, P.D. 97
 Hendry, A. 19
 Heneghan, J.M. 120
 Herman, J.R. 7,59
 Herron, T.J. 62
 Hickman, T.G. 11
 Hill, D.A. 27,130
 Hills, R. 101
 Hinteregger, H.F. 95,97
 Hobbs, R.W. 98
 Hodge, D.B. 23
 Hodges, J.C. 54
 Hoegy, W.R. 60
 Hollinger, J.P. 13
 Holtzman, J. 28
 Holzer, R.E. 79,80
 Howard, A.Q., Jr. 122
 Howard, J.E. 125
 Hrubesh, L.W. 14
 Hsiao, J.K. 135
 Hsu, Y.S. 52
 Huebner, D.A. 108
 Hunsucker, R.D. 44
 Ioannidis, G. 52
 Imbriale, W.A. 134
 Ippolito, L.J. 24
 Ishimaru, A. 119,120
 Itoh, T. 110
 Jaeger, H.D. 135
 Janssen, M. 101
 Jarem, J. 117
 Jenkins, R.W. 59
 Jensen, N.E. 123
 Johnson, R.C. 11
 Johnston, K.J. 98
 Jones, T.B. 53,66
 Kahn, W.K. 135
 Kalaghan, P.M. 90
 Kantor, I.J. 73
 Katsufakis, J.P. 75
 Kaufmann, P. 103
 Kay, I.W. 115
 Keller, J.B. 114
 Kenefick, J.F. 10
 Kennaugh, E.M. 109
 Kennel, C.F. 73
 Kerr, F.J. 98
 King, J.L. 21
 King, H.S. 92
 Klein, M.M. 49
 Klemperer, W.K. 127
 Knapp, G.R. 98
 Knight, C.A. 95,97
 Knowles, S.H. 95,96
 Ko, H.C. 92
 Koons, H.C. 83,84
 Konrad, T.G. 18

Kritikos, H.N. 30
 Kundu, M.R. 91
 Kuo, W.C. 121
 Laaspere, T. 71
 LaLonde, L.M. 103
 Lammers, U.H.W. 19
 Lang, R.H. 117
 Lanzerotti, L.J. 76
 Lashinski, H. 13
 Leadabrand, R.L. 43,54
 Lee, M.K. 58
 Lee, S.W. 129
 Leer, E. 73
 Legg, T.H. 96
 Lewis, R.L. 46
 Liemohn, H. 76
 Lin, J.C. 122
 Little, C.G. 17
 Liu, Yu-Ping 109
 Livingston, R.L. 55
 Lo, Y.T. 115
 Locke, J.L. 96
 Long, M.R. 123
 Love, A.W. 103
 Lytle, R.J. 26
 MacDoran, P.F. 97
 Mallinckrodt, A. 132
 Marandino, G.E. 95,97
 Marshall, R.E. 34
 Mason, V.B. 138
 Mathur, S.P. 134
 Matsumoto, J.H. 83
 Maurer, S. 129
 Mayr, H.G. 59,60
 McCormick, G.C. 19,34
 McAfee, J.R. 88
 McCullough, T.P. 91
 McDonough, T. 79,93
 McGuffin, A.L. 126
 McIntosh, R.E. 120
 McPherron, R.L. 75
 McPherson, D.A. 83,84
 Mechty, E.A. 59
 Meeks, M.L. 103
 Mei, K.K. 121
 Mennella, R.A. 13
 Miller, E.K. 109
 Miller, L.S. 37
 Mittal, R. 110,121,122
 Moe, R. 28
 Moffatt, D.L. 111
 Mohsen, A. 131
 Moore, R.K. 28
 Moran, J.M. 94
 Morgan, M.G. 70
 Moser, P.J. 67
 Mosier, S.R. 91
 Muhrleman, D.O. 102
 Muldrew, D.B. 85
 Newell, A.C. 11
 Nisbet, J.S. 58
 Nyquist, D.P. 134
 Ochs, G.R. 32
 Olsen, E.T. 102
 Olsen, R.L. 19
 O'Meara, T.R. 127
 Orphanoudakis, S.C. 71
 Ott, R.H. 130
 Park, C.G. 79
 Parker, H. 132
 Paul, A.K. 49,67
 Paymar, E.M. 80
 Peake, W.H. 28
 Peek, M.H. 69
 Perkins, F.W. 66,72
 Petriceks, J.D. 43,44,45
 Pickering, L.W. 120
 Pope, J.H. 72
 Porcello, L.J. 64
 Potemra, T.A. 54,55
 Preston, R.A. 97
 Pridmore-Brown, D.C. 136
 Ra, J.W. 112
 Rao, N.N. 62
 Rao, P.B. 88
 Reich, R. 132
 Resch, G.M. 95
 Richmond, J.H. 109
 Richter, K.R. 39
 Riegel, K.W. 100
 Rino, C.L. 45,63
 Robertson, D.S. 95,97
 Robertson, E.A. 22
 Robertson, S.C. 60
 Robison, F.L. 18
 Roche, J.F. 33
 Roederer, J.G. 69
 Rogers, A.E.E. 95,97
 Rogstad, D.H. 99
 Rosenbaum, S. 118
 Rosenberg, T.J. 55,71
 Rouse, J.W., Jr. 30
 Rowe, J.F., Jr. 52
 Rufenach, C.L. 68
 Safir, G. 28
 Salah, J.E. 51
 Seemann, D.R. 61
 Sengupta, D.L. 109
 Seshadri, S.R. 131
 Sessions, W.B. 61
 Sforza, P.F. 31
 Shapiro, I.I. 95,97
 Shawhan, S.D. 96
 Shostak, G.S. 99
 Showen, R.L. 66
 Simonson, S.C.III 99
 Siwiak, K. 129
 Skjerve, L. 97
 Smith, E.J. 79,80
 Smith, L.G. 59
 Smith, R.S. 110
 Smyth, J.B. 40
 Spitzmesser, D.J. 95,97
 Steinberg, B.D. 127
 Stenbaek-Nielsen, H.C. 69
 Stewart, G.E. 124,136
 Stiles, G.S. 82
 Stone, R.G. 7
 Straiton, A.W. 21
 Streifer, W. 112
 Strickland, J.I. 23
 Strohbehn, J.W. 33
 Stubenrauch, C.F. 130
 Stutzman, W.L. 34
 Suits, G.H. 28
 Sukhia, D.E. 22
 Summers, W.R. 81
 Swanson, P.N. 90
 Swazye, D.W. 36
 Tai, C-T. 130,138
 Tang, C.C.H. 40
 Tanenbaum, B.S. 52
 Tappert, F. 114
 Taylor, L.S. 119
 Telford, L.E. 10
 Theis, R.F. 59
 Thomas, J.B. 97
 Thomas, R.K. 30
 Thompson, A.D. 36
 Thorne, R.M. 80
 Thornton, D.D. 101
 Tierney, M.S. 47
 Toman, K. 58
 Tsao, C.K.H. 33
 Ulaby, F.T. 28
 Ulich, B.L. 90
 Urech, J. 97
 Uslenghi, P.L.E. 129
 Valeo, E.J. 72
 Vandenberg, N.R. 95,96,97
 Vargas-Vila, R. 47
 von Hoerner, S. 104
 Wait, J.R. 27,122
 Walton, E.K. 63
 Wand, R.H. 52
 Wang, Ting-I. 33
 Wang, T.N.C. 84
 Wang, T.S. 115
 Watt, T.M. 43
 Wefer, F.L. 90
 Weil, H. 81
 Welch, W.J. 101
 Weliachew, L.N. 101
 Wescott, E.M. 69
 White, D.P. 46
 Whitney, A.R. 95,97
 Whitney, H.E. 61
 Wiley, P.H. 34
 Wilk, J.M. 120
 Williams, D.J. 87
 Williams, J.G. 97
 Willim, D.K. 46
 Wilson, C.R. 56
 Winckler, J.R. 87
 Wong, M.S. 48
 Wright, J.W. 7,67
 Wright, M.C.H. 99,100
 Wulfsberg, K.N. 32
 Yen, J.L. 96,105
 Young, G.O. 125
 Young, J.D. 111
 Zeger, A.E. 125
 Zintsmaster, L.R. 23
 Zmuda, A.J. 54,55







1972 USNC-URSI FALL MEETING

11-15 December 1972

College of William and Mary

Williamsburg, Virginia

1973 USNC-URSI/GAP MEETING

22-24 August 1973

Boulder, Colorado

1974 USNC-URSI/GAP SUMMER MEETING

11-13 June 1974

Georgia Institute of Technology

Atlanta, Georgia

